NTNU – Trondheim
Norwegian University of
Science and Technology

# DEBRIS HANDLING AT SMALL HYDRO POWER INTAKES

Fredrik Holmeset

Civil and Environmental Engineering
Submission date: June 2013
Supervisor: Leif Lia, IVM
Co-supervisor: Hanne Nøvik, IVM

Norwegian University of Science and Technology
Department of Hydraulic and Environmental Engineering

# Acknowledgements

This master's thesis, *Debris Handling at Small Hydro Power Intakes*, is performed under the Department of Hydraulic and Environmental Engineering at The Norwegian University of Science and Technology.

The subjects discussed in this study have enriched the undersigned's enthusiasm for intake functionality and not at least the use of CFD-software. Even though the CFD-software provided a lot of frustration (especially in the beginning) it has proved to be a good companion through countless hours of clicking and typing. I am also satisfied with the result of the simulations performed in this thesis.

I use opportunity to express my gratitude to several people at the Department of Hydraulic and Environmental Engineering who supported me in accomplishing my study. Hanne Nøvik (PhD-student and co-supervisor) has supported me through interesting discussions and provided me with advices throughout the study. Samuel Vingerhagen, for his assistance through the use of VILJE and STAR CCM+. Geir Tesaker, for his assistance on building both the demonstration model and the scale model in the lab. Leif Lia (Professor and supervisor), for his ability of creating enthusiasm and interest within the field of hydro power!

Place and date

Fredrik Holmeset

## Abstract

In this study the handling of debris in small hydro power intakes is assessed by evaluating the concept of back flushing with a horizontally fixed trash rack.

The concept of back flushing is to reverse the flow over the trash rack for a short period of time in order to detach and evacuate clogged debris through a flushing pipe or gate.

In this study the concept of back flushing with a horizontal trash rack is evaluated for two different designs; a one chamber design and a two chamber design. The one chamber design is based on H. Brekke's conceptual idea. The two chamber design is also based on H. Brekke's idea but it is also inspired by Bergedammen. Bergedammen is an intake designed with two chambers making it possible to continue power production while back flushing one chamber at the time.

The efficiency of back flushing as well as the hydraulic performance during normal operation is mainly evaluated using numerical modelling and a CFD-software.

The concept of back flushing, general intake hydraulics and computational fluid dynamics (CFD) is covered by the literature study in this thesis.

The evaluation of the back flushing concept is initiated by a physical demonstration model with two chambers. The demonstration model is built and tested for flushing efficiency and performance during normal operation.

The following numerical tests are performed on 4 different model designs. The first model illustrates a full scale one chamber design. The second model illustrates a full scale two chamber design. The third model is identical to the demonstration model. The forth model is designed as a result of the demonstration model and the previous numerical models, where important model parameters were identified. The important model parameters for effective flushing and hydraulic performance during normal operation is identified as the height of the weir, the vertical position of the trash rack, the length of the model and the amount of water available for flushing.

The numerical analyses evaluate the flushing efficiency by assessing the velocity distribution over the trash rack. The hydraulic performance of the models during normal operation is evaluated by assessing streamlines, head loss and turbulent kinetic energy levels (TKE) by the outlet. During flushing the most important parameter is the height between the top of the weir and the trash rack. A high weir results in an even velocity distribution over the trash rack. A low weir results in uneven velocities with higher velocities along the weir. During normal production the length of the model and the height of the weir are important parameters affecting both the total head loss and TKE-values. The results achieved by the numerical modelling should be validated, as further research, on a scale model designed and built in the lab. The test program for the scale model is presented in this study.

# Samandrag

Denne rapporten tek føre seg drivgodshandtering på småkraftverksinntak ved å vurdere effektiviteten av tilbakespylingskonseptet med ei inntaksrist plassert horisontalt.

Tilbakespylingskonseptet går ut på å reversere vasstraumen over inntaksrista over ei kort periode, der målet er å rive drivgods laust frå rista og føre det ut gjennom spylerøyret.

I denne rapporten er tilbakespylingskonseptet evaluert for to ulike utformingar. Ei ein-kammer løysing og ei to-kammer løysing. Ein-kammer løysinga har sitt grunnlag i H. Brekke sin konseptuelle ide om å plassere rista horisontalt. To-kammer løysinga er også basert på H. Brekke men den er også inspirert av Bergedammen. Bergedammen er eit inntak med to kammer, noko som gjer det mogleg å fortsette kraftproduksjon samstundes som kammera tilbakespylast kvar for seg.

Effektiviteten av tilbakespylinga og dei hydrauliske forholda ved normal drift er hovudsakleg vurdert ved å nytte numerisk modellering og CFD-programvare.

Tilbakespylingskonseptet, generell inntakshydraulikk og numerisk modellering omfattar innhaldet i litteraturstudiet i denne rapporten.

Den første vurderinga av tilbakespylingskonseptet er gitt av bordmodellen med to kammer. Bordmodellen er bygd og testa for spylingseffektivitet og hydraulisk kvalitet under normal drift. Bordmodellen visualiserer at tilbakespylingskonseptet fungerer godt syner viktige modellparametrar for å oppnå god spyling.

Dei numeriske simuleringane er gjennomført på 4 ulike modellar. Den første modellen har ei ein-kammer løysing i fullskala. Den andre modellen har ei to-kammer løysing i fullskala. Den tredje modellen er lik bordmodellen. Den fjerde modellen er basert på resultata frå bordmodellen og dei føregåande simuleringane, der dei viktige modelparameterane vart identifisert. Dei viktige parameterane for effektiv tilbakespyling og god hydraulisk kvalitet ved normal produksjon er terskelhøgde, vertikal posisjon av inntaksrista, lengda mellom terskel og inntak til turbin og tilgjengeleg vatn for tilbakespyling.

Tilbakespylingseffektiviteten i dei numeriske simuleringane er vurdert ved å sjå på hastigheitsfordelinga over inntaksrista. Dei hydrauliske forholda ved normal produksjon er vurdert ved å sjå på strøymingslinjer, falltap og turbulent kinetisk energi (TKE) ved utløpet av modellen. Dei viktigaste parameterane for effektiv spyling er høgda mellom inntaksrista og terskeltoppen. Ein høg terskel fører til ei jamn hastigheitsfordeling over inntaksrista. Ein lav terskel gir ei ujamn hastigheitsfordeling med høgare hastigheit langs terskelen. Viktige modellparameterar ved normal drift er lengda på modellen og høgda av terskelen, som begge påverkar det totale falltapet og TKE verdiane. Som eit ledd for vidare forsking, bør resultata frå dei numeriske simuleringane validerast gjennom tilsvarande testing i ein fysisk modell som under denne studien er utvikla og bygd i laboratoriet.

# List of Tables

# List of Figures

# Contents

# 1. Introduction

Norway has for several years experienced a high increase of small power hydro power development, and 2012 is not an exception. In 2012 NVE handled concession cases worth 4.42 TWh in new production. 118 applications regarding small hydro power were handled by NVE in 2012, twice as much as in 2011. Of the 118 applications 60 were given concessions for a total amount of 583 GWh. In addition, 39 cases received exemption of concession for a total amount of 93 GWh. Norway has in comparison a total annual electricity production of about 125 TWh. (NVE, 2013)

Most of the small hydro power plants in Norway are so called run of the river power plants. Debris clogging the trash racks is a common problem for run of the river power plants. As the number of small hydro power plants increases and as current plant owners are distressed about their clogged trash racks, the developing of better intake solutions and trash rack cleaning processes will continue.

The two concepts of cleaning the trash rack assessed in this study are the concept of using a siphon cleaning system and the concept of back flushing on a horizontally fixed trash rack. The siphon cleaning system uses the siphon effect to create suction power which is applied through a nozzle directly onto the trash rack. Unfortunately, further study on the siphon concept was aborted due to a lot of ice at the intake where the instalment was planned and the fact that the siphon concept has already been externally tested and built.

This study therefore only concentrates on evaluating the efficiency and suitability of an intake solution using the concept of back flushing with a horizontally fixed trash rack. This design is based on H. Brekke's conceptual idea and will eliminate the need of manual cleaning of the trash rack.

The efficiency and suitability of the intake solution is validated by using physical models as well as numerical modelling. An initial demonstration model of the concept was built to identify important parameters for flushing efficiency and during normal operation. The result of the demonstration model is followed by several numerical simulations, where different model parameters were tested.

This study focuses on the use of numerical modelling and the CFD software STAR CCM+, including the intentions of validating the quality and correctness of the numerical results.

# 2. Intake Hydraulics

This chapter concentrates on explaining relevant theory used for this study. The headworks of river hydro power and intake hydraulics are the main subjects and are further adduced. The headwork is the first structure that encounters the production water used for hydro power production.

## 2.1. Composition of the Headwork Structure

A headwork has to be designed after the site surroundings which make every intake unique. Jenssen et al. (2006) explains the composition of a generalized headwork and it is displayed in figure 2-1.

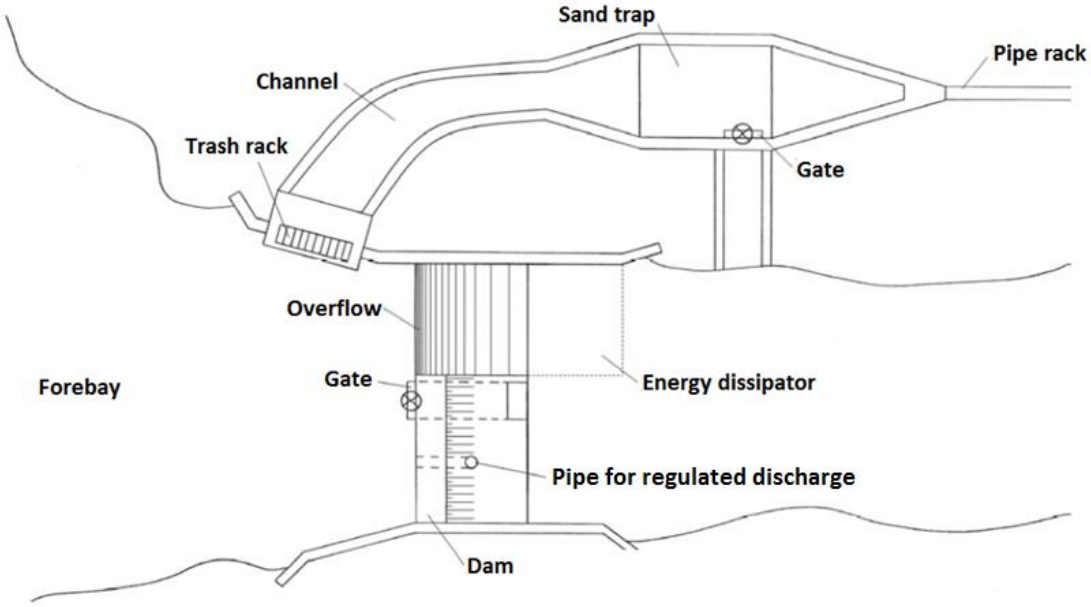


**Figure 2-1: The composition of a general stream headwork (Jenssen et al., 2006)**

The main parts of a stream headwork are marked in figure 2-1. Most stream headworks are designed with a dam to create a forebay or a small reservoir in front of the intake. The reservoir has several functions; it helps to create stable ice coverage, the water velocity is reduced, sediments in the river settle in the reservoir and can later be removed, the intake and the trash rack is submerged reducing risk of air entrainment and clogging and a sufficient surface area is created in order for the turbine water level regulator to work properly. The dam is designed with an *overflow* with sufficient capacity, *a bottom gate* for possibilities for flushing and emptying the reservoir, *a pipe* to ensure the regulated water flow and an *energy dissipater* if needed. The intake needs *a trash rack* to prevent debris from entering the water way. It is not unusual to install a coarse trash rack and a finer trash rack closer to the inlet. All trash racks need regular cleaning, manual or mechanically, to avoid clogged trash racks. For Norwegian conditions it is often sufficient with a small sand

trap to cope with sediments. The sand trap is usually placed between the coarse trash rack by the river and the pipe rack intake as illustrated in figure 2-1. A gate can be positioned in the bottom of the sand trap – this gives possibilities for emptying the sand trap by flushing. Depending on the topography and the position of the headwork the waterway may consist of a tunnel, a channel, a penstock or a combination of these. (Fladen et al., 2010, Jenssen et al., 2006)

## 2.2. Intake Functionality

Lysne et al. (2003) expresses the following main functional criterion for a hydro power plant: "*The plant shall remain in operation during all normal situations in order to secure a safe and regular power generation*" (p.43). Based on this criterion a list to ensure a well-functional headwork is presented:

1. Passage of floods
2. Passage of debris and ice
3. Passage of sediments
4. Bed control at the intake
5. Exclusion of suspended sediments and air
6. Safe operation and maintenance

**Passage of Floods**

All headwork shall be constructed in such a matter to safely handle flood water. The spillway must be designed to handle design flood without serious damage on any part of the headwork.

**Passage of Debris and Ice**

The headwork shall be designed in a way that prevents debris and ice to clog up in front of the trash rack and interfering with normal power production. Debris clogging to the trash rack is a common problem in Norwegian shallow river intakes. Cleaning of clogged trash racks can be done either manually with a rake or by several mechanical methods described later in this study. Deep reservoirs tend to be isolated from ice problem. Shallow intakes on the other hand, are often affected by drifting ice clogging the trash rack and direct freezing of ice on the trash rack. (Johnson, 1988)

**Passage of Sediments**

A well designed headwork has to manage both suspended sediments and bed-load. In steep rivers, attention to bed load in form of big boulders is important to prevent blockage of the intake or the flushing gates. It is also recommended with a free overflow crest design instead of gated weirs. Use of free overflow crests increases safety by eliminating the risk of gate blockage and gate malfunction. For steep rivers it is also recommended to have a low-level gate (flushing gate) for removal of deposits when needed. The flushing gate is preferable placed in the initial riverbed-level and close to or under the intake in order to remove interfering deposits during flushing.

**Bed Control at the Intake**

It is crucial to have control of the river floor in front of the intake in order to ensure a stabile water flow conditions as well as to prevent entrainment of sediments further down the water path. The riverbed shall never build up in front of the trash rack. Good bed control is obtained through good hydraulic design, by placing the trash rack close to the spillway and by use of flushing gates/sediment ejectors.

**Exclusion of Suspended Sediments and Air**

In parts of the world many rivers have the characteristics of high sediment transport – the headwork design must in these cases include good solutions for sediment handling. An average Norwegian river used for hydro power has low sediment transport and it is seldom necessary with sedimentation basins. In most cases a simple sand trap is sufficient to comprehend an acceptable water quality for power production.

Three main sources of air in pressurized tunnels are described by Lysne et al. (2003) as the following:

1. Air trapped in the tunnel during filling
2. Air supplied to the tunnel through the intake in forms of bubbles or air-conducted whirls
3. Air supplied to the tunnel through creek intakes

Air in pressurized tunnels are highly unwanted and causes pressure loss and flow disturbance. Air supplied through the intake may in most cases be solved by ensuring sufficient submerging of the intake.

**Safe Operation and Maintenance**

It is important that the trash rack, and the headworks in general, is designed in a way that ensures safe access at all times, also at extreme weather conditions, to perform maintenance like manually raking the trash rack.

## 2.3. Trash Rack Design

A trash rack is a gate placed in front of the intake and is designed to keep debris, ice and other obstacles away from the water path to prevent jamming or damage to the machinery and to ensure safe power production. Debris bigger than the smallest opening in the water-way, for instance the nozzle in Pelton turbines, shall not pass through the finest trash rack in order to avoid jamming, damage and production problems.

The trash rack should be fully submerged at all times to avoid the bars from freezing and to guarantee normal production after ice cover formation. If the trash rack is exposed to large quantities of frazil ice, which is frozen water particles suspended in the water flow, the risk of ice accumulation, even if the bars are heated, is overhanging. (Johnson, 1988)

A typical trash rack clearance is in the range of 10-50 mm. The trash rack can be designed as a perforated plate, a set of bars or as a wired network. Common in Norwegian small hydro power, is trash racks designed with parallel rectangular bars supplied with cross-overs for stiffness and vibration reduction. Hydraulically shaped bars are also available for trash racks, but due to higher costs this is often not feasible for small hydropower projects with low budgets. Corrosion protected trash racks are also available in form of coating, galvanic cell systems, stainless steel, high density polyethylene (HDPE) and fiber-reinforced polymer (FRP). Typical life expectancy of steel trash racks is 15 to 35 years and 25 to 50 for plastic or fiberglass trash racks. (Mesa Associates & Oak Ridge National Laboratory, 2011)

**Head Loss over the Trash Rack**

When designing a power plant it is important to study all sources of head loss through the water path. Any change in water flow results in a head loss. Higher head loss gives lower pressure head at the turbine and lower potential production. For small hydropower plants (less than 10MW) the trash rack area is often designed to achieve a gross water velocity of 0.5 m/s or less.

Calculating the head loss over the trash rack is done in various ways by different formulas. Kirschmer-Mosonyis formula is commonly used along with Idelchiks formula and the more advanced Meusburgers formula which also includes clogging of the trash rack. (Jenssen et al., 2006)

The Kirschmer-Mosonyis formula calculates the head loss over the trash rack as a function of gross water velocity ($V_R$), the thickness of the bars (t), the distance between the bars (b) and angled inflow through the trash rack ($k_\delta$).

$$\Delta H = k_F \cdot \left(\frac{t}{b}\right)^{4/3} \cdot \frac{V_R^{\,2}}{2g} \cdot \sin\alpha \cdot k_\delta \qquad [2\text{-}1]$$

$K_F$ is the shape factor of the bars and is typically set as 2.42 for rectangular bars and 0.76-1.04 for hydraulically shaped bars. The angle $\alpha$ is the angle between the trash rack and the

horizontal plane. $k_\delta$ is the coefficient for angled inflow through the trash rack and varies from 1.00-6.05 depending on the inflow angle and the relation between *t* and *b*. The entire table for different $k_\delta$-values is available in Jenssen et al. (2006) but only based on rectangular rods with thickness and length of 10 mm and 50 mm. $V_R$ is the gross water velocity through a vertically projection of the trash rack calculated as the following:

$$V_R = \frac{Q_R}{H_R \cdot B_R} \qquad [2\text{-}2]$$

Where $Q_R$ is the water flow through the trash rack, $H_R$ is the height of the trash rack and $B_R$ is the width of the trash rack.

## 2.4. Handling of Debris

A well designed headwork shall include solutions for handling all types of debris considered to appear in the river. The concentration of river debris is highest during floods and during autumn defoliation. Based on the debris characteristics, Jenssen et al. (2006) divides debris into four groups:

- Natural floating debris
- Submerged and bed load materials
- Man-made waste
- Ice related debris

*Natural floating debris* consists of a wide variation of materials. Leaves, moss, grass, branches and threes are examples of natural floating debris. Most of the natural floating debris, as leaves, is small and soft materials and will seldom harm the turbine if it passes the trash rack. The problem with natural floating debris is its varying size and potential of clogging the trash rack resulting in head loss and higher maintenance costs.

*Submerged and bed load materials* consists of mainly saturated vegetation, gravel and stone as well as dead animals. The bed load will settle in in the reservoir where the water velocity is lower than in the river up streams. If the reservoir is too small, bed load will settle in front of the intake and small stones may be carried through the trash rack causing damage to the turbine in its passage. If the settling basin or the reservoir is insufficient and the area is suspected of high sediment transport a sand trap between the trash rack and the intake might be needed. Saturated leaves are often a problem when it tends to submerge and follow the water path and clogs over the trash rack.

*Man-made waste* is a wide description and contains everything from branches and fishing gear to furniture and hay bales. The trash rack can easily stop man-made waste but the risk

of plastic or other debris totally clogging the trash rack is overhanging, and will lead to shut down of the power plant. The risk of having man-made debris in the river shall be considered in the planning phase, as for other debris.

*Ice related debris* is a common problem in cold areas. Ice clogging the trash rack appears when ice freezes directly on the trash rack and when shifting ice jams in front of the trash rack. In rare occurrences even entire ice blocks is sucked under blocking the entire trash rack. (Jenssen et al., 2006)

Keeping floating debris clear from the trash rack can be a challenge, especially in small intakes where a large percentage of the river discharge is used for power production. Keywords to achieve good handling of floating debris are intake orientation, booms, submerging and knowledge about velocity distribution and turbulence intensity of the river.

**Intake orientation**

The intake shall be designed in a way that prevents debris and ice from clogging up in front of the trash rack. To prevent clogging it is preferred to place the trash rack close to the overflow with an angle to the water flow as well as a ledge to further prevent debris being pushed under and instead following the cross flow with the wall and over the overflow. The concept of an angled river intake is presented in figure 2-2.

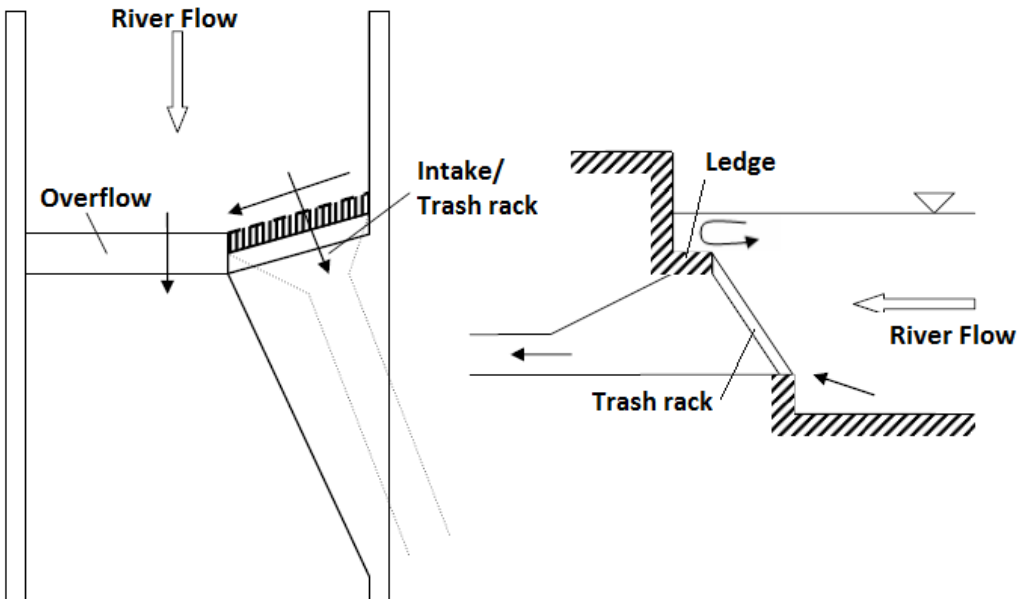


**Figure 2-2: Angled river intake with ledge to prevent debris clogging (Jenssen et al., 2006)**

**Floating Booms and Skimmer Walls**

Installations of floating booms, if done correctly, are in many cases an effective way of diverting floating debris past the thrash rack. When using floating booms as a diverting measure it is preferred to have water velocity below 0.5 m/s in the river. The boom must also be deep enough to ensure adequate freeboard. The boom and anchoring must be designed to withstand the applied forces from the water flow and direct impacts from heavy debris. The angle (θ) between the flow direction and the boom must not exceed $30^{o}$ - $45^{o}$ to effectively direct the debris along the boom. It is not recommended to place the boom close to the intake where the water velocity tends to be high. Figure 2-3 illustrates the concept behind placing the boom.

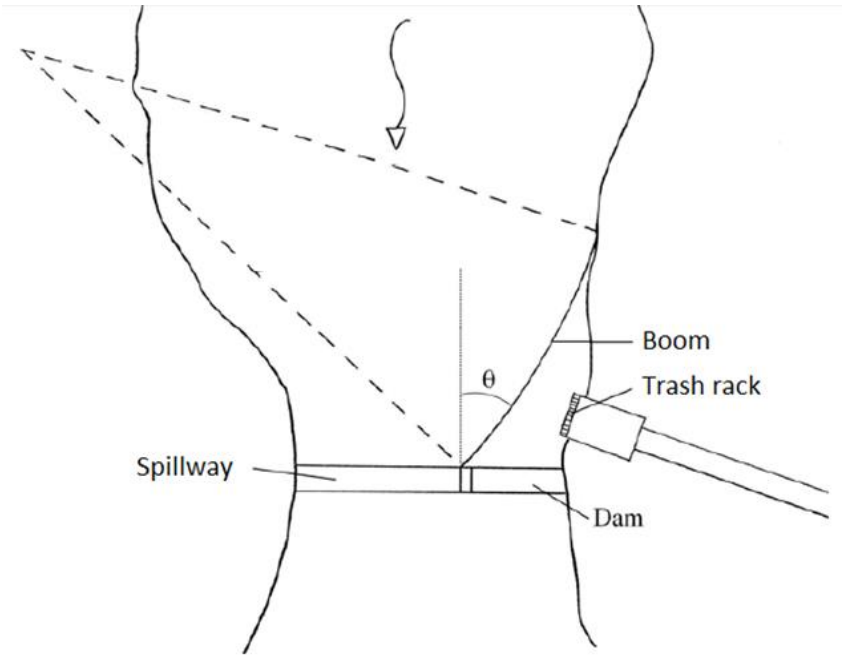


**Figure 2-3: Recommended placement of booms to direct debris past the trash rack (Jenssen et. al., 2006)**

**Submerging**

Sufficient submerging of the intake is important to avoid air entrainment and vortexes guiding debris under the surface resulting in clogging of the trash rack. Knauss (1987) and Guttormsen (1989) among others present different methods for estimating necessary submerging of intakes. It is important to note that these formulas express limits for air entrainment and not when vortexes guides debris under the surface. Consciousness about debris being guided under the surface by vortexes before air is important.

Most of the calculation methods for sufficient submerging are based on a function of the Froude number at the inlet. The Froude-number is defined as:

$$F = \frac{v}{\sqrt{gd}} \qquad [2\text{-}3]$$

Where:
F = The Froude-number
v = Water velocity at the inlet
g = Gravity
d = Inner diameter at the inlet or the inlet height

Knauss (1987) presents the following formula for sufficient submerging of intakes:

$$\left(\frac{h}{d}\right)_{cr} = \frac{1}{2} + 2F \qquad [2\text{-}4]$$

$$\left(\frac{h'}{d}\right)_{cr} = 1 + 2{,}3F \qquad [2\text{-}5]$$

The result of formula 2-4 shall not apply if it is less than 1.5. In general the formula resulting in deepest submerging is advised. The submerging (h and h') and the diameter (d) is visualized in figure 2-4.

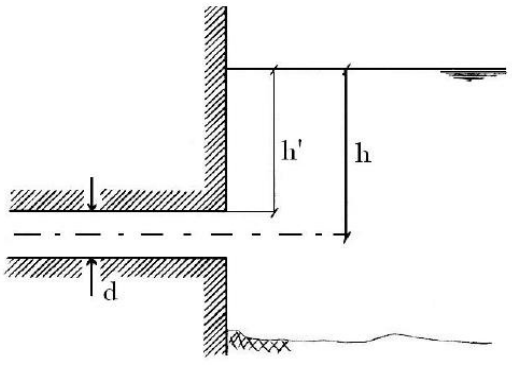


**Figure 2-4: Submerging of intakes (Jenssen et. al., 2006)**

## 2.5. Conventional Cleaning of Trash Racks

Cleaning of trash racks can be divided into mechanical and manual cleaning. Small hydropower plants with low budgets tend to use manual cleaning but are eager to find cheap and effective ways of automatic cleaning.

**Manual Cleaning**

Most manual cleaning processes are based on some form of raking. The rake is usually special made to fit between the clearings in the trash rack. Manual cleaning is not commonly used in bigger hydropower plants where the economy allows instalment of automatic cleaning equipment.

Manual cleaning of trash racks is dependent on available manpower. In some cases manual cleaning is expensive due to remotely placed intakes. Manual cleaning is also a risk of safety when raking may be needed during extreme weather or in the dark. During the most intense periods it is not unusual to clean the trash rack several times a day. (Jenssen et al., 2006)

**Mechanical Cleaning**

There are numerous patents for trash rack cleaners on the market. Many of the rack cleaners are based on a mechanical raking device able to move vertically over the rack when needed. Mechanical cleaning systems are commonly custom made due to different type of debris and structures at the site. Cleaning systems based on hollow trash rack rods with pressurized air and a design with rotating brushes moving across the trash rack area are two among other additional concepts. The different cleaning systems can be automatically directed by time intervals or by head-loss sensors, reducing the need of manual workforce. Automatic trash rack cleaners are often only installed on bigger power plants. The price for an automatic trash rack cleaner varies a lot depending on manner of operation and rack area. For small cleaners less than $15m^2$ rack area the price lies between 150.000 – 600.000 NOK. (Fladen et. al., 2010)

## 2.6. The Concept of Back Flushing

Back flushing is an alternative to manual and mechanical cleaning of trash racks. The concept of back flushing is to reverse the flow over the trash rack for a short period of time in order to detach and evacuate clogged debris through a flushing pipe or gate. The back flushing method has proven to be efficient for trash rack cleaning at small hydro power plants, but the suitability is highly dependent on the extra costs compared with a conventional intake design and the cost of lost production water during flushing. The flushing velocity and the pressure difference over the trash rack are important factors describing the back flushing efficiency. The clogging force applied to the debris due to the pressure difference over the trash rack, visualized by the head loss, will affect the flushing efficiency. (Nøvik, Lia and Jørstad, 2011).

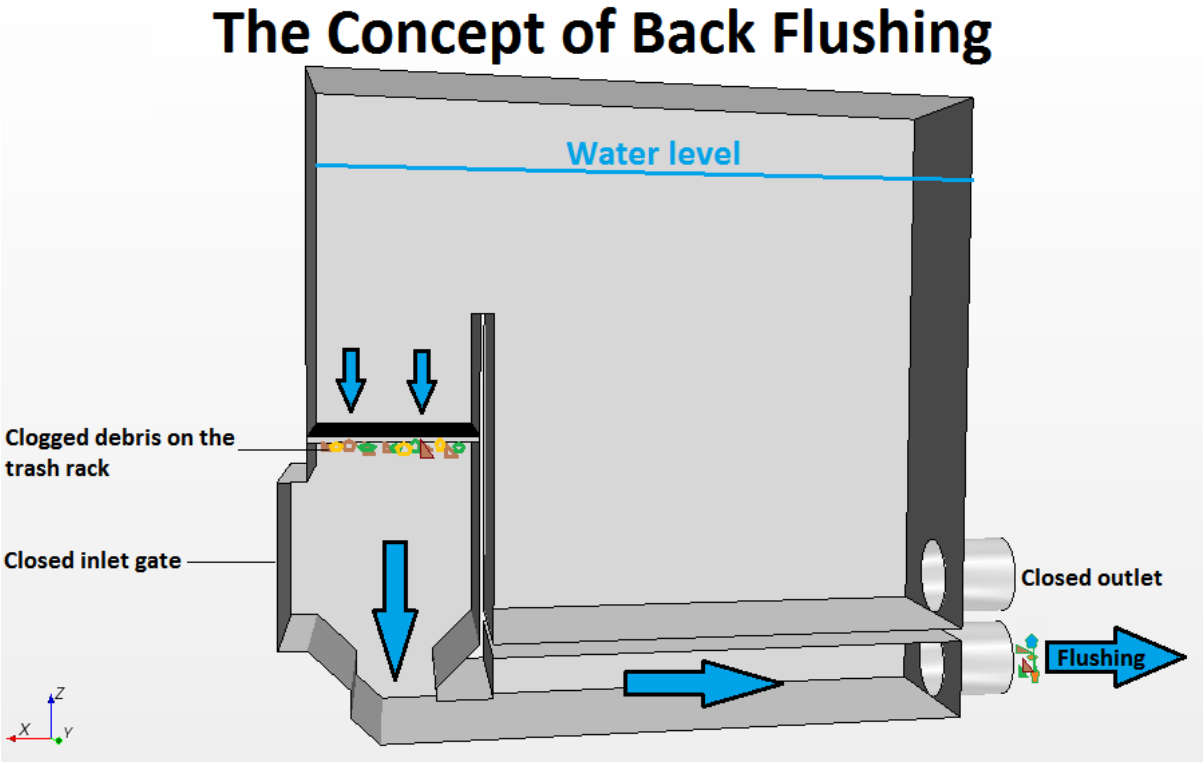


**Figure 2-5: Illustration of the concept of back flushing**

Figure 2-5 illustrate back flushing on an intake designed with a horizontally fixed trash rack. The inlet gate is closed. There is no power production and the flushing gate is open resulting in reversed water flow over the trash rack.

### 2.6.1. Examples of Headworks using the Concept of Back Flushing

In Norway there are several headworks already in operation using the concept of back flushing for cleaning the trash rack. Three examples are given in more detail.

***Bergedammen***

*Bergedammen* is the intake for a small hydro power plant in *Eidsdal*, Norway. The power plant is owned by *Eidsdal Kraft AS*. The power plant started production in 2006. The turbine capacity is 3.5 $m^3/s$ and the average production is 25 GWh. (Jørstad, 2010)

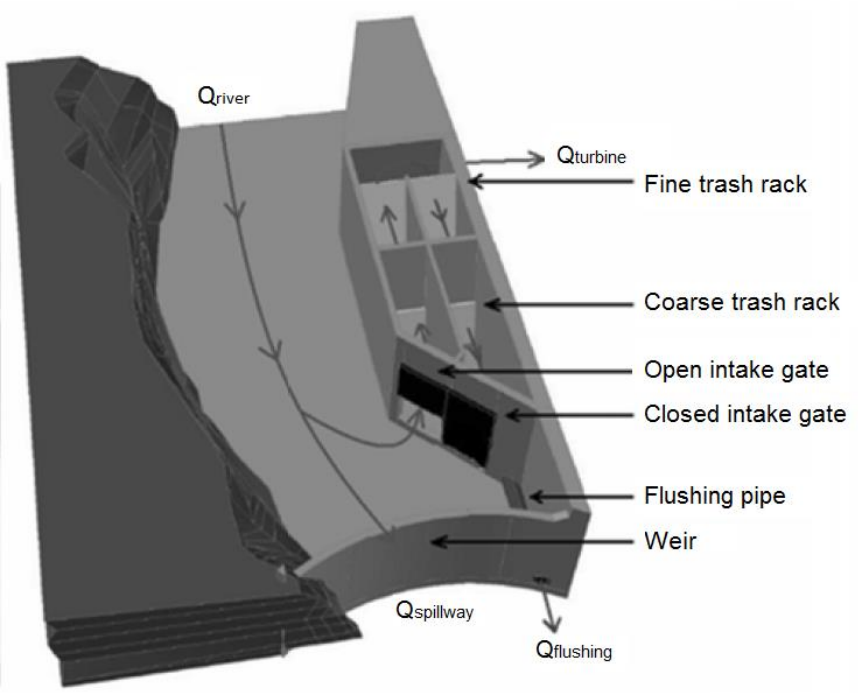


**Figure 2-6: Bergedammen (Nøvik, Lia and Jørstad, 2011)**

Figure 2-6 displays how *Bergedammen* with its two-chamber design flush the trash racks in sequence while producing power. In normal operation both intake gates are open. While back flushing one of the chambers the related intake gate is closed and the flushing gate is opened reversing the flow over the trash racks evacuating loosened debris through the flushing pipe. The power production while flushing is reduced in order to use the excessive water for flushing.

***Utvik* Power Plant**

*Utvik* power plant is owned by *Utvik Elektrisitetsverk* and was converted into a back flushing design in 2002. Figure 2-7 displays the headwork of *Utvik* power plant. The river enters from the right. Durig normal operation water passes through the coarse trash rack, through the intake gate and passes through the fine trash rack before it enters the intake pipe. While flushing, the power plant shuts down and the intake gate closes leaving chamber III and IV filled with water. The draining gate is then opened forcing the water back through the fine trash rack detaching clogged debris and evacuates it downstream.

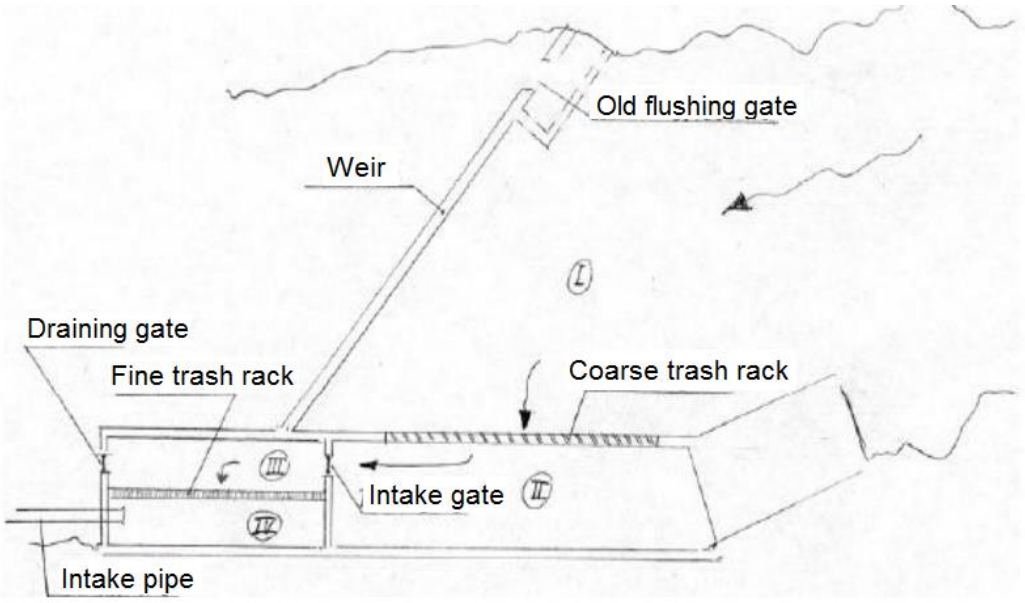


**Figure 2-7: Utvik Power Plant (Nøvik & Jørstad, 2011)**

### *Viddal* Power Plant

*Viddal* power plant, owned by *Tussa kraft AS*, operates with water from the river *Viddalselva* and the used production water from *Draura* Power Plant. The turbine in *Viddal* power plant has a maximum capacity of 3 $m^3/s$. *Viddal* Power Plant uses the concept of back flushing to clean the trash rack by reversing the water flow over the trash rack. Figure 2-8 shows the flow patterns in normal operation and while back flushing. To reverse the water flow the intake gate is closed and the flushing gate is opened. The water used for back flushing comes from *Draura* Power Plant. (Aune, 2011)

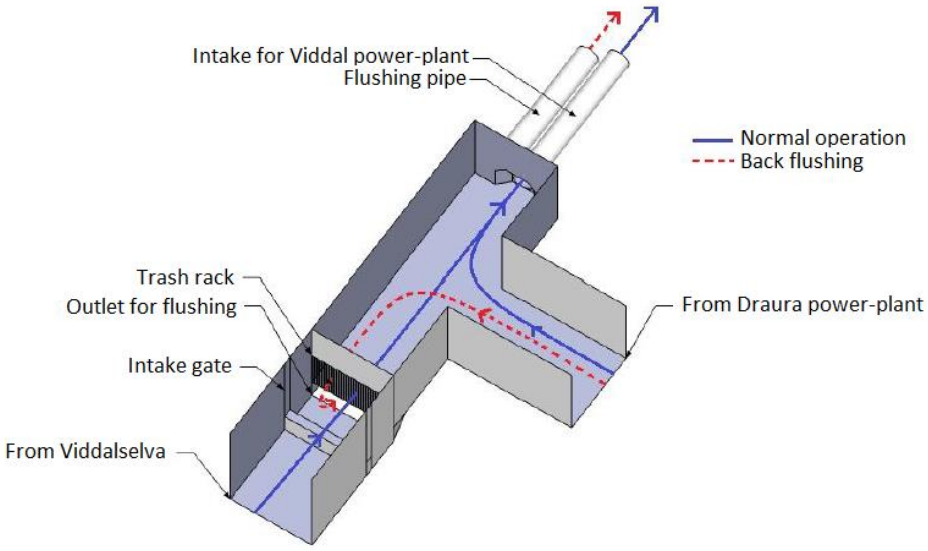


**Figure 2-8: Viddal Power Plant (Aune, 2011)**

### 2.6.2. Necessary Flushing Velocities

A laboratory back flushing experiment was performed at The Norwegian University of Science and Technology by the Department of Hydraulic and Environmental Engineering in 2011. The experiment included how the relative flushing velocity affected the back flushing efficiency. The result of the relative flushing velocity test is displayed in figure 2-9.

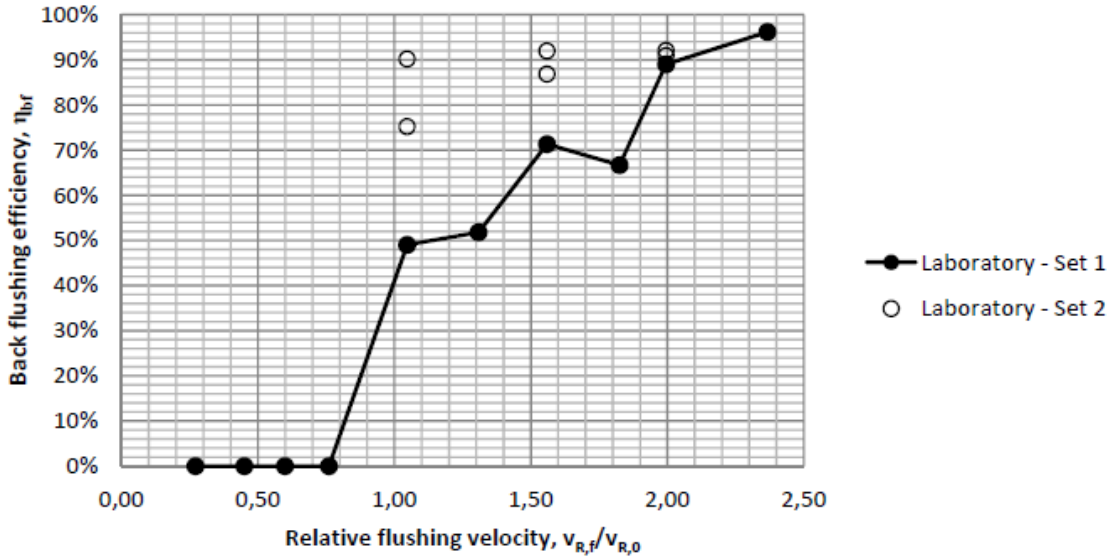


**Figure 2-9: Results from the relative flushing velocity test (Nøvik, Lia and Jørstad, 2011)**

The relative flushing velocity is based on the ratio between the flushing velocity, $v_{R,f}$, and the velocity of normal operation, $v_{R,0}$. The back flushing efficiency is quantified by the reduction of head loss after flushing compared to the initial head loss over the trash rack.

The relative flushing velocity test indicated that most of the clogged debris is loosened early in the flushing process, leaving some areas of the trash rack clean. The flow tended to concentrate through the open areas resulting in lower velocities through the clogged areas making it harder to successively clean the remaining areas of the trash rack. In the laboratory test the debris started to detach with a relative flushing velocity value of 1.4. As figure 2-9 displays, a relative flushing velocity of 2.0 results in a cleaning efficiency of 90 %. Some tests were also performed at *Bergedammen* where acceptable cleaning efficiency was measured at a relative flushing velocity of 2.0 which corresponds to a flushing velocity of 0.26 $^{m}/_{s}$. (Nøvik, Lia and Jørstad, 2011).

### 2.6.3. Adhesion of Different Debris

Adhesion between the clogged debris and the trash rack is an important factor for back flushing efficiency. Type of debris is one major factor afflicting the adhesion. Tests reveal that rivers where the debris is dominated by leaves generally results in a lower adhesion than debris dominated by grass or moss or a combination of leaves, moss and branches (Gotvassli, 2012).

For measuring adhesion PEETRA was used. PEETRA is a simple tool measuring the pulling force needed to detach clogged debris from trash racks and is developed by the NTNU and the Department of Hydraulic and Environmental Engineering. Adhesion is measured as the force per area needed to detach the clogged debris. Gotvassli (2012) tested the adhesion of clogged debris at Bergedammen, and some of the results are given in the following table.

**Table 2-1: Adhesion of different debris (Gotvassli, 2012)**

| Type of debris | Adhesion (water head in meters) |
|---|---|
| Leaves | 0.047 |
| Leaves and moss | 0.151 |
| Leaves, moss and branches | 0.164 |

The adhesion values in table 2-1 give a rough average of what adhesion value to expected and is also in accordance with the conclusion of the experiment where leaves alone results in lower adhesion than a combination of leaves and moss.

# 3. Computational Fluid Dynamics

Computational fluid dynamics (CFD) is a powerful tool for simulating the flow of fluids and gasses in simple and complex systems by using numerical methods and algorithms. STAR CCM+ is the CFD software used for this study and will be introduced further in this chapter.

## 3.1. Introduction

In the last twenty years the usage and evolution of computers has gone sky high, both for personal use and within technology and research. Many of the numerical algorithms invented in the 1970's are still used today. Today's fast and powerful computers have changed the use of numerical algorithms entirely, making it possible to solve most practical flow problems in sophisticated software.

Modern CFD-software is today capable of solving many problems, but the accuracy is still uncertain. It is important for the user of the computer software to have sufficient knowledge about the numerical methods used and their limitations to achieve reasonable result. An inexperienced user can easily produce a convincing result with nice looking figures but the reliability behind the result might be questionable and not trustworthy in practical engineering. (Olsen, 2011)

## 3.2. STAR CCM+

The company behind STAR CCM+ is CD-Adapco. STAR CCM+ is one of many available CFD-software and is based on object-oriented programming and supports different turbulence and multiphase models.

### 3.2.1. Grids

Establishment of grid systems (a system of cells) are one of the main principals in CFD-modelling. The grid system splits the geometry into cells where equations are solved for each cell. As Olsen (2011) portrays, grid systems can be classified in relations to several points:

- **Shape** – Usually triangular or quadrilateral
- **Orthogonality** – Determined by the angle between crossing gridlines
- **Structure** – A grid system is structured or unstructured
- **Adaptive or moving grids** – Grid changing during simulations
- **Nesting** – A finer grid inside a coarser grid
- **Outblocking** – A procedure where specified cells are made inactive

STAR CCM+ contains three main types of core meshing models (grid systems):

- Trimmed
- Tetrahedral
- Polyhedral

A trimmed, a tetrahedral and a polyhedral mesh are displayed in figure 3-1 also including number of cells, CPU time and size of the mesh. The meshes in figure 3-1 are all based on the same criteria of target size (50 mm), maximum size (50 mm) and minimum cell size (1 mm).

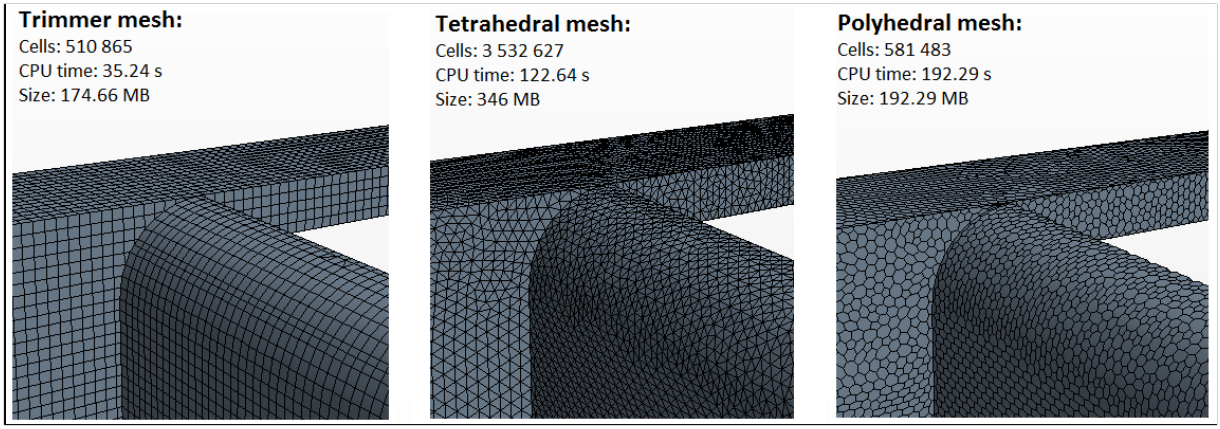


**Figure 3-1: Trimmer, tetrahedral and polyhedral mesh**

The fastest volume mesh type in terms of number of cells constructed per minute is the tetrahedral mesh. However, the tetrahedral mesh needs five to eight times more cells to produce the same accuracy as a trimmed or polyhedral mesh. Given the same amount of cells, a polyhedral or a trimmed mesh gives a more accurate solution compared with a tetrahedral mesh.

The choice of mesh type is dependant of several factors. Some of the factors may be available time for building the mesh, the desired solution accuracy, the convergence rate and available computer memory. Higher cell resolution results in a bigger model, requests longer calculation time and a better resolution of the solution. A grid system is recommended to have at least three cells between two boundaries, one intermediate cell confined by two surface incorporated cells.

Both tetrahedral and polyhedral meshes are dependent on the quality of the starting surface. If the starting surface, for instance the imported geometry from AutoCAD, has bad quality and errors the results of the volume mesh will be highly affected. The trimmer mesh, however, is not influenced by the starting surface and is therefore more likely to produce a better volume mesh. The trimmer mesh is the most commonly used type of grid and has the advantage of easy organize the mesh parallel to a horizontal water surface. (Olsen, 2011) (CD-Adapco, 2012)

### 3.2.2. Discretization

Olsen (2011) describes discretization as transforming the partial differential equation into a new equation where the variable in one cell is a function of the variable in the neighbouring cells. As the iterations continue the equation of the current cell is calculated based on an average of its neighbouring cells. When a first order discretization is applied, only the mediate neighbouring cells are used for the calculations. When a second order discretization is applied, a double set of neighbouring cells is used. Figure 3-2 portrays a visual explanation of the concept of first and second order discretization.

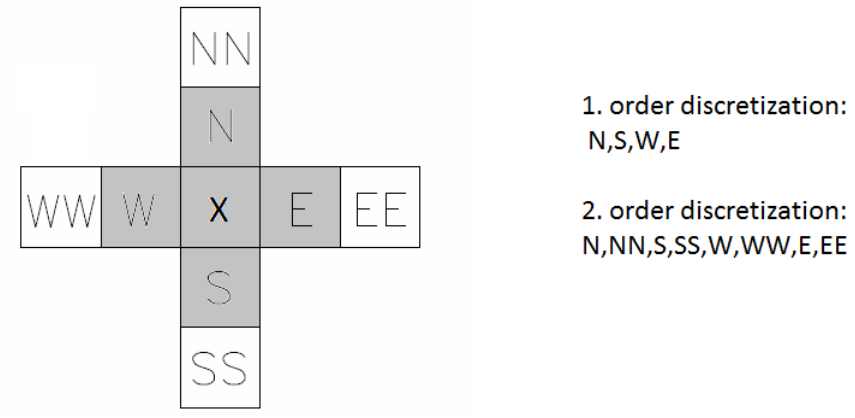


**Figure 3-2: The concept of first and second order discretization**

**Temporal Discretization in the Implicit Unsteady Solver**

In the implicit unsteady solver controls the time-step size and enables the user to apply the temporal discretization of 1st or 2th order. The first order temporal scheme is set as default in the implicit solver and is often referred to as Euler Implicit and discretizes the unsteady solution by using the solution at current time step (n+1) and one from the previous time step (n) as described:

$$\frac{d}{dt}(\rho\chi\phi V)_0 = \frac{(\rho_0\phi_0)^{n+1} - (\rho_0\phi_0)^n}{\Delta t} V_0 \qquad [3\text{-}1]$$

The 2th order temporal discretization scheme discretizes the solution by using the solution for the current time step (n+1) as well as two solutions from precious time steps (n and n-1) as described:

$$\frac{d}{dt}(\rho\chi\phi V)_0 = \frac{3(\rho_0\phi_0)^{n+1} - 4(\rho_0\phi_0)^n + (\rho_0\phi_0)^{n-1}}{2\Delta t} V_0 \qquad [3\text{-}2]$$

### 3.2.3. Turbulence Models

Turbulence models are inexact representations of the fluid turbulence in reality. Different models give different solutions and no single turbulence model is the best for a given simulation. STAR CCM+ uses three approaches for modelling turbulence.

- Reynolds-Averaged Navier Stokes equations (RANS)
- Large eddy simulation (LES)
- Detached eddy simulation (DES)

RANS is a commonly used approach and is also used for the simulations performed in this study and will therefore be described in more detail. LES and DES are for advanced users with knowledge about applicable literature and grid resolution and scaling requirements. (CD-Adapco, 2012)

**Reynolds-Averaged Navier-Stokes Equations (RANS)**

The Navier-Stokes equations govern fluid turbulence and describes the instantaneous velocities and pressure fields in fluids. The Navier-Stokes equations are based on equilibrium on a small volume of water in laminar flows. For turbulent flow the Reynolds averaged version (RANS) of the Navier-stokes equations is commonly used. Formula 3-3 shows the Navier-Stokes equation where U is velocity, $\rho$ is density, P is pressure, v is viscosity and $\delta_{ij}$ is the Kronecker delta. (Olsen, 2011)

$$\frac{\partial U_i}{\partial t} + U_j \frac{\partial U_i}{\partial x_j} = \frac{1}{\rho}\frac{\partial}{\partial x_j}\left(-P\delta_{ij} + \rho\nu\left(\frac{\partial U_i}{\partial x_j} + \frac{\partial U_j}{\partial x_i}\right)\right) \qquad [3\text{-}3]$$

As Durbin & Reif (2010) promptly states, the phenomenon of turbulence is a chaotic, spatially and temporally complex solution for the Navier-Stokes equations. The problem is that these solutions are hard to obtain even with supercomputers. An easier method of obtaining the solutions of turbulence is by decomposing the Navier-Stokes equations of instant velocity and pressure fields into a mean value and a fluctuating component – this becomes the RANS-equations. The resulting equation of the decomposition of the Navier-Stokes equations (RANS) consists of an additional term in the momentum transport equation called the Reynolds stress tensor and is described as following:

$$\mathbf{T}_t \equiv -\rho\overline{v'v'} = -\rho\begin{bmatrix} \overline{u'u'} & \overline{u'v'} & \overline{u'w} \\ \overline{u'v'} & \overline{v'v'} & \overline{v'w'} \\ \overline{u'w'} & \overline{v'w'} & \overline{w'w} \end{bmatrix} \qquad [3\text{-}4]$$

Where $T_t$ is the Reynolds stress tensor which is also often modelled with the Boussinesq' approximation, $\rho$ is density and the average velocity components described by u', v' and w'.

STAR CCM+ uses two approaches to solve the Reynolds stress tensor, $T_t$ :

- Eddy viscosity models
- Reynolds stress transport models

**Eddy Viscosity Models**

The Eddy viscosity models calculate the Reynolds stress tensor $(T_t)$ as a function of mean flow scalar quantities by using the concept of turbulent viscosity and turbulent kinetic energy (TKE). There are three models included in the Eddy viscosity models:

- K-Epsilon
- K-Omega
- Spalart-Allmaras

*The K-Epsilon models* provide a good compromise between accuracy, robustness and computational cost. The K-Epsilon models are so called two-equation models where transport equations are solved for the turbulent kinetic energy **κ** and its dissipation rate **ε**. The K-Epsilon model is used for the simulations in this study because it is commonly used and has many verification cases for free surface simulations.

*The K-Omega model* is, similar to K-Epsilon, a two-equation model, but where the transport equations are solved for the turbulent kinetic energy **κ** and a quantity called **ω**. The quantity **ω** is defined as the dissipation rate per unit turbulent kinetic energy. The K-Omega models are recommended as an alternative for Spalart-Almaras models.

*The Spalart-Allmaras model* is suitable for simulations where boundary layers are largely attached, for example flow over a wing or other aerospace flow applications. These models are not suited for simulations with dominating free-shear layers, flows with complex recirculation or natural convection. (CD-Adapco, 2012)

### 3.2.4. Turbulent Kinetic Energy (TKE)

The turbulent kinetic energy defines the work done per unit of time by the turbulent dispersion force in water or in other phases, which tells us how much energy is absorbed due to velocity fluctuations and turbulence in the water path. The turbulent dispersion force accounts for the interaction between the dispersed phase and turbulent eddies, also referred to as velocity fluctuations, and is defined as:

$$\mathbf{F}^{TD}{}_{ij} = A^{D}{}_{ij}\frac{v_c^t}{\sigma_\alpha}\left(\frac{\nabla\alpha_j}{\alpha_j} - \frac{\nabla\alpha_i}{\alpha_i}\right) \qquad [3\text{-}5]$$

Where $A^{D}_{ij}$ is the linear drag coefficient, $v_c^t$ is the turbulent kinetic viscosity for the continuous phase and $\sigma_\alpha$ is the turbulent Prandtl number. The Prandtl number describes the ratio between the momentum eddy diffusivity and the heat transfer eddy diffusivity (CD-Adapco, 2012).

### 3.2.5. Multiphase Flows and Volume of Fluid (VOF)

Multiphase flow is a term referring to simulations with several phases (solids, liquids and gasses) within the same system, where the different phases are mixed at the macroscopic scale. Multiphase flows are classified into two categories:

- Dispersive flows: Bubbly, droplet and particle flows.
- Stratified flows: Free surface flows and annular film flow in pipes.

STAR CCM+ presents five different models to meet the multiphase flow requirements. VOF is one of the five models and is provided for systems containing two or more fluid phases where each of them constitutes large parts of the system. Free surface flow and sloshing flow in a water tank are typical examples where VOF is favourably used. Using VOF will require a fine mesh if bubbles and droplets are likely to appear. Three or more cells across each bubble are recommended to produce small errors. (CD-Adapco, 2012)

VOF classifies each cell by their content, for instance it can consist of water, air or a combination. If the cell is full the given value is 1, if it is empty the given value is 0. In a multiphase flow model with water and air, the water surface is typically defined where the VOF-value is 0.5 (half full). In order to acquire an exact water surface you should not have more than a few cells with VOF-value between 0-1 at the surface zone. Figure 3-3 shows an example of a defined and an undefined water-surface.

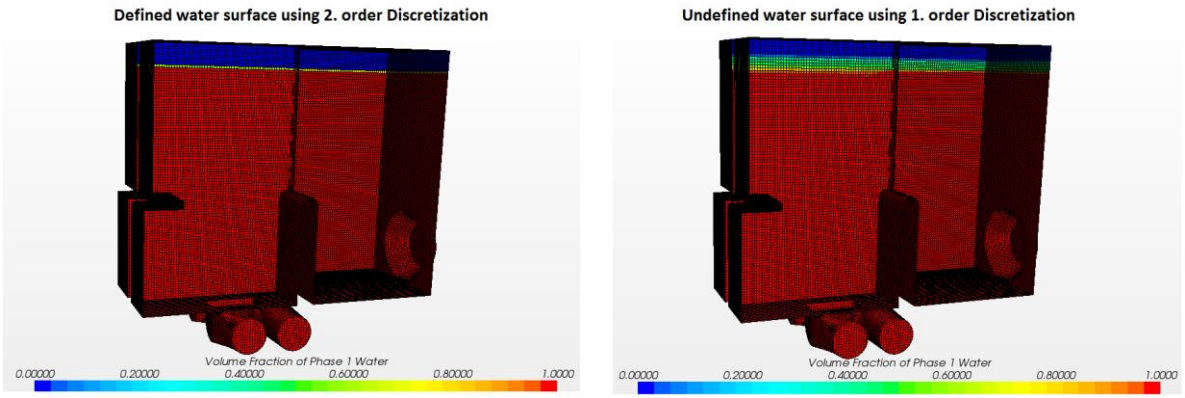


**Figure 3-3: Defined and undefined water surface using 1st and 2th order discretization**

To obtain a sharper boundary between phases, for example the line between air and water, it is recommended to use the 2nd order discretization scheme, as supported by figure 3-3. Performing more iterations and using a finer mesh are also inflicting on the quality of the boundary surface. Increasing the sharpening factor parameter will also result in interface sharpening, but might result in a non-physical alignment of the free surface line with the grid. (CD-Adapco, 2012)

### 3.2.6. Relaxation

The relaxation factor determines how fast a calculation converges to a final solution on a scale from 0-1, where 1 is the fastest. The relaxation factor is a scaling factor used to relax all corrections before they are applied to the variables. A relaxation factor of 1 results in 100% of the corrections being applied to the next set of variables. A high relaxation factor provides fast calculations but may also lead to instability (diverging solutions) caused by the complexity of most simulations. The relaxation factor should be set in a way that gives a solution which is on an acceptable level for both speed and stability. In most cases, an acceptable relaxation factor will lie between 0.75-0.85, but simulations with high-speed flow might need a relaxation factor as low as 0.2 to maintain stability. There are several relaxation factors to assess in STAR CCM+ and they are referred to as *under relaxation factors*. (Cd.Adapco, 2012) (Olsen, 2011)

When applying a multiphase model with RANS and the K-Epsilon turbulence model, these are the following relaxation factors dealt with in the solver node:

- Under-relaxation factor for velocity
- Under-relaxation factor for pressure
- Under-relaxation factor segregated VOF
- Under-relaxation factor K-Epsilon turbulence
- Under-relaxation factor K-Epsilon turbulent viscosity

### 3.2.7. Steady or Unsteady State

Steady state flow is characterized by a stabile flow not changing over time. Unsteady flow is characterized by fluctuation and flow inconsistencies over time. The steady state model in STAR CCM+ is used for all steady flow calculations. The concept of time is useless in steady state simulations. Simulations that are time dependant will require an unsteady model simulation (implicit or explicit) which would include:

- Time varying boundary conditions
- Free surface (VOF) problems
- Sliding or deformation mesh problems
- Transient heat transfer

**The Implicit Unsteady Model**

The implicit unsteady model in STAR CCM+ is the only model which includes Segregated Flow and Segregated Fluid Energy models. Implicit unsteady is an alternative to explicit unsteady and which one to choose is based on the times scale of interests. The implicit unsteady model is appropriate if the time scale of the phenomena of interest (vortexes) is in the same order as the convection and diffusion processes. (CD-Adapco, 2012)

### 3.2.8. Time Steps and Iterations

With the unsteady approach you are required to choose a physical time step size and thus the Courant number. A courant number higher than 1 indicates that a particle moves through a cell in less than one time step and the calculation is skipped. The general equation for the Courant number is portrayed in equation 3-6 for n-dimensions:

$$C = \Delta t \sum_{i=1}^{n} \frac{u_{x_i}}{\Delta x_i} \leq C_{max} \qquad [3\text{-}6]$$

Where $\Delta t$ is the given time-step, $u$ is the velocity for the given direction and $\Delta x$ the length interval of a cell (Courant, Friedrichs & Lewy, 1967). Implicit models (solvers) are in fact usually stable with local maximum Courant numbers in the range of 10-100, but with a mean Courant number of ~1. (CD-Adapco, 2012)

The number of iterations needed to achieve convergence varies a lot and depends, among others, by the complexity of the simulation, the grid resolution and the time-step size. By using smaller time-steps the solution changes less from one iteration to the next. The implicit unsteady model uses inner iterations. Inner iterations are performed within each time-step and the number of inner iterations needed is reduced by smaller time-steps. Generally, the number of inner iterations needed, can be determined by how the residuals converge within each time-step. There is no need to apply more inner iterations if the residuals do not change or improve sufficiently within each time step. (CD-Adapco, 2012)

### 3.2.9. Sources of Errors and Uncertainties

There are numerous uncertainties with CFD-modelling. The following list presents common sources of errors with CFD-modelling, ranged in the order of what is most relevant for the simulations performed in this study.

1. **Errors in Boundary Conditions and Input Data**
   Errors in boundary conditions and input data are the most common sources of errors in CFD-modelling. It is difficult to precisely determine the boundary conditions for the different parts in the model. The roughness properties of a wall and the velocity distribution of the inlet are two examples of parameters hard to precisely determine realistically. (Olsen, 2011)

2. **Human Errors Due to Inexperience of the User**
   Human error is expected while performing computations in CFD. Inexperienced users are more likely to do bad choices when it comes to deciding between different parameters than experienced users. (Olsen, 2011)

3. **Numerical Approximation Errors**
   False diffusion and when discretization the equations are typical sources of error in numerical approximations. The discretization error is described as the difference between the exact solution of the equation and the approximated solution. False diffusion appears when velocity vectors and concentrations are calculated incorrectly due to coarse grids, grids not properly aligned to the flow direction or not using higher order schemes. (Ferziger & Peric, 2002) (Olsen, 2011)

4. **Convergence Error**
   Convergence is not always easy to achieve, and it depends on different factors like mesh type and time-step. If convergence is not reached it will lead to inaccuracies. A proper convergence criterion should be used in order to prevent results without convergence being used. In time dependant simulations, convergence may not be reached within each time step. (Ferziger & Peric, 2002) (Olsen, 2011)

5. **Modelling Errors**
   The difference between the real flow and the simulated solution based on mathematical equations is called the modelling error. The error also occurs when the geometry in the model is different from the real examined geometry and when the geometry is simplified by estimation of boundary conditions. (Ferziger & Peric, 2002) (Olsen, 2011)

6. **Bugs in the Software**
   It is most likely that every CFD-software has bugs in it. An estimate often used is one bug per 1 000 – 10 000 lines of programming. A typical CFD-program has about 100 000 – 1 000 000 lines of programming. A CFD-program is often updated and improved. Each time a CFD-program is updated it is possible that new bugs are put into the system. (Olsen, 2011)

7. **Round-off Errors**
   The round-off errors are limited to the accuracy of the computers processors. Today, while most computers use a 64 bit system with 12 digits accuracy, this error is mostly insignificant. (Olsen, 2011)

# 4. Demonstration Model of the Two-Chamber Horizontal Trash Rack Concept

The purpose of building a demonstration model of the two-chamber horizontal trash rack concept is to visualize the concept, making it displayable and to identify the back-flushing efficiency. The model is also built to compare head loss and streamlines with numerical simulations.

## 4.1. Designing and Building the Demonstration Model

The demonstration model is designed as a two-chamber setup with two separate inlet gates and two horizontally fixed trash racks. The model has one outlet for normal production and two flushing gates. The two-chamber setup makes it possible to produce electricity while back flushing one chamber at the time. A detailed CAD-drawing of the model follows in figure 4-1 and an inflated version in appendix 1.

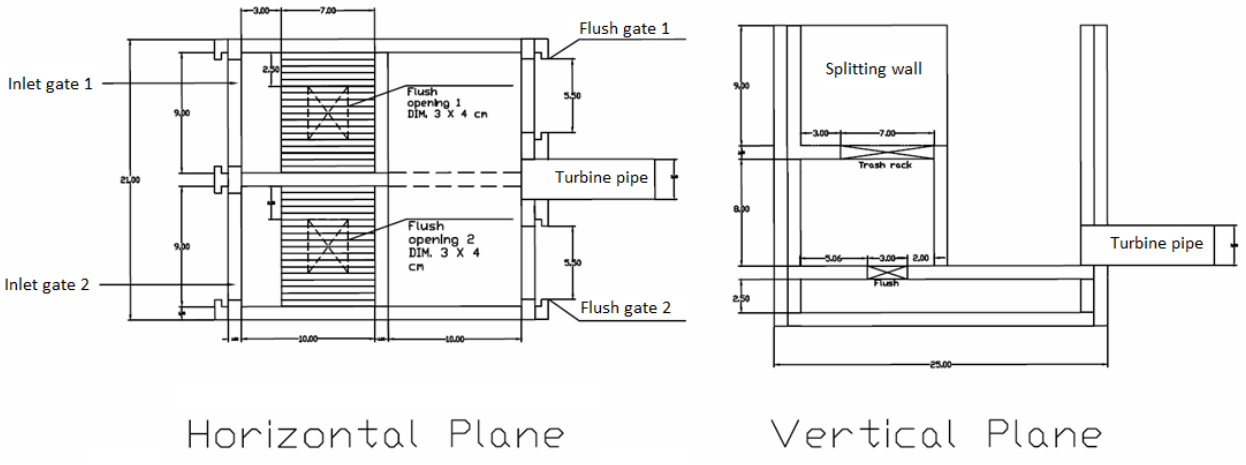


**Figure 4-1: CAD-drawing of the Demonstration Model**

The total length of the model is 250 mm. The dimension of each horizontal trash rack is 90 x 70 mm. During normal operation both inlet gates are open allowing water to flow up through the horizontal trash racks before the flow bends down towards the outlet to the right. The trash racks are shifted 30 mm right of the wall to illustrate a concrete floor where a hatch is installed to ensure access for maintenance under the trash rack.

## 4.2. Evaluation of Streamlines and Head Loss

An assessment of streamlines and head loss for the demonstration model under normal production is performed. Comparing the stream line and head loss results for the demonstration model with a correspondent numerical model would help us verify the quality and correctness of the numerical result.

The evaluations of streamlines and head loss are performed under a normal production state with constant discharge of 1.2 litres per second. The discharge is measured by the pump which ensures a continuous water flow.

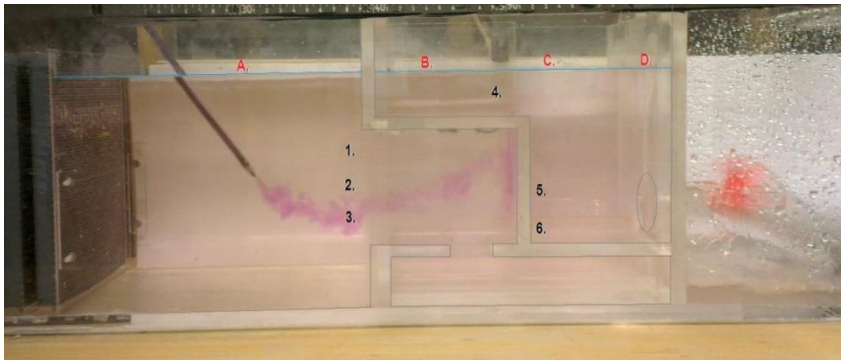


**Figure 4-2: The Demonstration Model during normal production**

**Evaluation of Streamlines**

The streamlines are evaluated by inserting a dyed solution in the flow path. The dyed solution is injected in points 1-6, displayed in figure 4-2, in order to portray a complete image of the flow pattern.

**Evaluation of Head Loss**

The head loss is evaluated by comparing the height of the water table before entering the intake construction and within the intake construction. The height is measured by a digital ruler at point A-D as marked in figure 4-2.

## 4.3. Evaluation of Back Flushing Performance

The back flushing efficiency of the model is tested by adding small pieces of fabrics and threads to the water flow. The fabric gets clogged to the trash rack and the model suffers increased head loss. Flushing is performed by closing one of the inlet gates and sudden opening of the belonging flushing gate. There is an understanding of the fact that the added fabrics and threads do not behave or clog the trash rack as real debris, but it will reveal the concept of back flushing.

# 5. Numerical Modelling of the Horizontal Trash Rack Concept

The following chapter contains the procedure and setup for the numerical simulations performed for this study. The simulations for the horizontal trash rack concept are performed in STAR CCM+ and special attention is given to back flushing efficiency and the hydraulic performance of the model during normal production.

## 5.1. Test Program for the Numerical Simulations

The goal of the test program is to analyse the back flushing efficiency and assess the head loss and streamlines during normal operation for different models and geometries. The back flushing efficiency is evaluated by assessing the velocity distribution over the horizontal trash rack while back flushing. During normal operation the streamlines are analysed, turbulent kinetic energy is measured and the total system head loss is plotted.

The tests are performed on the following 4 main models and sub models:

1. **One Chamber Model**
2. **Two Chamber Model**
    a. Without trash rack
    b. With trash rack
    c. With modified weir
3. **Demonstration Model**
4. **Scale Model**
    a. Stretched model with low weir
    b. Stretched model with high weir
    c. Shortened model with low weir

All models illustrate the back flushing concept using a horizontal trash rack. Model 1 and 2 are both full scale models. Model 1 has one chamber while model 2 has two chambers making power production possible while back flushing one trash rack at the time. Model 3 is identical to the demonstration model presented in chapter 4. Model 4 is a scale model which is based on the visual results of the Demonstration Model as well as from the numerical results of model 1, 2 and 3. The geometry of the models is further adduced in chapter 5.2.

The details of the tests are described in table 5-1. The tests are ordered in two groups, one for back flushing and one during normal operation.

**Table 5-1: Test program for the numerical simulations**

| Tests: | Test Parameters | Model | Model Characteristics | Model Parameters: | | |
|---|---|---|---|---|---|---|
| | | | | L/D | $H_R/D$ | $V_{OTR}/V_{UTR}$ |
| **1. Back flushing** | | | | | | |
| **1.1.** | Velocity distribution | 1. | One chamber, full scale model | 2,25 | 3,19 | 1,55 |
| **1.2.** | Velocity distribution | 2a. | Two chamber, full scale model | 2,7 | 2,15 | 2,27 |
| **1.3.** | Velocity distribution | 4a. | One chamber, scale model, low weir | 6 | 3 | 3,94 |
| **1.4.** | Velocity distribution | 4b. | One chamber, scale model, high weir | 6 | 4 | 2,40 |
| **2. Normal operation** | | | | | | |
| **2.1.** | Head loss, TKE | 1. | One chamber, full scale model | 2,25 | 3,19 | 1,55 |
| **2.2.** | Head loss, TKE | 2a. | Two chamber, full scale model | 2,7 | 2,15 | 2,27 |
| **2.3.** | Head loss, TKE | 2a. | Two chamber model, low water-level | 2,7 | 2,15 | 0,88 |
| **2.4.** | Head loss, TKE | 2b. | Two chamber model, with trash rack | 2,7 | 2,15 | 2,27 |
| **2.5.** | Head loss, TKE | 2c. | Two chamber model, with modified weir | 2,7 | 2,15 | 2,27 |
| **2.6.** | Head loss, TKE | 3. | Demonstration model, two chamber model | 3,3 | 3 | 1,32 |
| **2.7.** | Head loss, TKE | 4a. | One chamber, scale model stretched, low weir | 6 | 3 | 3,94 |
| **2.8.** | Head loss, TKE | 4c. | One chamber, scale model shortened, low weir | 2 | 3 | 1,31 |
| **2.9.** | Head loss, TKE | 4b. | Scale model, stretched, high weir | 6 | 4 | 2,40 |

Every test is performed on different models except test 2.3 which is similar to test 2.2, where the only difference is the initial water level. The test program describes three important model parameters in order to relate the test results with model geometry. The important model parameters are developed by analysing the Demonstration Model as well as the initial numerical results. The model parameters are described in figure 5-1. L is described as the length of the lower chamber, measured between the penstock and the weir. $H_R$ is described as the weir height. D is the diameter of the penstock. $V_{OTR}$ is described as the volume of water over the horizontal trash rack and is also the available volume for back flushing. $V_{UTR}$ is described as the volume of water in the zone between the gate inlet and the horizontal trash rack.

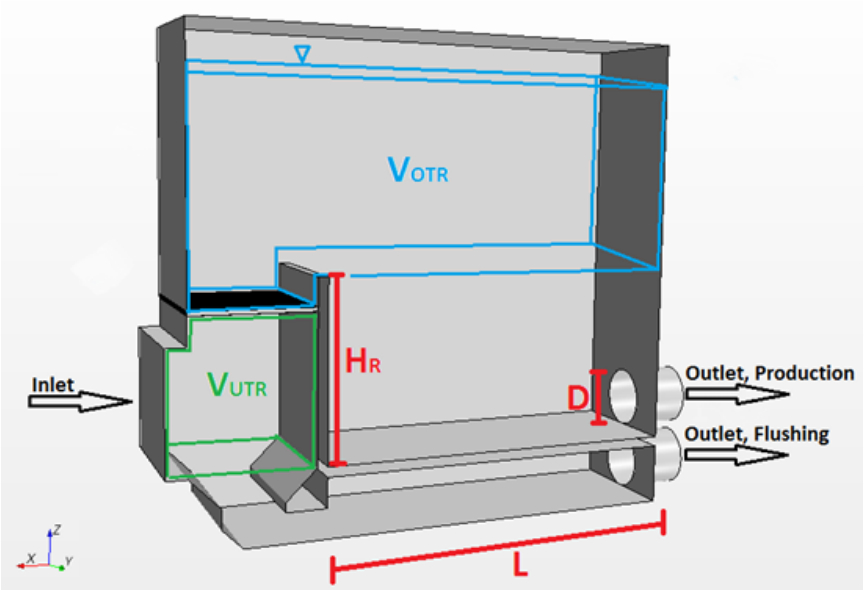


**Figure 5-1: Explanation of the model parameters in model 4a**

## 5.2. Model Geometry and Boundary Conditions

The 3D models described in chapter 5.1 were all prepared in AutoCAD. The geometry of each model is presented in this chapter along with its general boundary conditions. Additional information of the boundary conditions for each test is given in chapter 5.3.

### 5.2.1. Model 1 – The One Chamber Model

The One Chamber model is the initial model for the horizontal trash rack concept, based on Hallbjørn Brekke's conceptual idea. The model is not optimized in terms of flow preference; it is compact and has several bad geometric solutions. Access for maintenance under the trash rack is ensured through a hatch in the concrete ledge on the same level as the trash rack (See Fig 5-2).

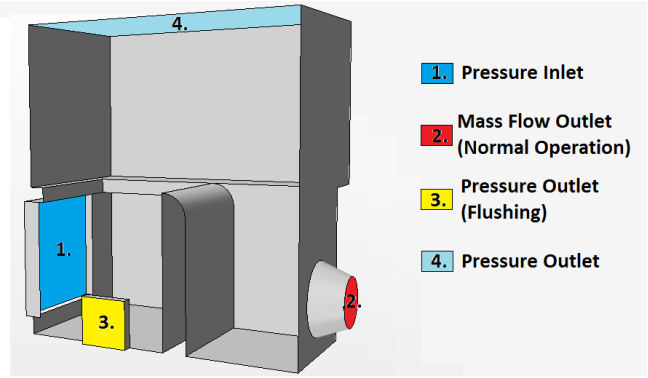


**Figure 5-2: Geometry and boundary conditions for model 1 – The One Chamber Model**

**Table 5-2: Key geometry sizes in Model 1 – The One Chamber Model**

| Geometry | | Dimensions [m] | Area [$m^2$] |
|---|---|---|---|
| Inlet (1) | [Length x Height] | 2 x 2 | 4 |
| Outlet for normal operation (2) | [Diameter] | 0.8 | 0.79 |
| Outlet for flushing (3) | [Length x Height] | 0.8 x 0.8 | 0.64 |
| Horizontal trash rack | [Length x Width] | 2 x 2 | 4 |

Figure 5-2 displays the geometry and boundary conditions for model 1, the one chamber model. Model 1 is in full scale with a design discharge of 2 $m^3/s$. Important geometry sizes are presented in table 5-2.

During normal operation point 1 is active ensuing water inflow and consequently point 2 ensures outflow to the penstock and later the turbine (See Fig. 5-2). The outflow in point 2 is directly controlled by selecting mass per second value. While back flushing, inflow and outflow through point 1 and 2 is deactivated while the outlet for flushing in point 3 is activated. The flushing outlet is defined as a pressure outlet, resulting in a discharge regulated by the water pressure. The roof of the model, referred to as point 4, is defined as a pressure outlet making air transport in and out of the construction possible.

### 5.2.2. Model 2 – The Two Chamber Model

The two chamber model is an enhanced edition of the one chamber model with an additional chamber, inspired by Egil Berge's design of Bergedammen described in chapter 2.6.1. Egil Berge`s design makes it possible to continue power production while back flushing one trash rack at the time. The Two Chamber model is better hydraulically shaped than the one chamber model, by implying symmetry and a curved weir. Access for maintenance under the trash rack is achieved through a hatch in the ledge by the left exterior wall at the same level as the trash rack (See Fig. 5-3).

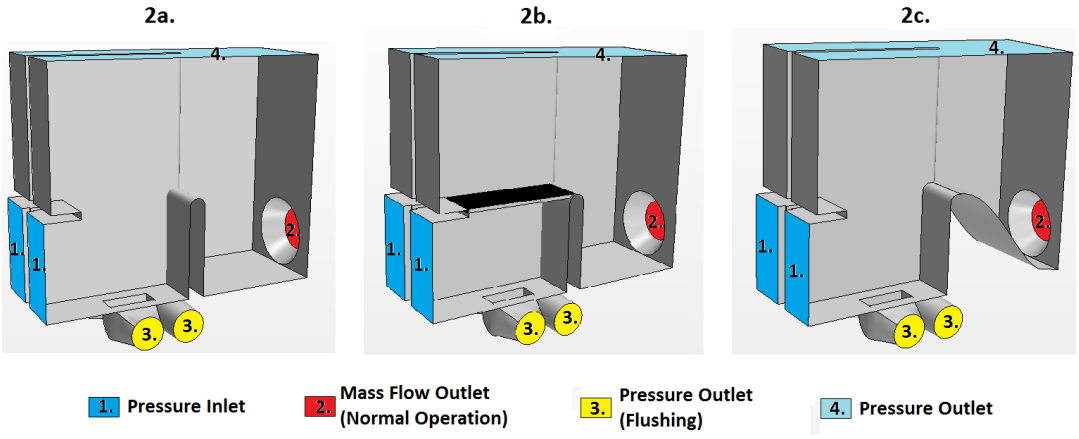


**Figure 5-3: Geometry and boundary conditions for model 2 - The Two Chamber Model**

**Table 5-3: Key geometry sizes in Model 2 – The Two Chamber Model**

| Geometry | | Dimensions [m] | Area [$m^2$] |
|---|---|---|---|
| Inlet (1) | [Length x Height] | 1 x 2 | 2 |
| Outlet for normal operation (2) | [Diameter] | 1 | 0.50 |
| Outlet for flushing (3) | [Diameter] | 0.7 | 0.38 |
| Horizontal trash rack | [Length x Width] | 1 x 2 | 2 |

Figure 5-3 displays the geometry and the boundary conditions for model 2. Model 2 is a full scale model with two inlet gates and two horizontal trash racks with a design discharge of 2 $m^3/s$. Important geometry sizes are presented in table 5-3.

The difference between model 2a and 2b is the presence of the trash rack in model 2b. Performing simulations for both models makes it possible to measure the isolated head loss due to the trash rack alone and the total head loss. As figure 5-3 displays, model 2c is modified by introducing a more hydraulically shaped weir for eddy and TKE reduction purposes. The trash rack in model 2b is 1000 mm wide and 2350 mm long with 30 mm bearings.

### 5.2.3. Model 3 – The Demonstration Model

Model 3 is a copy of the demonstration Model presented in chapter 4. The physical demonstration model is built in Plexiglas and has been used for exhibition purposes where the concept of back flushing is visualized. Model 3 is identical to the Demonstration Model in order to compare simulated streamlines and head loss with real measurements. The demonstration model has a simple structure, only concentrating on visualizing the back flushing concept. However, it would be interesting to compare the flow characteristics of the real model with the numerical simulation.

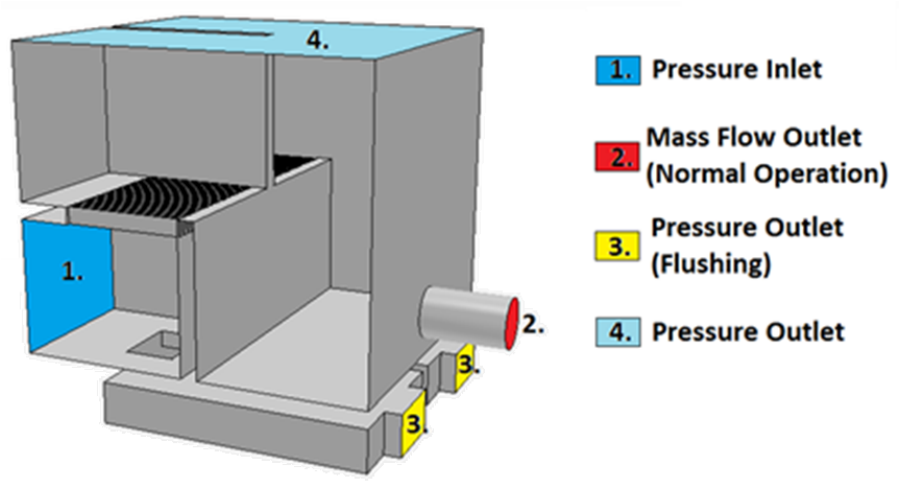


**Figure 5-4: Geometry and boundary conditions for model 3 – The Demonstration Model**

**Table 5-4: Key geometry sizes in Model 3 – The Demonstration Model**

| Geometry | | Dimensions [cm] | Area [$cm^2$] |
|---|---|---|---|
| Inlet (1) | [Length x Height] | 8 x 9 | 72 |
| Outlet for normal operation (2) | [Diameter] | 3 | 7.1 |
| Outlet for flushing (3) | [Length x Height] | 4 x 2.5 | 10 |
| Horizontal trash rack | [Length x Width] | 7 x 9 | 63 |

Model 3 is presented in figure 5-4, displaying both its geometry and boundary conditions. Model 3 is based on the two chamber design and has two identical inlet gates followed by two horizontally fixed trash racks. Model 3 has a design discharge capacity of 1.2 litre/s. Key geometry sizes are presented in table 5-4 and a more detailed sketch of the physical Demonstration Model is presented in appendix 1.

### 5.2.4. Model 4 – The Scale Model

The geometry of the Scale Model is based on the results of the previous models. The Scale Model is tested with different model parameters resulting in several sub models. The different model parameters include the length (L) between the weir and the outlet and the height of the weir ($H_R$). The Scale Model is also designed with considerations to continue physical testing on a similar model in the lab.

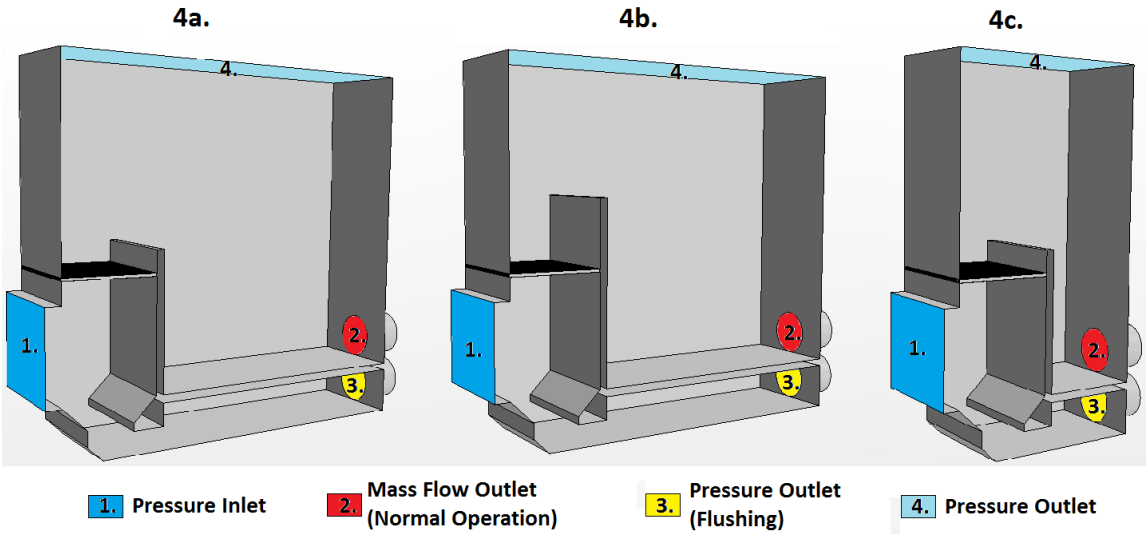


**Figure 5-5: Geometry and boundary conditions for model 4 – The Scale Model**

**Table 5-5: Key geometry sizes in Model 4 – The Scale Model**

| Geometry | | Dimensions [cm] | Area [$cm^2$] |
|---|---|---|---|
| **Inlet (1)** | [Length x Height] | 35 x 30 | 1050 |
| **Outlet for normal operation (2)** | [Diameter] | 15 | 177 |
| **Outlet for flushing (3)** | [Diameter] | 15 | 177 |
| **Horizontal trash rack** | [Length x Width] | 35 x 30 | 1050 |

Model 4 is presented in figure 5-5, displaying both its geometry and boundary conditions. Three different editions of the scale model has been produced for simulation purposes, with the intention of comparing the flushing efficiency with varying weir height (model 4a and 4b) and how the length of the model afflicts the turbulence level and head loss (model 4a and 4c). Model 4 is scaled by using Froude similarity and has a design discharge of 20 litre/s. Key geometry sizes are presented in table 5-5. The boundary conditions are the same for each model.

## 5.3. Establishment of Grids

The simulations in this study are all performed with trimmer grids. The trimmer grid achieves high accuracy compared to number of cells. The simulations performed in this study are dominated by flows in every direction. However, the water surface is more or less always horizontally oriented in the intake chamber. An advantage with the trimmer grid is how it easily can be oriented parallel to the water surface making it suitable for a precise measure of the water surface.

As the super computer at NTNU is available, larger simulations with higher cell resolution can be performed effectively. Because of the super computers availability a high cell resolution is used for all simulations. For all simulations the maximum cell size is set as the same value as the target cell size in order to achieve a uniform cell-size arrangement also inside the volume mesh. A uniform high resolution mesh, also inside the volume, is recommended in order to reach accurate solutions and to preserve the natural movement of the water.

An overview of the grid preferences for each model is given in table 5-6.

**Table 5-6: Grid preferences for numerical simulations**

| Model | Volume Mesh | Number of cells | Cell-size [mm] | Relative Minimum surface size [mm] | Mesh size [MB] | Mesh CPU-Time [s] |
|---|---|---|---|---|---|---|
| **1.** | Trimmer | 712 000 | 45 | 10 | 264.80 | 42.19 |
| **2a.** | Trimmer | 554 200 | 50 | 10 | 240.14 | 45.53 |
| **2b.** | Trimmer | 2 885 100 | 50 | 10 | 1038.13 | 276.25 |
| **2c.** | Trimmer | 701 300 | 45 | 10 | 276.87 | 56.59 |
| **3.** | Trimmer | 1 170 700 | 2.5 | 0.5 | 431.38 | 92.41 |
| **4a.** | Trimmer | 1 892 100 | 10 | 5 | 656.99 | 155.12 |
| **4b.** | Trimmer | 1 479 229 | 10 | 5 | 577.52 | 147.78 |
| **4c.** | Trimmer | 1 637 425 | 10 | 5 | 529.59 | 134.22 |

**Volumetric Control Volumes**

Volumetric control volumes are applied to specify areas of the model which need separate sets of grid specifications. For better grid quality and to achieve necessary grid resolution a volumetric control volume is used to define the grid resolution for the trash rack in model 2b, 3, 4a, 4b and 4c.

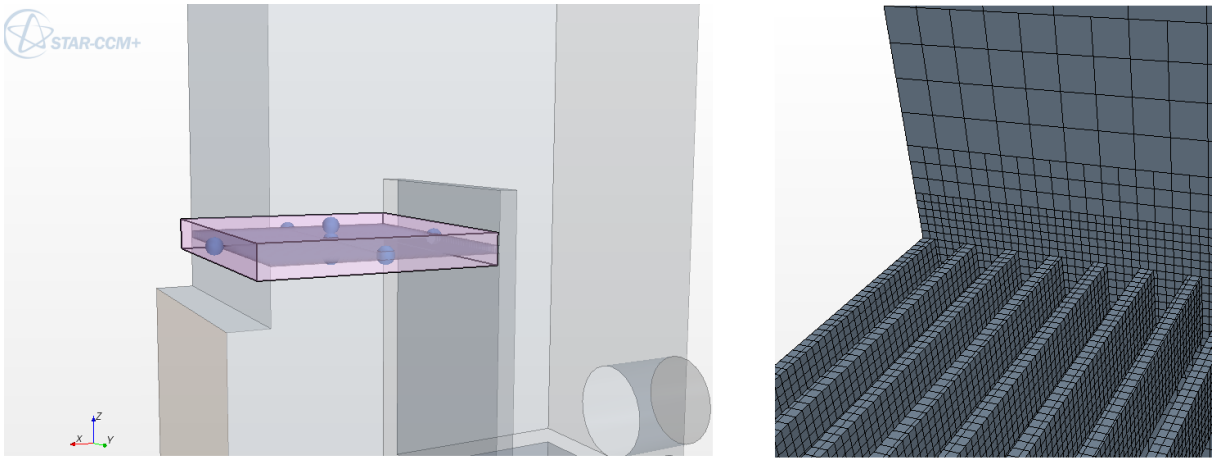


**Figure 5-6: Applying volumetric shape over the trash rack in model 4c**

Figure 5-6 displays the position of the applied volumetric control volume to the left and the resulting grid resolution over the trash rack to the right. The volumetric control volume makes it possible to define a finer mesh grid around the trash rack without affecting the general mesh structure for the model. The main criterion for the mesh around the trash rack is to achieve at least 3 cells across the clearance between the bars. In model 4c the number of cells between the bars is 4 or more. The volumetric control volume continues a distance past the trash rack in order to achieve a compatible transition zone.

## 5.4. Numerical setup

The numerical setup is individual for each simulation but there are similarities between them. The chosen numerical setup is based on the STAR CCM+ User manual (CD-Adapco, 2011) and the results of sensitivity analysis performed in the undersigned's project-thesis (Holmeset, 2012) and Åsmund Hasaas's master thesis (Hasaas, 2012).

### 5.4.1. Boundary Conditions

The boundary conditions for each test are presented in appendix 2 and they are denoted to as in chapter 5.2. Each model has one or two inlet boundaries, an outlet for normal production, one or two outlets for flushing and a top boundary titled as the roof.

The inlet boundary condition for all tests is defined as a *pressure outlet*. In Star CCM+ the mass flow may travel in both directions through the *pressure outlet* also making it useable as an inlet. The pressure distribution over the inlet is defined using a field function imitating local water pressure. The field function is described in more detail in chapter 5.4.2.

The outlet boundary condition for normal production is defined as a *mass flow inlet.* Even though *mass flow inlet* is defined as an inlet condition, it may be applied as an outlet condition by inducing negative mass flow values. The *mass flow inlet* boundary conditions results in a discharge of constant values.

For the outlet boundary condition for flushing, two different boundary conditions have been used. A *mass flow inlet* boundary condition is used for test 1.1 and 1.2. A p*ressure outlet* boundary condition is used for test 1.3 and 1.4, making the simulation more realistic with a varying discharge as the water-level changes. Every test simulating flushing is performed by suddenly opening of the flushing gate.

The boundary condition of the roof is in all tests defined as a *pressure outlet*, allowing free movement of air and atmospheric conditions.

The interior walls of the models are specified as smooth surfaces. For the tests concerning flushing efficiency (test 1.1, 1.2, 1.3 and 1.4) the flushing discharge is based on Nøvik's results on back flushing described in chapter 2.6.2 as two times the gross velocity over the trash rack during normal production (Nøvik, 2011).

### 5.4.2. Initial Conditions and Field Functions

Field functions have been created for the test program in order to define the initial water level, the pressure distribution over the inlet and for plotting water level change during flushing.

**Defining the Initial Water Level**

Outlining the initial conditions for the tests included defining the initial water surface. The initial water surface is defined by designing a field function which is applied to the volume fraction part in the initial condition part under the continua properties as displayed in figure 5-7.

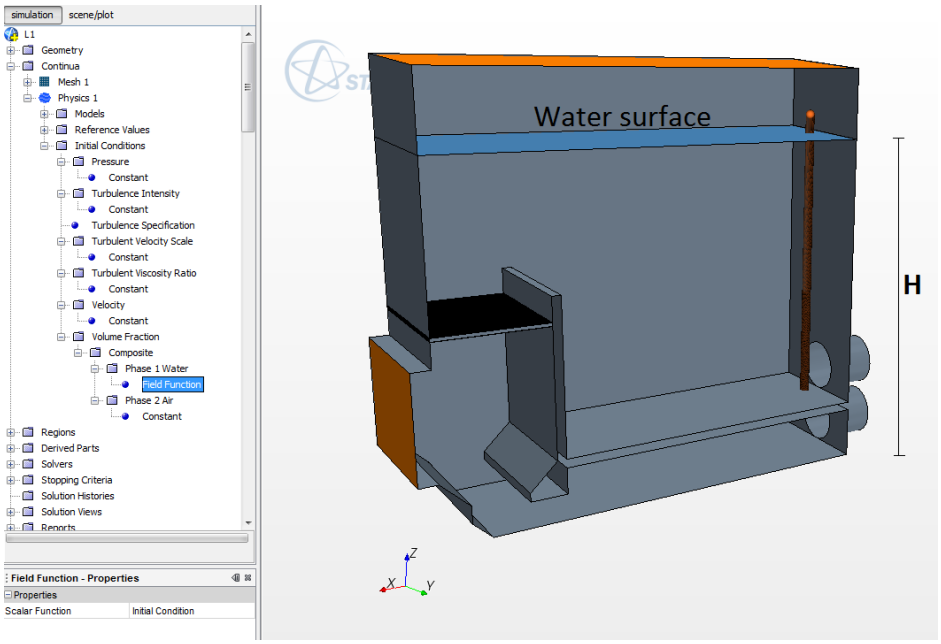


**Figure 5-7: Initial water surface in model 4a.**

The field function defining the initial water level is as follows:

***($$Position[2]<=H)?1:0***

The field function describes in which height (H) in Z-direction the concentration of water should be 1. Above the given height (H) the concentration of water is defined as 0 (air).

**Defining the Pressure Distribution over the Inlet**

A realistic inlet is essential for a realistic result. In order to achieve a realistic inlet it is important to have knowledge about the conditions upstream the inlet. In a best-case-scenario and within a given period of time, the water level upstream the headwork is more or less stationary with a low level of cross flows. By defining the intake as a pressure cell where the pressure is defined as a section of the hydrostatic pressure at the given depth you obtain more or less realistic inlet conditions. Figure 5-8 describes the section of the hydrostatic pressure used for defining the inlet boundary condition. The water level outside the intake is defined as constant over time also making the pressure inlet persistent.

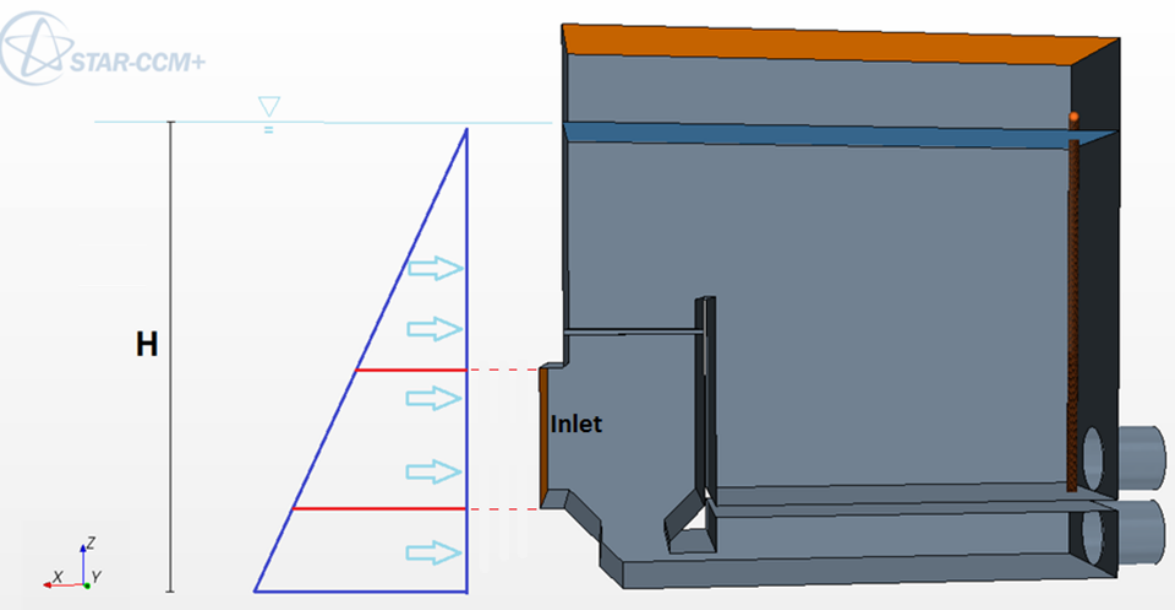


**Figure 5-8: Applying hydrostatic pressure as the inlet boundary condition**

All simulations performed in this study use the hydrostatic pressure as the inlet condition, where only the water level height varies. The field function defining the pressure inlet condition is as follows:

***($Density*9.81*(H-$$Position[2])***

The hydrostatic pressure over the boundary is defined as the density of water multiplied by its mass acceleration and each point's depth under the water surface. Each point's depth under the surface is defined as the difference between the total water depth (H) and the Z-coordinate for the current point.

**Plotting Change of Water Level During Flushing**

While simulating flushing it would be interesting to plot the varying water level over time. In model 4, the scale model, the water level was plotted for two positions - directly over the horizontal trash rack and at the penstock outlet. For monitoring the water level along the z-axis two line probes were generated from $Z_0 – Z_1$ as displayed in figure 5-9.

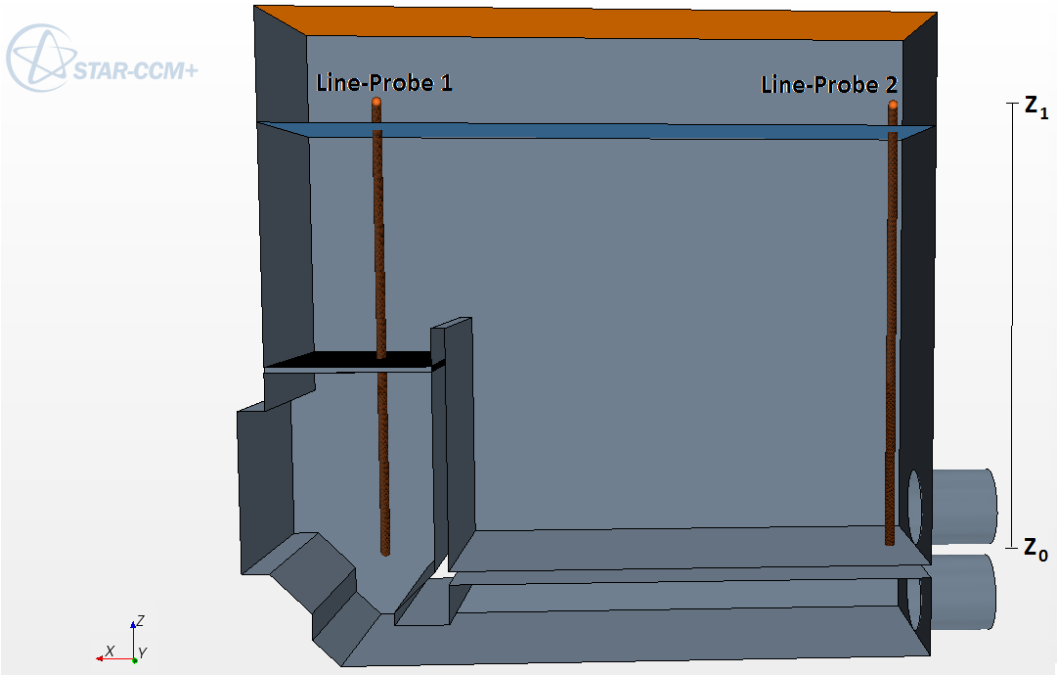


**Figure 5-9: Line-probes for water level monitoring**

Each of the two Line-Probes contains 1000 probes. The field function defining the water level is as follows:

$$\${VolumeFractionPhase\ 1\ Water}*((Z_1-Z_0)/P)$$

The field function is generated by referring to the volume fraction of water function which defines the water content in each cell. The volume fraction function is then multiplied by the difference between the z- coordinate of $Z_1$ and $Z_0$, and divided by the number of probes (P). A report with the sum of the field function over the line probes was generated and plotted with time at its x-axis and water level at its y-axis.

### 5.4.3. Choice of Viscous Regime and Turbulence Models

The viscous regime in STAR CCM+ is divided into three parts; viscid, laminar and turbulent. The simulations performed in this study are all subjected to turbulence flow and hence sets the viscous regime. The turbulent regime is divided into RANS, DES and LES, as described in chapter 3.2.3. RANS is the turbulence model used for the simulations in this study. RANS is chosen due to it being commonly used in general and due to numerous comparable studies performed in the Department of Hydraulic and Environmental Engineering at NTNU.

Both K-Epsilon and K-Omega are usable turbulence models for the open flow characteristics of the horizontal trash rack model. By looking at past studies, there are small differences in velocity distribution when comparing the K-Epsilon and K-Omega turbulence model (Holmeset, 2012, Hasaas, 2012). Because of the small differences and the fact that K-Epsilon is set as the default turbulence model for RANS in STAR CCM+, K-Epsilon it is used as the turbulence model for all simulations in this study.

Table 5-7 describes the initial values and inputs for the turbulence model chosen for every simulation performed in this study.

**Table 5-7: Properties for the turbulence model (RANS)**

| Properties | Value | Description |
|---|---|---|
| Turbulence Model: | Realizable K-Epsilon Two-Layer | A version of the K-Epsilon model which combines the realizable K-Epsilon model with the two-layer approach, adding flexible wall treatment. |
| Convection Scheme: | 2nd order Upwind Scheme | A scheme introduces a dissipative error helping the solver to achieve robust convergence. |
| Turbulence Specification: | Intensity + Viscosity Ratio | Specifies the method for defining the turbulence profile at boundaries. |
| Turbulent Velocity Scale: | 1 m/s | A representative velocity scale for the simulation used for estimating the initial turbulent kinetic energy (TKE) |
| Turbulent Viscosity Ratio: | 10 | A boundary value and initial condition value describing the ratio of turbulent to laminar viscosity. |
| Turbulence Intensity: | 0.01 | A measure of the root mean square of the local velocity fluctuations v’ relative to the mean or reference velocity v. (CD-Adapco, 2012) |

### 5.4.4. Choice of Multiphase Flow Models

As the physics of the model includes separate materials, water and air, a multiphase mixture setup is chosen. The multiphase mixture in STAR CCM+ has two flow models to choose between:

- Multiphase segregated flow
- Volume of Fluid (VOF)

As chapter 3.2.4 states, VOF is suitable for the conditions present in the models for this study and is therefore used for all simulations.

**Multiphase interactions**

The interaction between phases is identified under Physics -> Models -> Multiphase Interactions in the properties window. A single general phase interaction is created for all simulations in this study. The VOF-phase-interaction identifies the primary phase as water and the secondary as air. The initial interaction between water and air, describing the initial water level, is pronounced as a field function in chapter 4.4.2. The chosen properties for the multiphase model is presented in table 5-8.

**Table 5-8: Properties for the multiphase model (VOF)**

| Properties | Value | Description |
|---|---|---|
| Convection Scheme: | 2nd order | Sharper interfaces between phases are obtained by using the 2nd order discretization scheme. It is essential for the simulation result to identify a sharp boundary between water and air. |
| Sharpening Factor: | 0.0 | Increasing the sharpening factor results in further sharpening of interfaces between phases, but it may cause non-physical alignment. Applying a sharpening factor for the simulations was not necessary when an already gratifying interface was achieved by using the 2nd order discretization scheme. |
| Angle Factor: | 0.05 | Default angle factor in HRIC[1] scheme for interface tracking |
| CFL_l: | 0.5 | Default lower Courant number limit in HRIC[1] scheme |
| CFL_u: | 1.0 | Default upper Courant number limit in HRIC[1] scheme |

[1]HRIC = High-Resolution Interface Capturing. HRIC mimics the convective transport of immiscible fluid components making it suitable for tracking sharp interfaces.

### 5.4.5. Defining Relaxation Factors

All simulations are performed with an identical set of relaxation factors. The relaxation factors are accessible in the solver node and default values are implied by STAR CCM+ (CD-Adapco, 2012). The relaxation factors used for the simulations are presented in table 5-9.

**Table 5-9: Selection of under-relaxation factors**

| Type: | Under-Relaxation factor: |
|---|---|
| Velocity | 0.7 |
| Pressure | 0.3 |
| Segregated VOF | 0.9 |
| K-Epsilon Turbulence | 0.8 |
| K-Epsilon Turbulent Viscosity | 1.0 |

### 5.4.6. Time Steps and Iterations in the Implicit Unsteady Model

While running the simulations with the implicit unsteady approach, special attention was given to Courant numbers, convergence and mass balance.

**The time step size is regulated to meet Courant number requirements**

The applied time step differs between the simulations with and without the trash rack and for the back flushing simulations where the velocity is higher. The goal has been to establish a mean Courant number smaller than 1, as suggested in chapter 3.2.7. The user guide for STAR CCM+ allows local courant numbers in the area of 10-100, but to ensure stability the local Courant numbers are maxed at ~1 for all simulations in this study by reducing the time step.

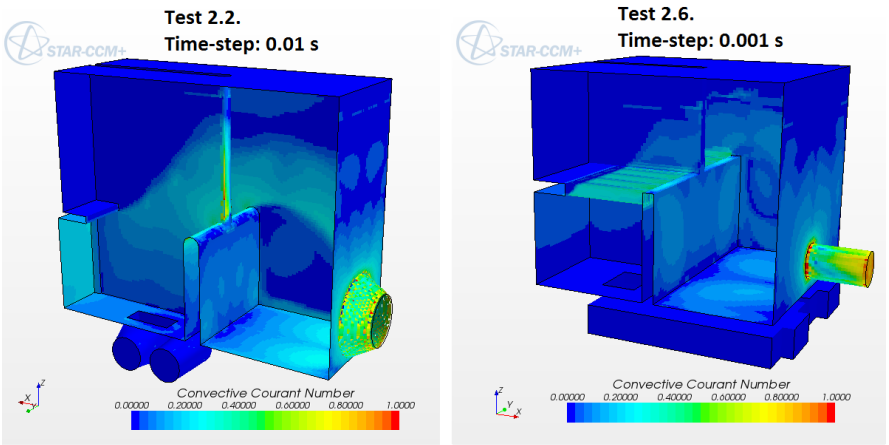


**Figure 5-10: Global Courant numbers for test 2.2 and 2.6.**

Figure 5-10 displays an overview of the Courant number for test 2.2 and 2.6. Generally for all tests, the highest courant numbers appear at the thrash rack and by the outlet pipe.

While flushing, the highest Courant numbers appear in the flushing pipe and over the trash rack where the velocity also is highest.

Some of the simulations experienced local Courant numbers of 3-5 at the outlet. In order to control the exactness of the result with high Courant numbers, the local Courant number was reduced to less than 1 by reducing the time-step size for at least 2000 iterations. The result differences between the simulations with high local Courant numbers and low Courant numbers were more or less absent. The results of the Courant number comparison test are displayed in Appendix 3. The TKE values after 2000 iterations with lower Courant numbers experienced only a reduction of 1.3 % and this reduction is most likely due to small oscillations in mass balance.

**Number of iterations needed is regulated by the requirement of mass balance**
For each simulation, the number of needed iterations to achieve mass balance differs depending on the complexity of the model and the time-step size as mentioned in chapter 3.2.7. Each simulation in this study has been evaluated for sufficient mass balance before accepting the results. The mass balance is evaluated by plots describing the mass entering the model, the mass exiting the model and the difference between these.

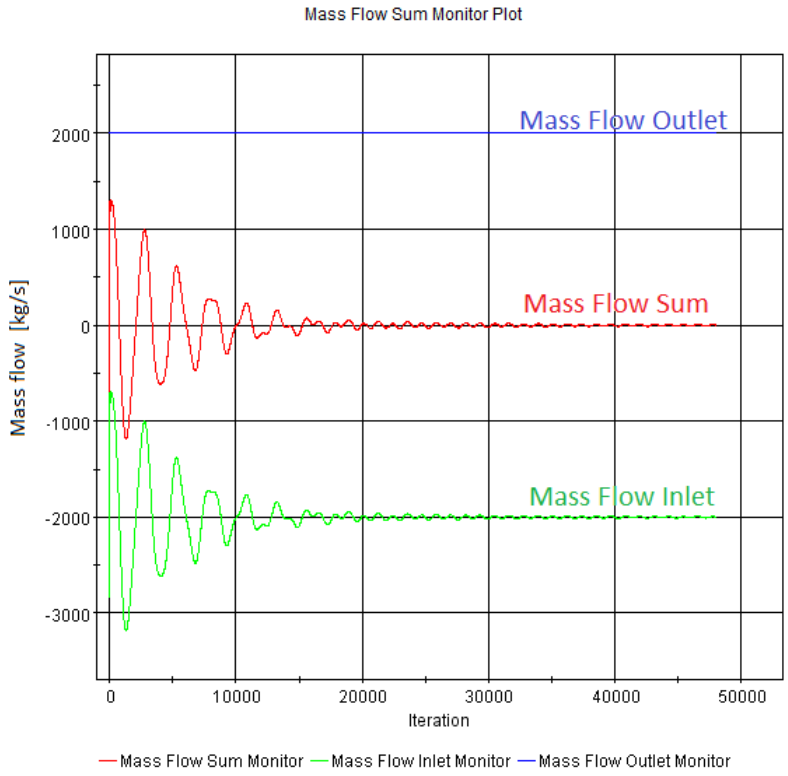


**Figure 5-11: Example of a satisfying mass balance plot**

Figure 5-11 presents a satisfying mass balance result where the sum of masses entering and leaving the model converges towards zero. The blue line, the mass flow through the outlet, is constant throughout every simulations performed in this study due to its constant

boundary condition. The green line, the mass flow through the inlet, varies due to its pressure controlled boundary condition.

A number of 4 inner iterations are used for all simulations performed in this study, when it appears that adding more inner iterations does not change the residuals within each time step any more.

An overview of time steps, iterations performed and physical time simulated for every test is displayed in table 5-10.

**Table 5-10: Time-steps and iterations used for the numerical simulations**

| Test | Time-Step [seconds] | Iterations | Physical Simulation Time [s] |
|---|---|---|---|
| **1.1.** | 0.01 | 8 800 | 22 |
| **1.2.** | 0.01 | 32 000 | 80 |
| **1.3.** | 0.0005 | 32 000 | 4 |
| **1.4.** | 0.0005 | 24 000 | 3 |
| **2.1.** | 0.01 | 32 000 | 80 |
| **2.2.** | 0.01 | 48 000 | 120 |
| **2.3.** | 0.01 | 32 000 | 80 |
| **2.4.** | 0.01 | 56 000 | 140 |
| **2.5.** | 0.01 | 48 000 | 120 |
| **2.6.** | 0.001 | 32 000 | 8 |
| **2.7.** | 0.001 | 64 000 | 16 |
| **2.8.** | 0.001 | 64 000 | 16 |
| **2.9.** | 0.001 | 72 000 | 18 |

# 6. Results

The results from the physical demonstration model and the results from the test program of the numerical simulations are presented in this chapter. A visual presentation of the results has been emphasised in order to present the results in an effective and understandable way.

## 6.1. Results for the Physical Demonstration Model

The results for the physical demonstration model include an evaluation of the total flow pattern displayed by streamlines and measurement of the total head loss during normal operation. The performance of the back flushing is also analysed. The result from the numerical simulation of the demonstration model is presented in chapter 6.3.6.

**Evaluation of streamlines and water level**

Figure 6-1 displays a total image of the flow pattern, based on the performed dyed solution test presented in chapter 4.

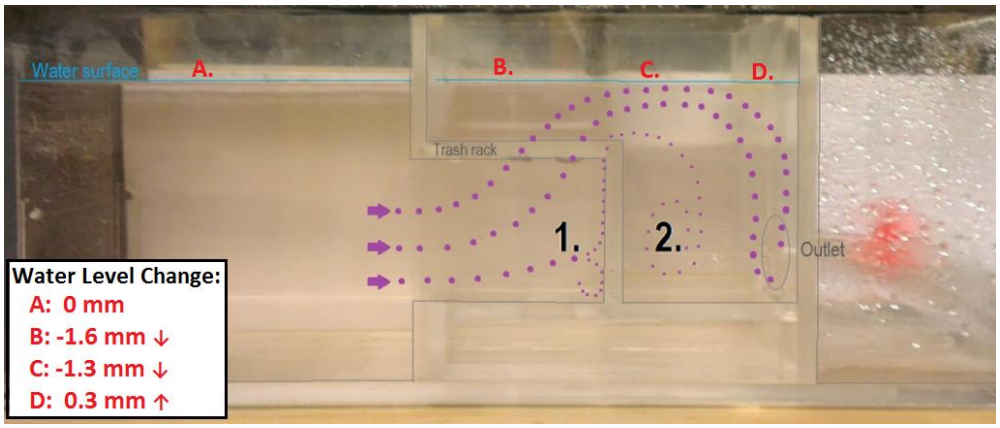


**Figure 6-1: Main streamlines in the physical Demonstration Model**

From the evaluation of streamlines two zones with eddies appear, marked in figure 6-1 as point 1 and 2.

The change in water level is measured in point B, C, and D compared to the initial water level outside the intake at point A (See Fig. 6-1). The water level is lowered by 1.6 mm over the trash rack (point B). Downstream the weir (point C) the water level is 1.3 mm lower than the initial water level at point A. In front of the penstock intake (point D) the water level rises 0.3 mm over the initial water level at point A.

**The performance of back flushing**

The back flushing tests identified that the concept works. When the flushing gate is suddenly opened, the fabrics are detached from the rack. It is identified that sufficient water available for flushing is important for the debris to detach and follow the flow through the flushing gate. The water level in the demonstration model is only 50 mm above the trash rack, which is close to the limit of successful flushing.

## 6.2. Results for the Back Flushing Efficiency

The back flushing efficiency is analysed by evaluating the velocity distribution over the horizontal trash rack in the One Chamber Model (Test 1.1), the Two Chamber Model (Test 1.2) and in the one chambered Scaled Model (Test 1.3 and 1.4). Animations are made for test 1.1, 1.3 and 1.4 showing the velocity distribution over time during flushing. The velocity distribution is presented as a vector scene and a scalar scene which also displays the water level.

The residuals for each simulation are presented in appendix 4. Mass flow plots are presented for test 1.2, 1.3 and 1.4 in appendix 5. Mass flow is not plotted for test 1.1 where the mass outflow is constant (4 $m^3/s$) throughout the simulation.

### 6.2.1. Test 1.1 – Back Flushing in the One Chamber Model

Test 1.1 is performed on model 1 - The One Chamber Model. The back flushing is performed by activating the flushing outlet and closing both the inlet and the outlet for normal production as described in the boundary conditions in appendix 2. The velocity distribution over the trash rack is measured as the water level decreases. The velocity distribution is presented at three time-stages, at 0.2, 1.6 and 3.2 seconds after the back flushing initiation. The velocity distribution is presented in animation 1 and in figure 6-2, 6-3 and 6-4 at different time-stages. The horizontal trash rack experiences higher velocities along the edges, especially along the weir.

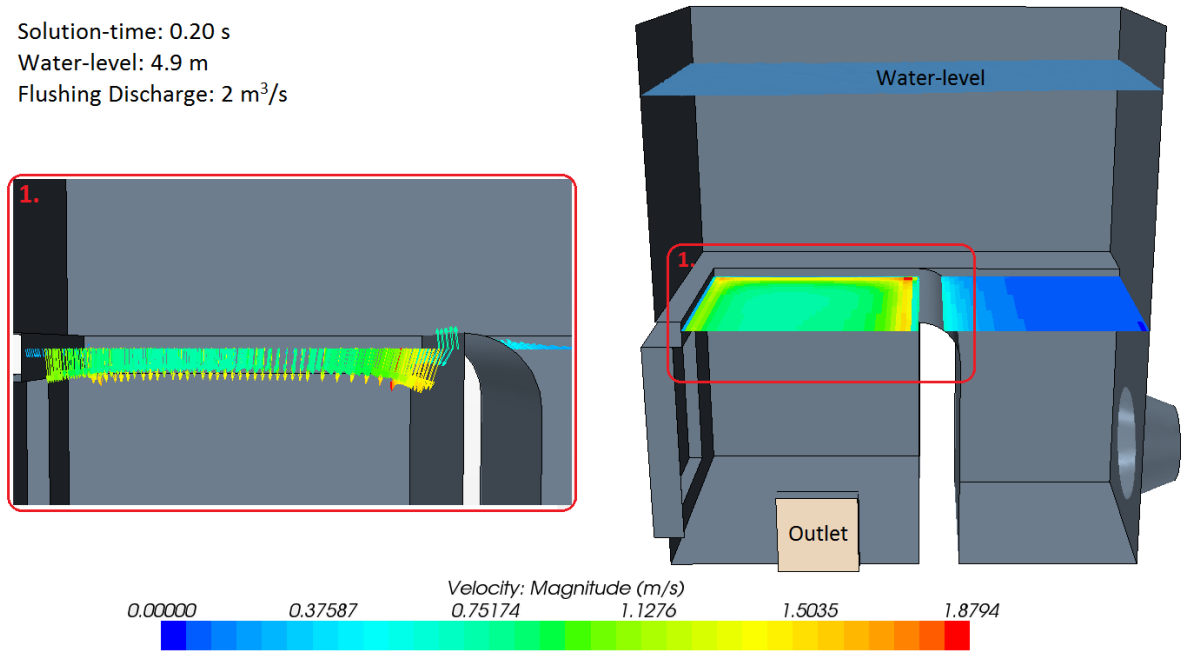


**Figure 6-2: Test 1.1. Velocity distribution over the trash rack at 0.20 seconds**

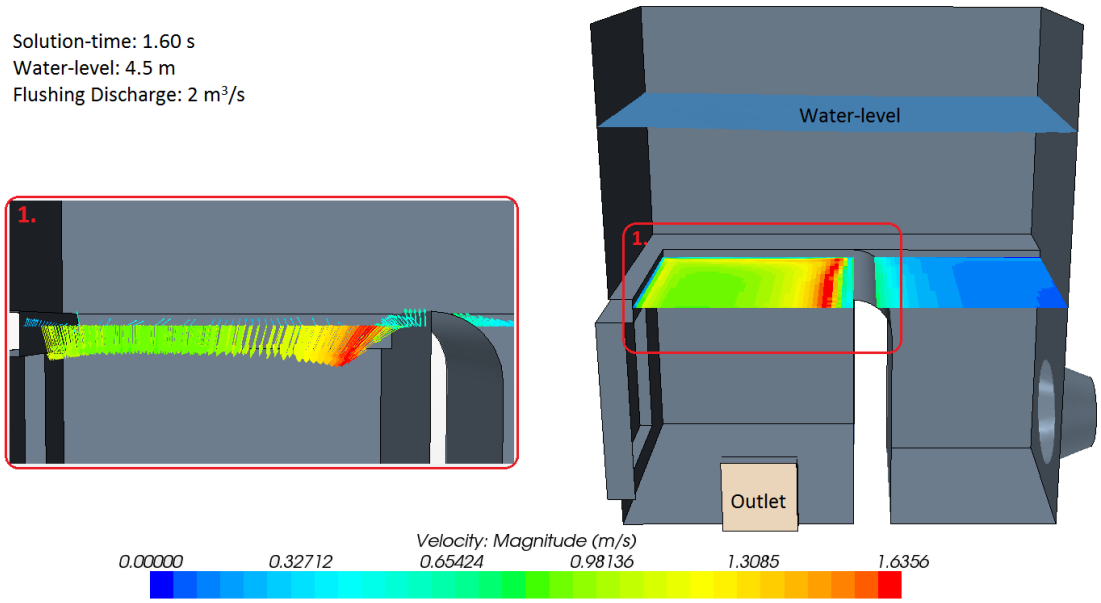


**Figure 6-3: Test 1.1. Velocity distribution over the trash rack at 1.60 seconds**

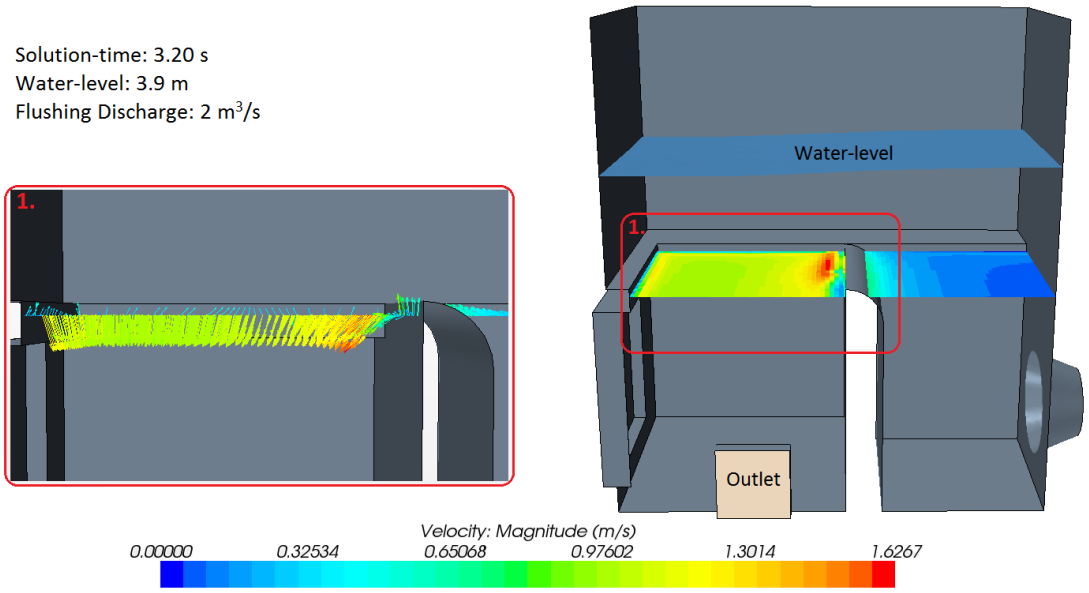


**Figure 6-4: Test 1.1. Velocity distribution over the trash rack at 3.20 seconds**

### 6.2.2. Test 1.2 – Back Flushing in the Two Chamber Model

Test 1.2 is performed on model 2a, the Two Chamber Model. As described in the boundary conditions in appendix 2 the test is performed with 15% of normal production discharge and a constant flushing discharge of 2 $m^3/s$. The water level is simulated to be stationary when the secondary inlet gate is open supporting the model with sufficient water inflow. The horizontal trash rack experiences more or less even velocities of ~1 m/s along the centre of the rack but suffers low velocities of ~0.2 m/s at the upper right corner at the weir and by the left edge (See Fig. 6-5).

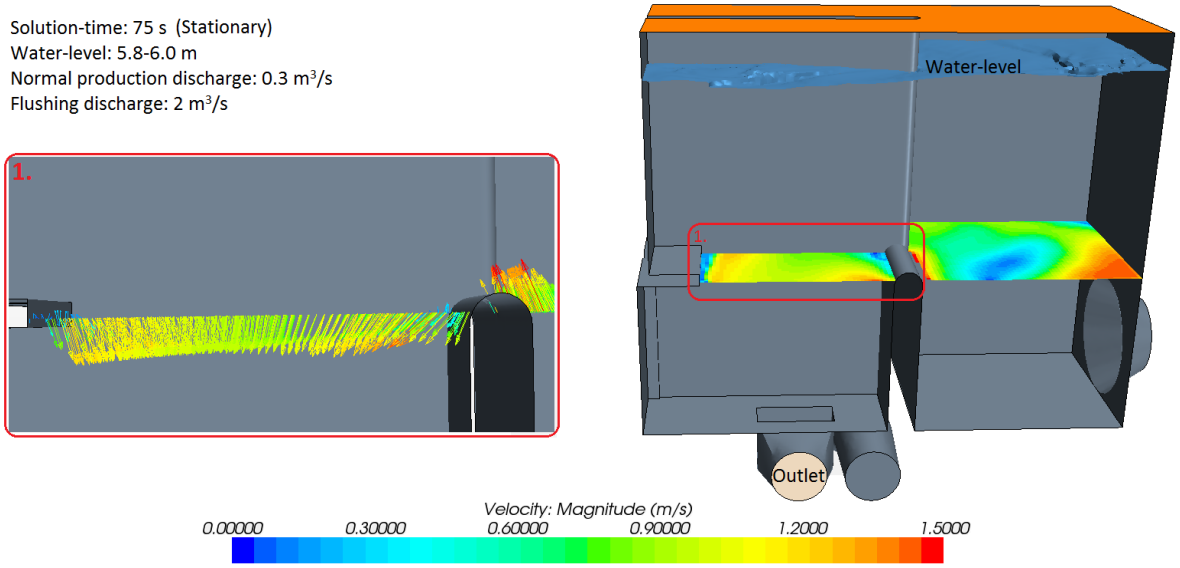


**Figure 6-5: Test 1.2. Velocity distribution over the trash rack (stationary)**

### 6.2.3. Test 1.3 – Back Flushing in the Scale Model with Low Weir

Test 1.3 is performed on model 4a, the Scale Model with a low weir. The velocity distribution over the trash rack is evaluated as the water-level decreases. The outlet is defined as a pressure outlet, resulting in a realistic water flow with changing discharge over time. The flow discharge satisfies the design discharge within the area of 0.25-2.50 seconds after flushing initiation as presented in the mass flow plot in appendix 5. Figure 6-6, 6-7 and 6-8 presents the velocity distribution at 0.5, 1.50 and 2.50 seconds after flushing initiation. The characteristic of the velocity distribution clearly varies over time during flushing. A high velocity line moves across the trash rack to the left as time passes and the water level reduces. The high velocity line can be explained as an eddy emerging and developing in the right parts of the trash rack as the water level is reduced.

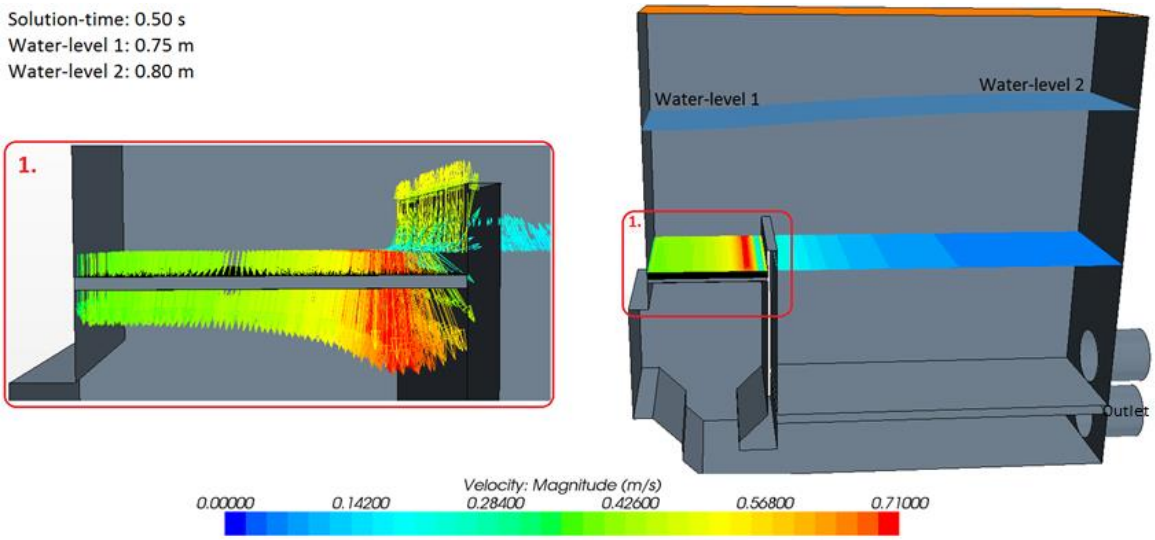


**Figure 6-6: Test 1.3. Velocity distribution over the trash rack at 0.50 seconds**

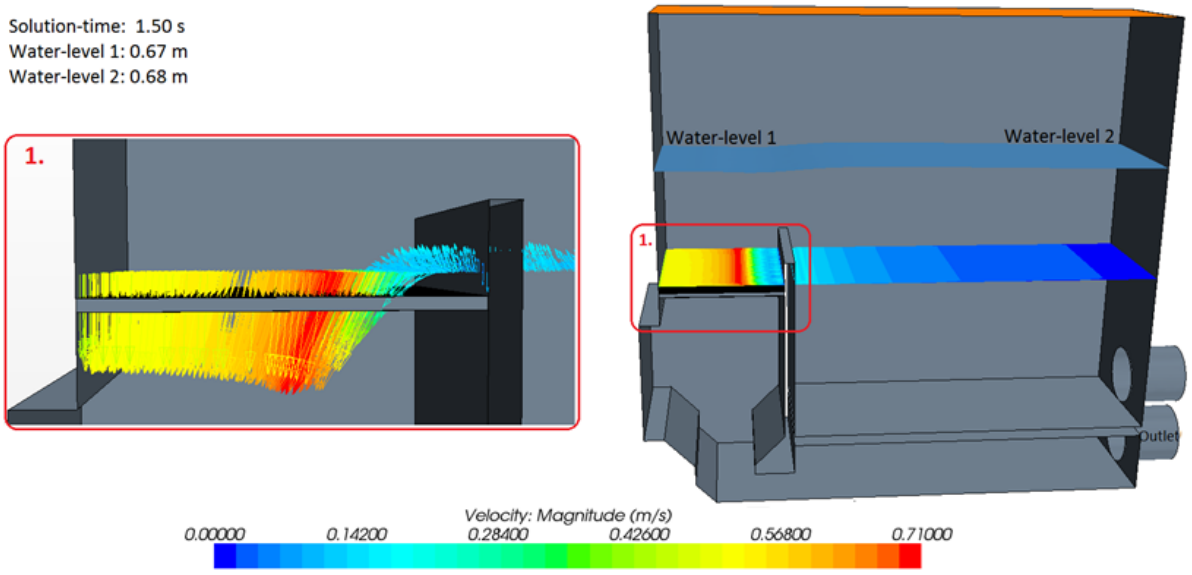


**Figure 6-7: Test 1.3. Velocity distribution over the trash rack at 1.50 seconds**

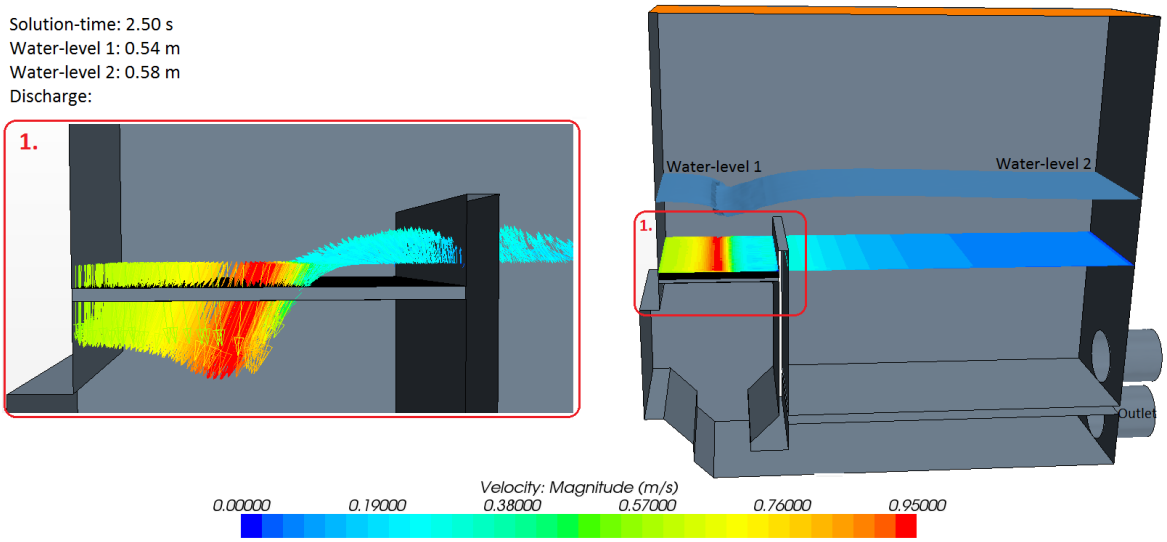


**Figure 6-8: Test 1.3. Velocity distribution over the trash rack at 2.50 seconds**

### 6.2.4. Test 1.4 – Back Flushing in the Scale Model with High Weir

Test 4.1 is performed on model 4b, the Scale Model with a high weir. The velocity distribution over the trash rack is evaluated as the water level decreases. As in test 1.3 with the low weir, the outlet is defined as a pressure outlet, resulting in a realistic water flow with changing discharge over time. The flow discharge satisfies the design discharge within the area of 0.25-1.75 seconds after flushing initiation as presented in appendix 5. Figure 6-9, 6-10 and 6-11 presents the velocity distribution at 0.5, 1.50 and 2.50 seconds after flushing initiation. As the back flushing is initiated the velocity distribution starts of being even across the entire trash rack with a typical velocity of 0.4 m/s (which is the design flushing velocity). The velocity distribution is characterized as even the first second after initiation. After the first second a recirculation zone is created at the weir resulting in local upward directed flows. As the water-level decreases towards the top level of the weir, the water surface over the trash rack decreases rapidly and a free water fall emerges.

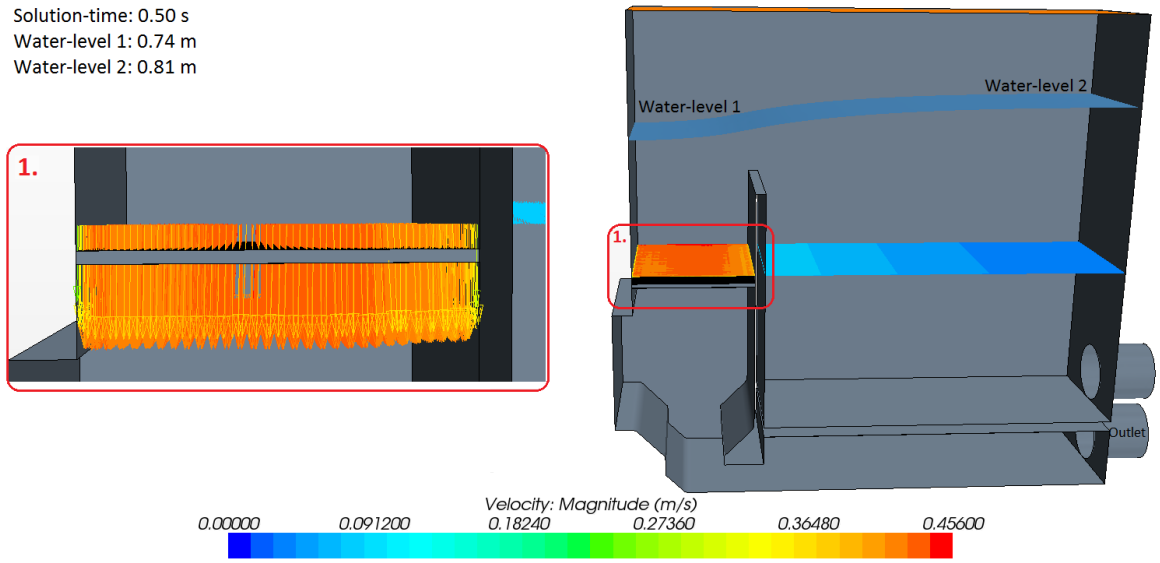


**Figure 6-9: Test 1.4. Velocity distribution over the trash rack at 0.50 seconds**

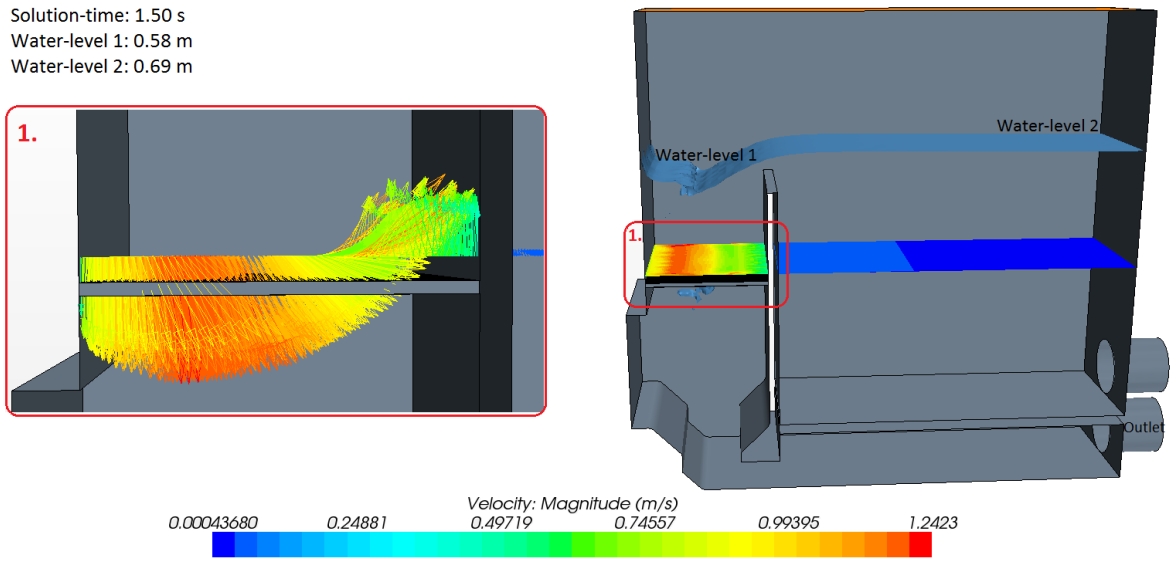


**Figure 6-10: Test 1.4. Velocity distribution over the trash rack at 1.50 seconds**

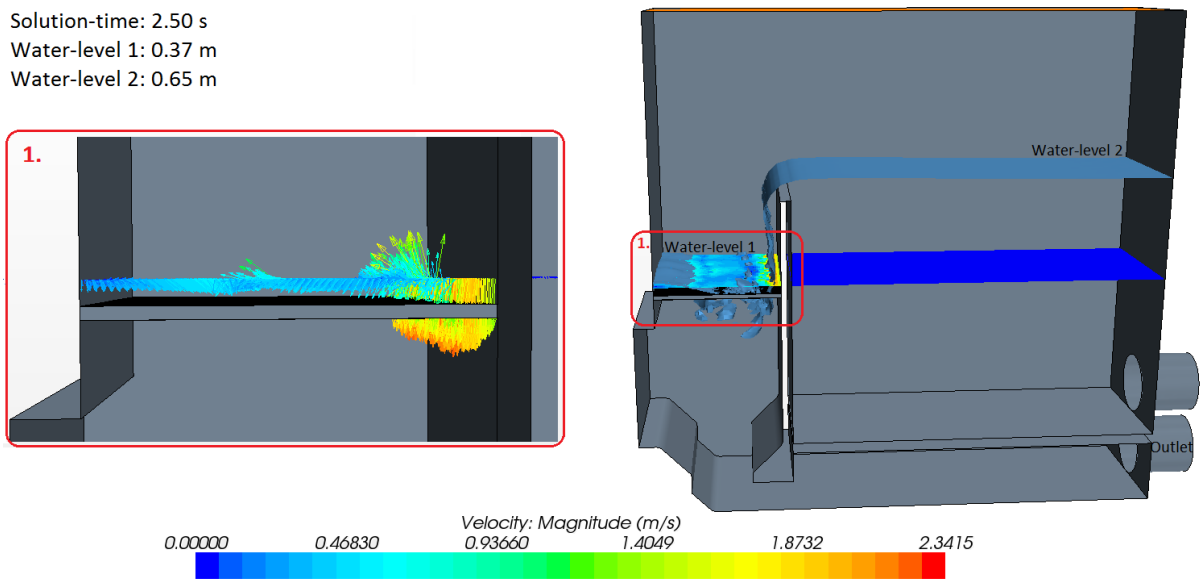


**Figure 6-11: Test 1.4. Velocity distribution over the trash rack at 2.50 seconds**

## 6.3. Results of Hydraulic Performance during Normal Production

The hydraulic performance during normal production is assessed by looking at the following test parameters:

- Streamlines
- Turbulent Kinetic Energy levels at the outlet (TKE)
- Head loss measurements
- Velocity distribution over the trash racks (Appendix 6)

The streamlines are visually presented on a volume-fraction-of-water layout for all tests. Streamline-views are great for revealing an image of the total flow pattern.

The TKE-values are visually portrayed across the outlet of the model. The TKE-levels are measured at the outlet because this is the point where the water exits the model also making it a suitable area for comparing with other simulations. Average TKE-values are also measured by extracting every cell value over the outlet in STAR CCM+.

The head loss through a model is calculated by using the total pressure height, plotted horizontally through a continuous line from inlet to outlet. The total head loss is calculated as the total pressure height difference between the outlet and the inlet position. By the outlet the pressure height is often embossed by fluctuations making it hard to choose the exact outlet pressure value. An average pressure value over the last 10 measures is therefore used as an average outlet pressure height.

The velocity distribution across the inlet and over the horizontal trash racks are visually portrayed in Appendix 6, as this velocity is a main design criteria for the models.

### 6.3.1. Test 2.1 – The One Chamber Model

Test 2.1 is performed on model 1, the One Chamber Model during normal operation with active inlet and outlet boundaries. The results for test 2.1 are further portrayed here.

The streamlines of test 2.1 are portrayed in figure 6-12. There are secondary flows at the bottom of the upper chamber by the flushing gate and after passing the horizontal trash rack. The main water flow is pushed against the right end wall before moving through the outlet pipe.

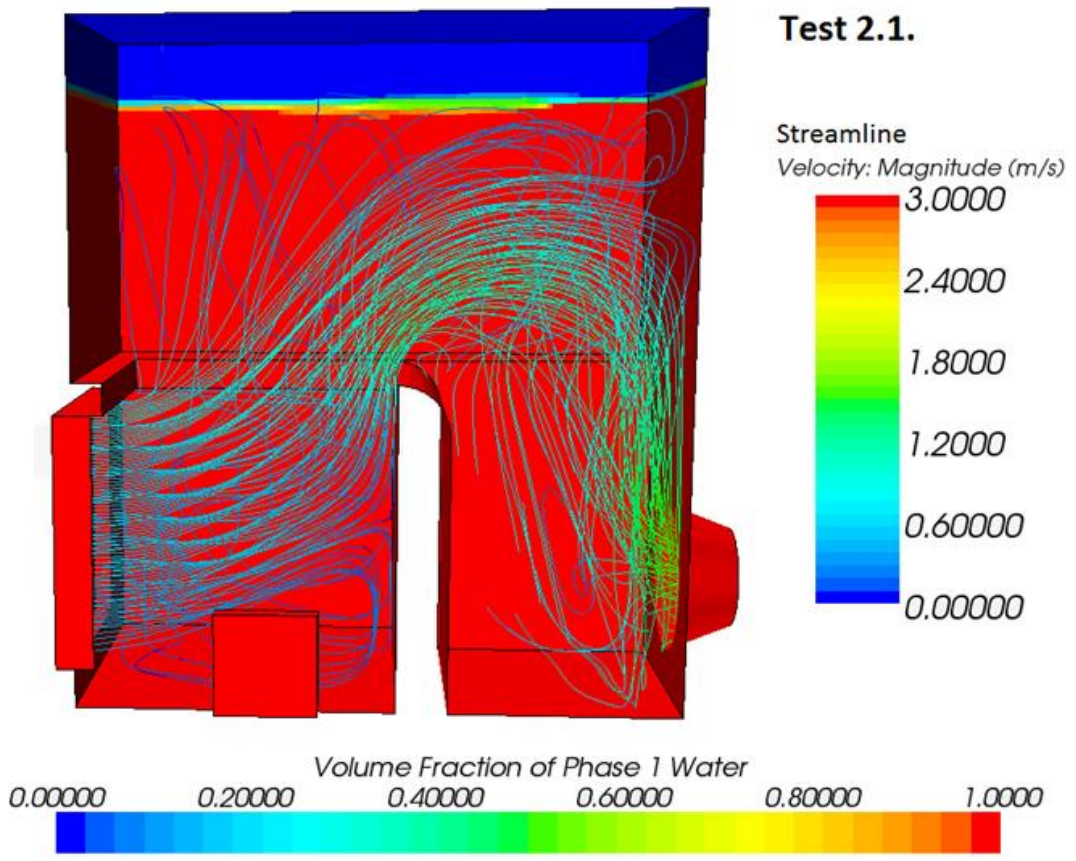


**Figure 6-12: Streamlines and volume fraction of water for test 2.1 – The One Chamber Model**

The TKE-values at the outlet for test 2.1 are portrayed in figure 6-13. The geometry of the model used for test 2.1 is not symmetrical, neither are the TKE-values. Average TKE is measured as 0.698 J/kg.

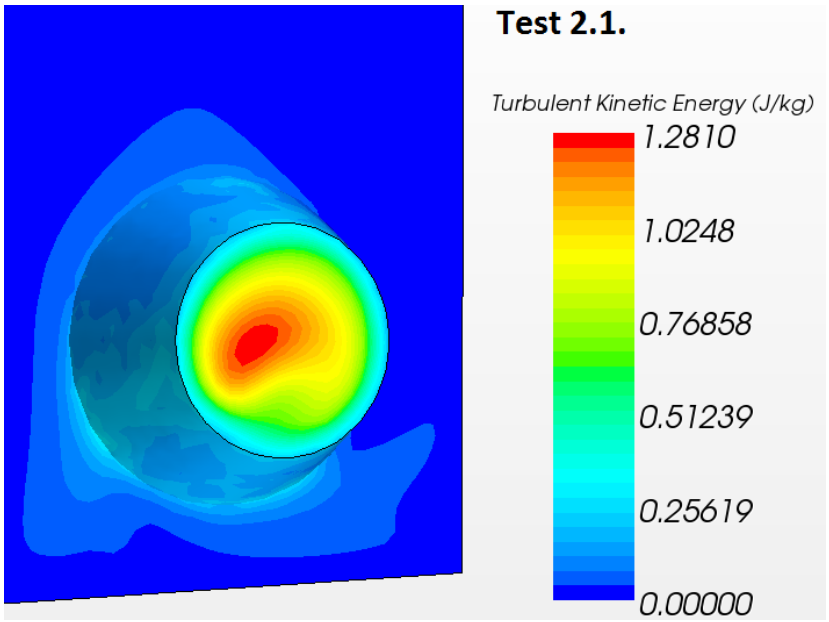


**Figure 6-13: Turbulent kinetic energy (TKE) for test 2.1 – The One Chamber Model**

The total head loss for test 2.1 is calculated as 0.143 m by using the graph displayed in figure 6-14.

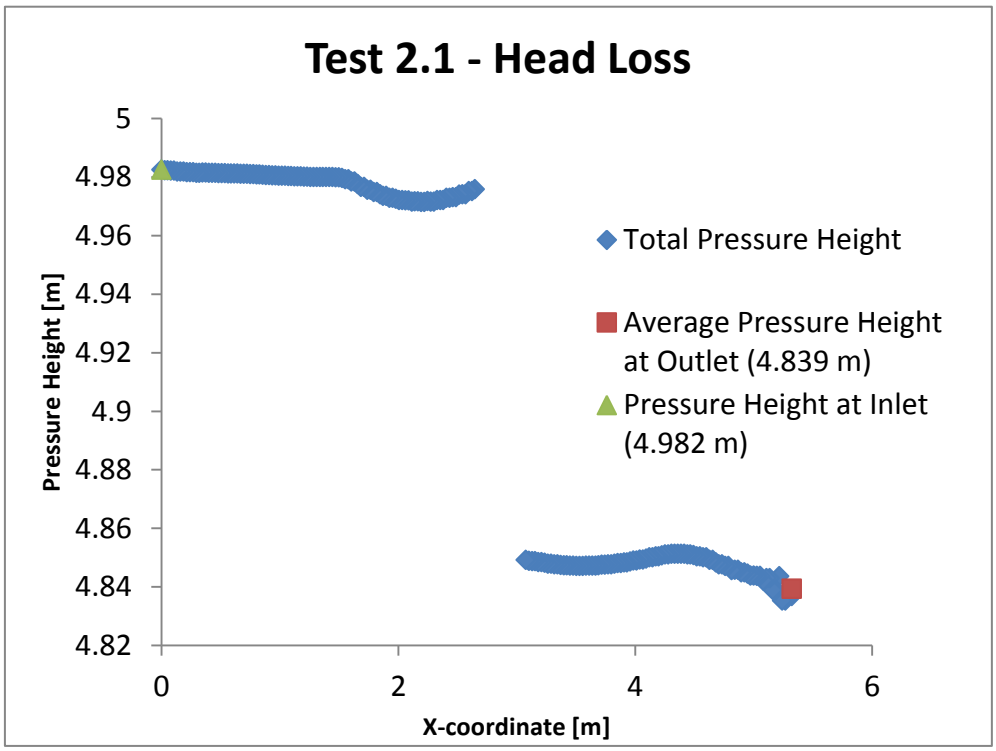


**Figure 6-14: Head loss for test 2.1 – The One Chamber Model**

### 6.3.2. Test 2.2 – The Standard Two Chamber Model

Test 2.2 is performed on model 2a, the Two Chamber Model, during normal operation with active inlet and outlet boundaries. The results for test 2.2 are further portrayed here.

The streamlines of test 2.2 is portrayed in figure 6-15. There are low-velocity-secondary-flows by the foot of the weir on the downstream side and at the surface.

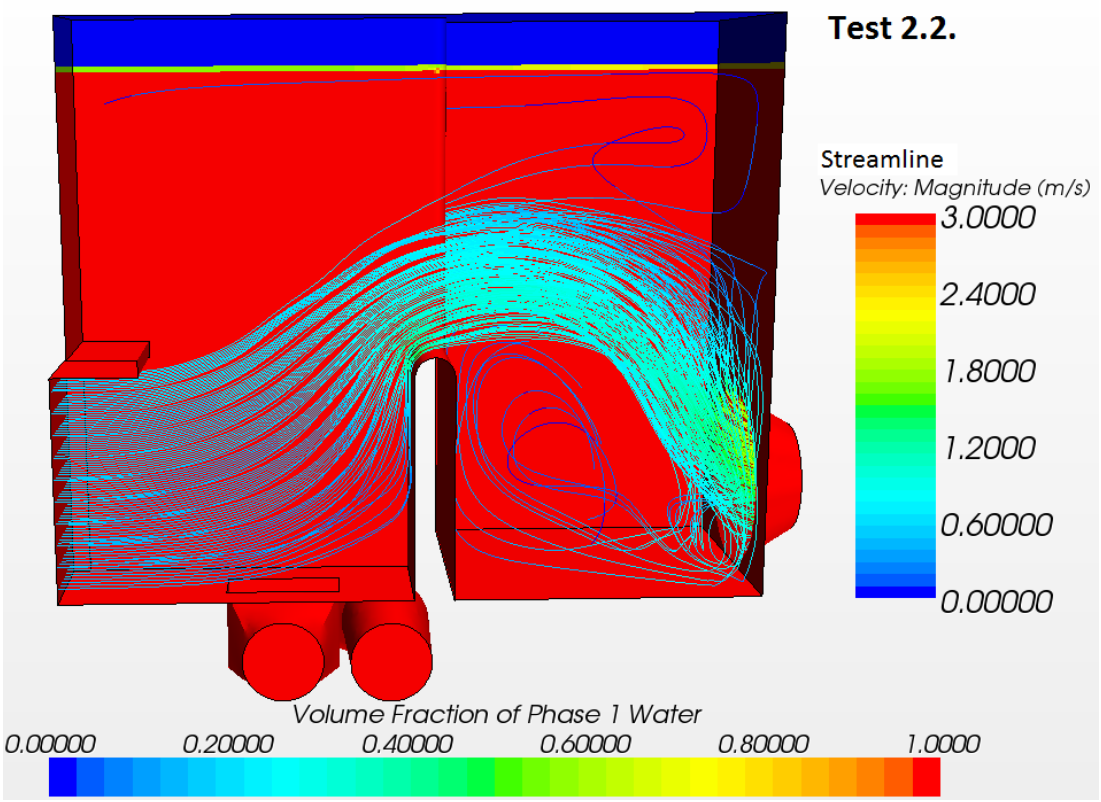


**Figure 6-15: Streamlines and volume fraction of water for test 2.2 – The Two Chamber Model**

The TKE-value at the outlet for test 2.2 is portrayed in figure 6-16. The geometry of the model used for test 2.2 is symmetrical and so are the TKE-values. Average TKE is measured as 0.139 J/kg.

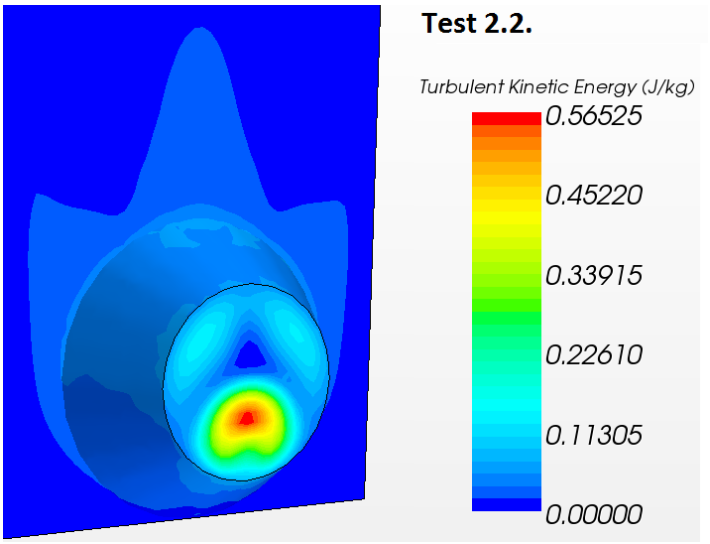


**Figure 6-16: Turbulent kinetic energy (TKE) for test 2.2 – The Two Chamber Model**

The total head loss for test 2.2 is calculated as 0.008 m by using the graph displayed in figure 6-17.

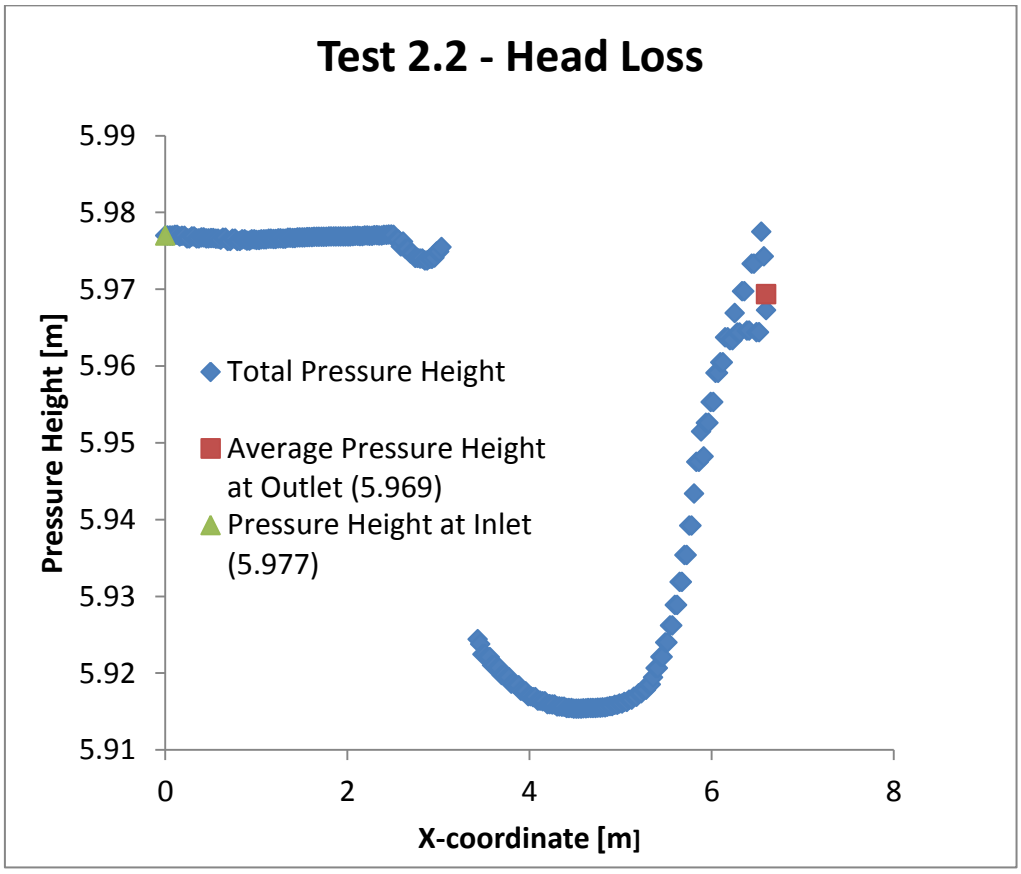


**Figure 6-17: Head loss for test 2.2 – The Two Chamber Model**

### 6.3.3. Test 2.3 – The Two Chamber Model with Low Water Level

Test 2.3 is performed on model 2a, the Two Chamber Model with a lower water level and active inlet and outlet boundaries. The results for test 2.3 are further portrayed here.

The streamlines for test 2.3 are displayed in figure 6-18. A low water level results in a more concentrated water flow and a higher velocity over the weir. There are low velocity secondary flows at the foot of the weir on the downstream side. The low water level also inflicts the interface between water and air in the right half of the model.

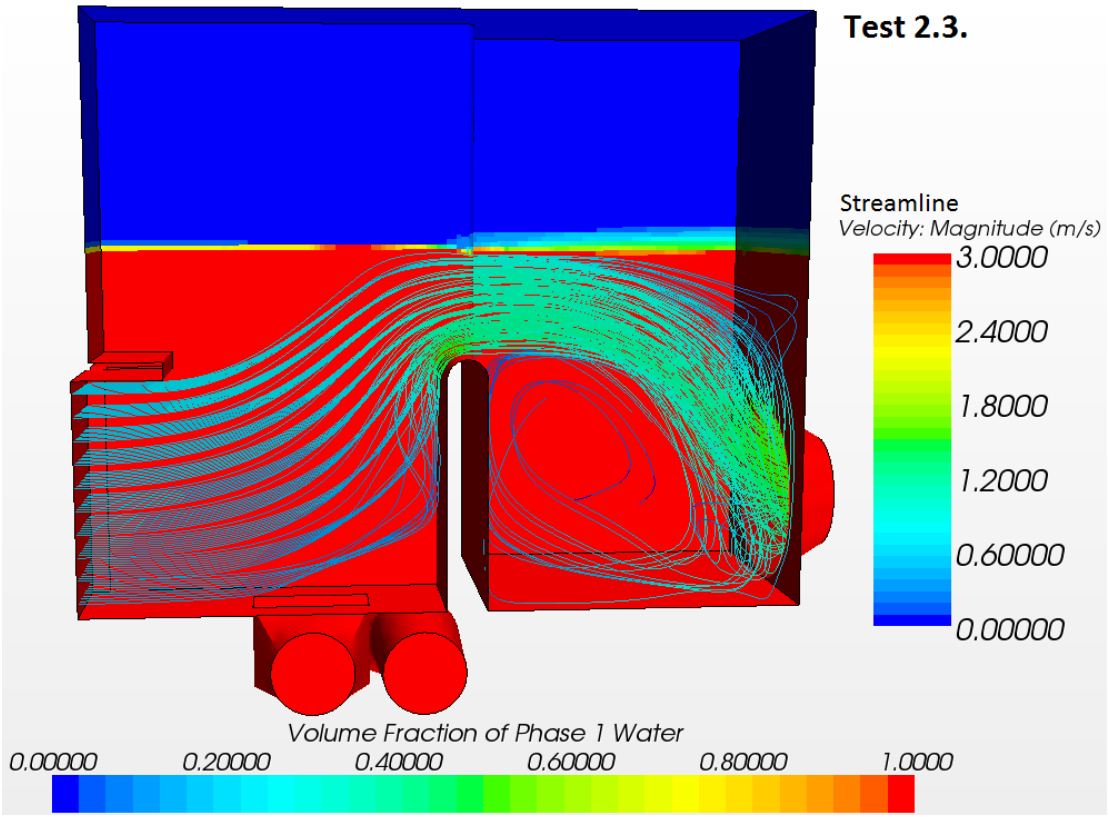


**Figure 6-18: Streamlines and volume fraction of water for Test 2.3 – The Two Chamber Model with low water level.**

The TKE-value at the outlet for test 2.3 is portrayed in figure 6-19. The geometry of the model in test 2.3 is symmetrical and so are the TKE-values. Average TKE is measured as 0.150 J/kg.

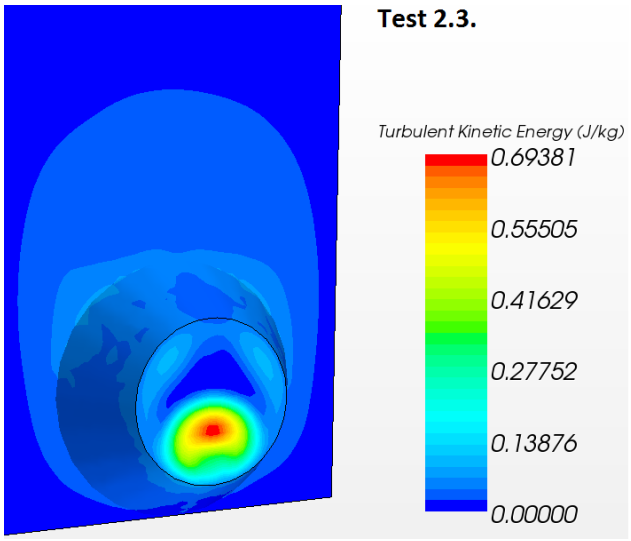


**Figure 6-19: Turbulent kinetic energy (TKE) for test 2.3 – The Two Chamber Model with low water level.**

The total head loss for test 2.3 is calculated as 0.032 m by using the graph displayed in figure 6-20.

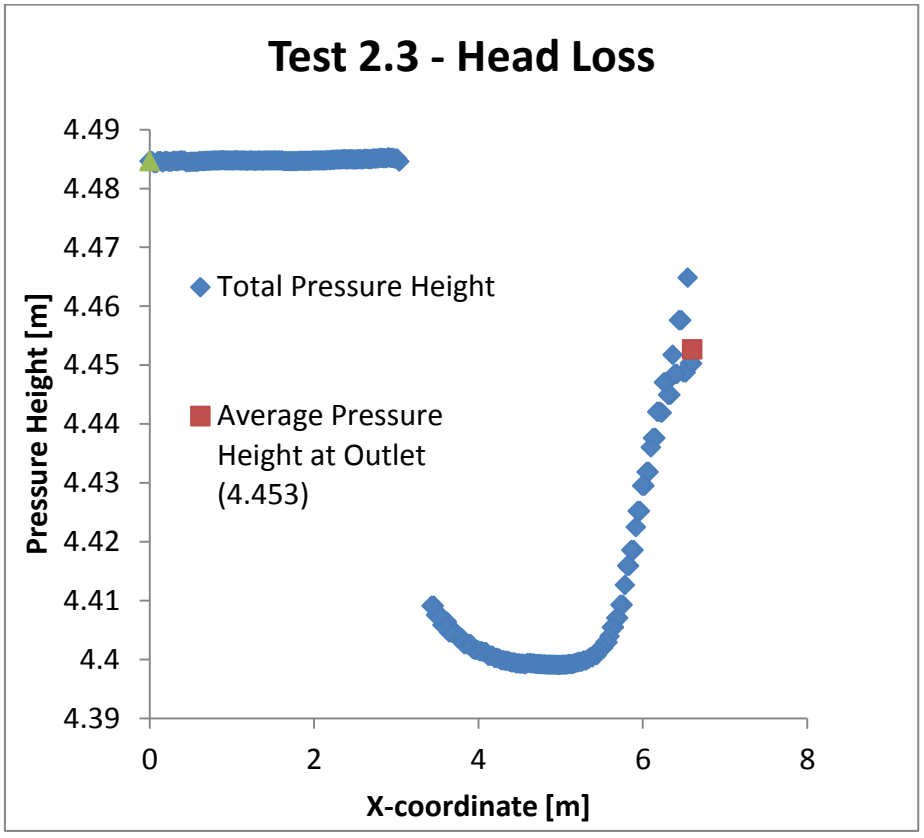


**Figure 6-20: Head loss for test 2.3 – The Two Chamber Model with low water level.**

### 6.3.4. Test 2.4 – The Two Chamber Model Included the Trash Rack

Test 2.4 is performed on model 2b, the Two Chamber Model with a modelled trash rack, with active inlet and outlet boundaries. The results for test 2.4 are further portrayed here.

The streamlines of test 2.4 is portrayed in figure 6-21. There are low-velocity-secondary-flows at the bottom of the weir on the downstream side as in the previous tests on the Two Chamber model.

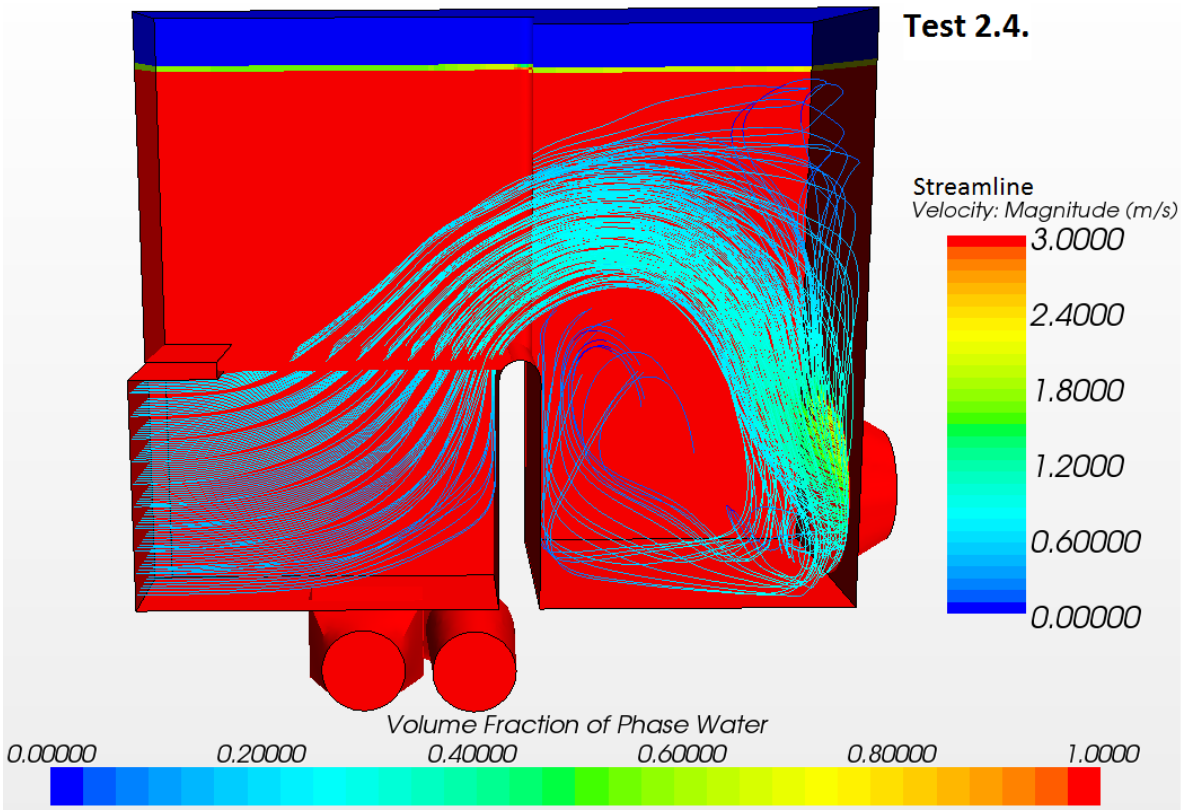


**Figure 6-21: Streamlines and volume fraction of water for test 2.4 – The Two Chamber Model with trash rack.**

The TKE-value at the outlet for test 2.4 is portrayed in figure 6-22. The geometry of the model used for test 2.4 is symmetrical but the TKE-values are slightly asymmetrical. Average TKE is measured as 0.182 J/kg.

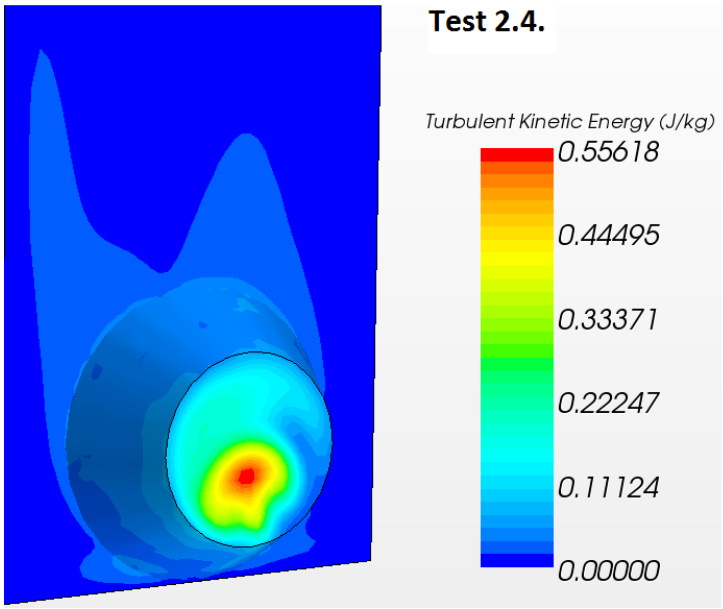


**Figure 6-22: Turbulent kinetic energy (TKE) for test 2.4 – The Two Chamber Model with trash rack**

The total head loss for test 2.4 is calculated as 0.034 m by using the graph displayed in figure 6-23.

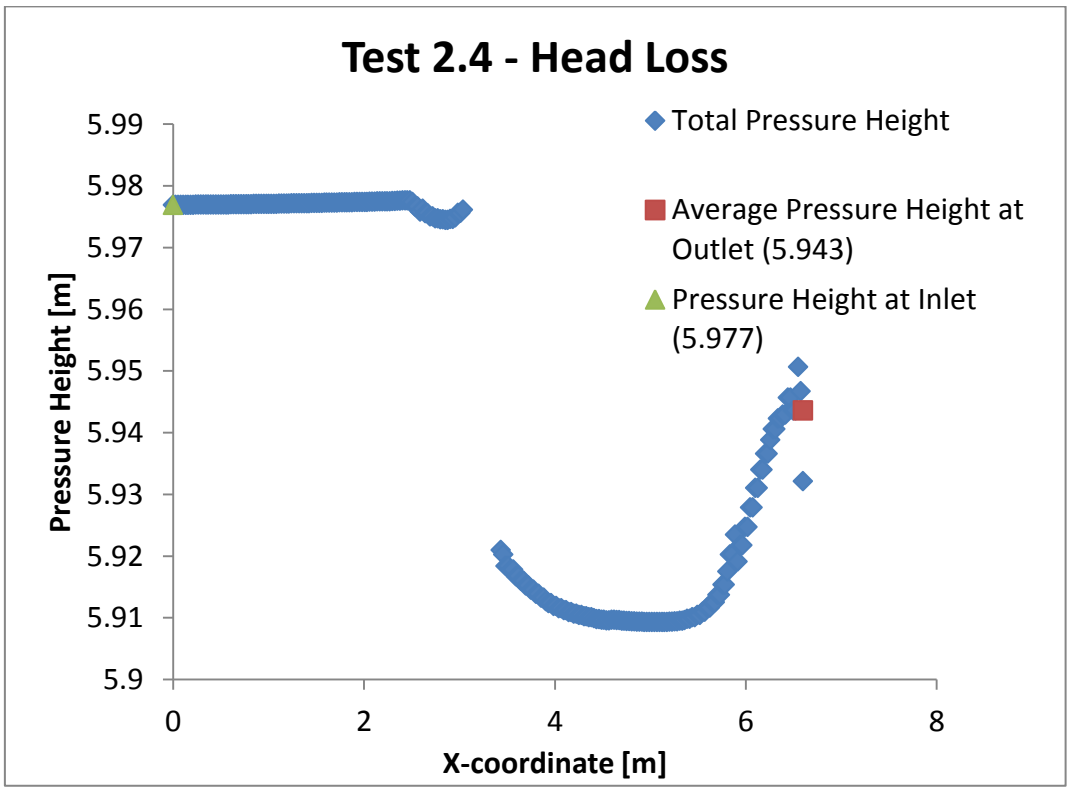


**Figure 6-23: Head Loss for Test 2.4 – The Two Chamber Model with trash rack**

### 6.3.5. Test 2.5 – The Two Chamber Model with Modified Weir

Test 2.5 is performed on model 2c, the Two Chamber Model with a modified weir, with active inlet and outlet boundaries. The results for test 2.5 are further portrayed here.

The streamlines of test 2.5 is portrayed in figure 6-24. There are no secondary flows at the bottom of the weir at the downstream side. However, secondary flows with low velocity appear at the foot of the weir on the upstream side of the weir and at the surface.

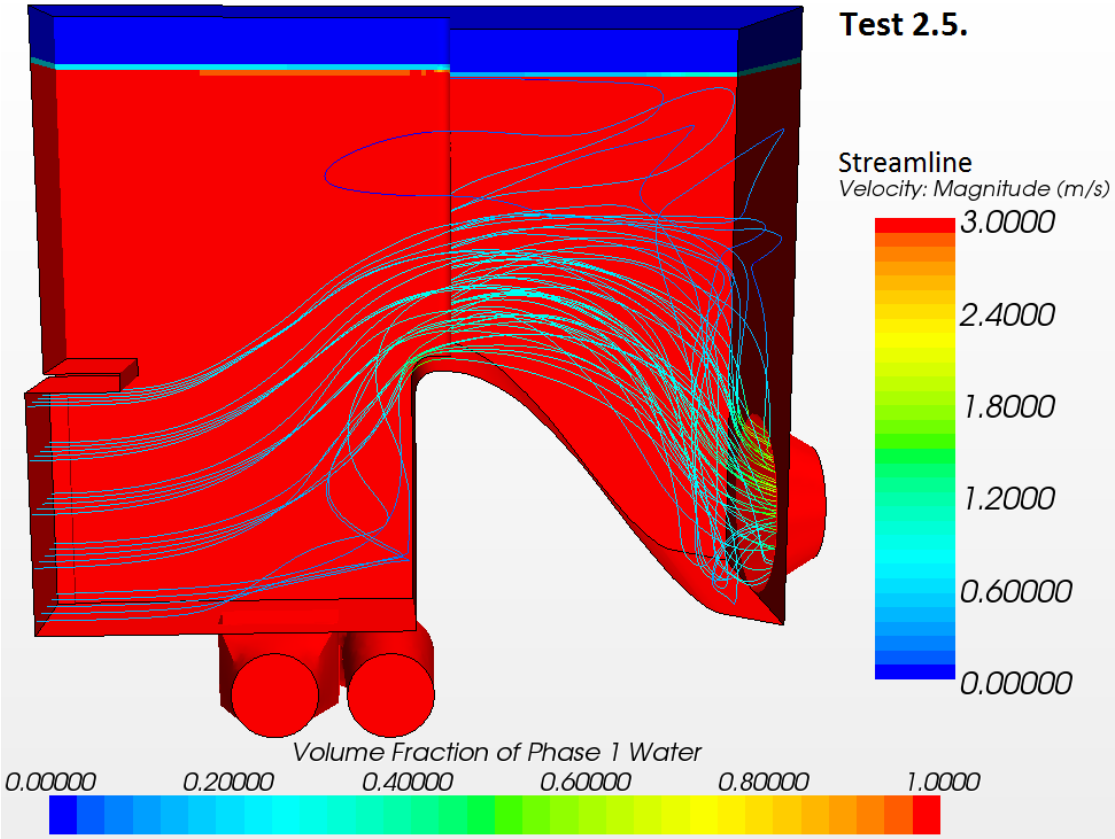


**Figure 6-24: Streamlines and volume fraction of water for test 2.5 – The Two Chamber Model with modified weir**

The TKE-value at the outlet for test 2.5 is portrayed in figure 6-25. The geometry of the model used for test 2.4 is symmetrical but the TKE-values are slightly asymmetrical. Average TKE is measured as 0.310 J/kg.

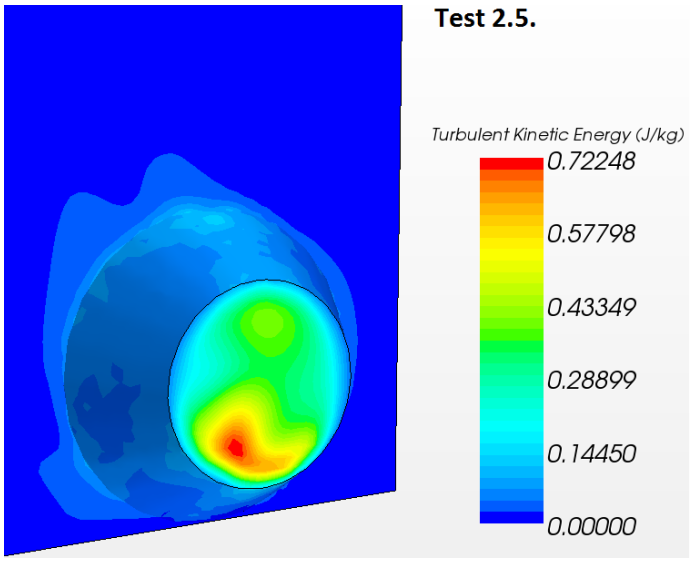


**Figure 6-25: Turbulent kinetic energy (TKE) for test 2.5 – The Two Chamber Model with modified weir**

The total head loss for test 2.5 is calculated as 0.018 m by using the graph displayed in figure 6-26.

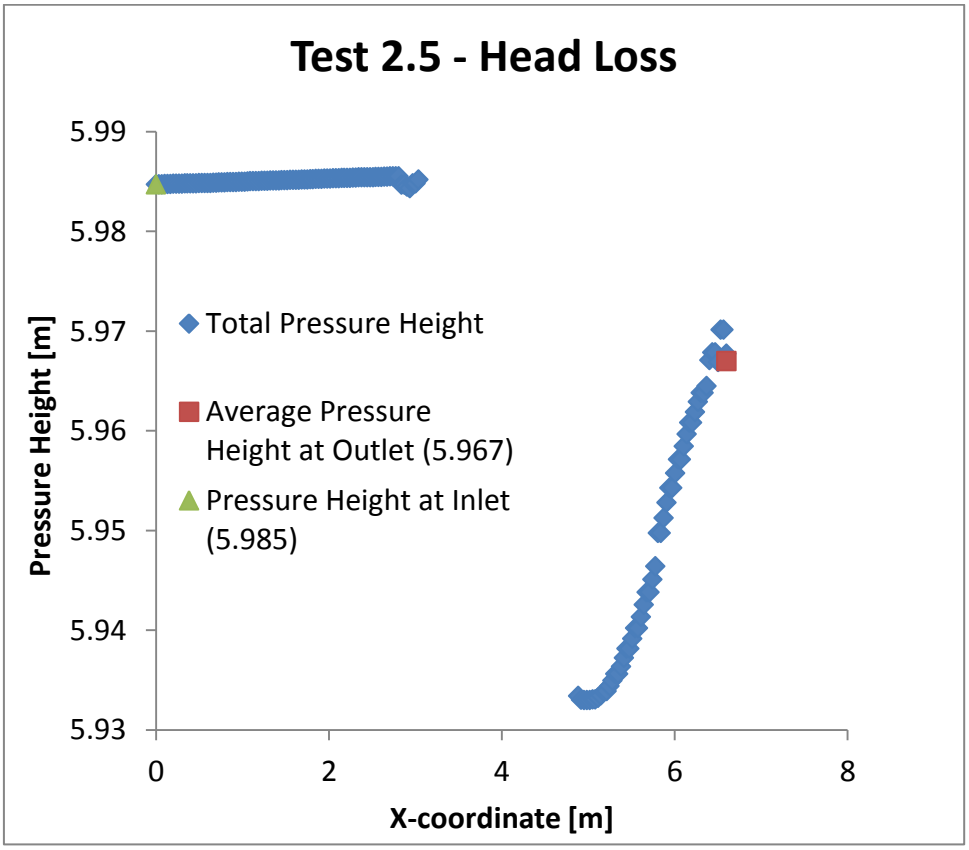


**Figure 6-26: Head loss for test 2.5 – The Two Chamber Model with modified weir**

### 6.3.6. Test 2.6 – The Demonstration Model

Test 2.6 is performed on model 3, the Demonstration Model. The simulation is performed in order to compare head loss and streamlines with the physical model described in chapter 5. The results for test 2.6 are further portrayed here.

The streamlines of test 2.6 is portrayed in figure 6-27. Secondary flows appear at the bottom of the weir on the downstream side. The interface between water and air is also less defined in the right half of the model.

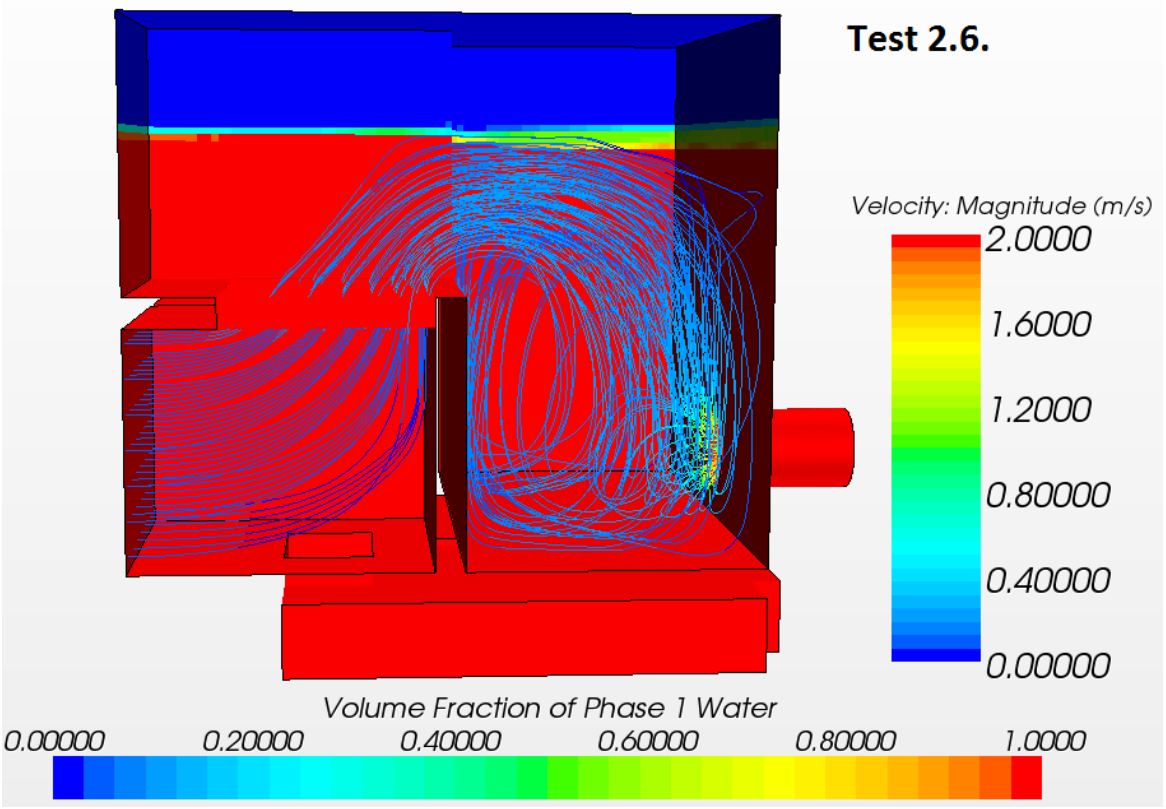


**Figure 6-27: Streamlines and volume fraction of water for test 2.6 – The Demonstration Model**

The TKE-value at the outlet for test 2.6 is portrayed in figure 6-28. The TKE values are symmetrically distributed over the outlet and with highest concentration at the upper parts of the pipe. Average TKE is measured as 0.158 J/kg.

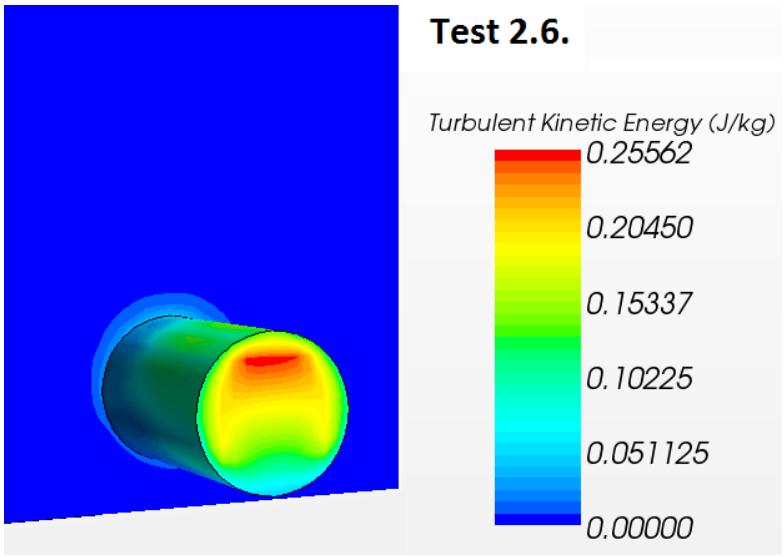


**Figure 6-28: Turbulent kinetic energy (TKE) for test 2.6 – The Demonstration Model**

The total head loss for test 2.6 is calculated as 0.016 m by using the graph displayed in figure 6-29. The water level for test 2.6 is plotted in appendix 7.

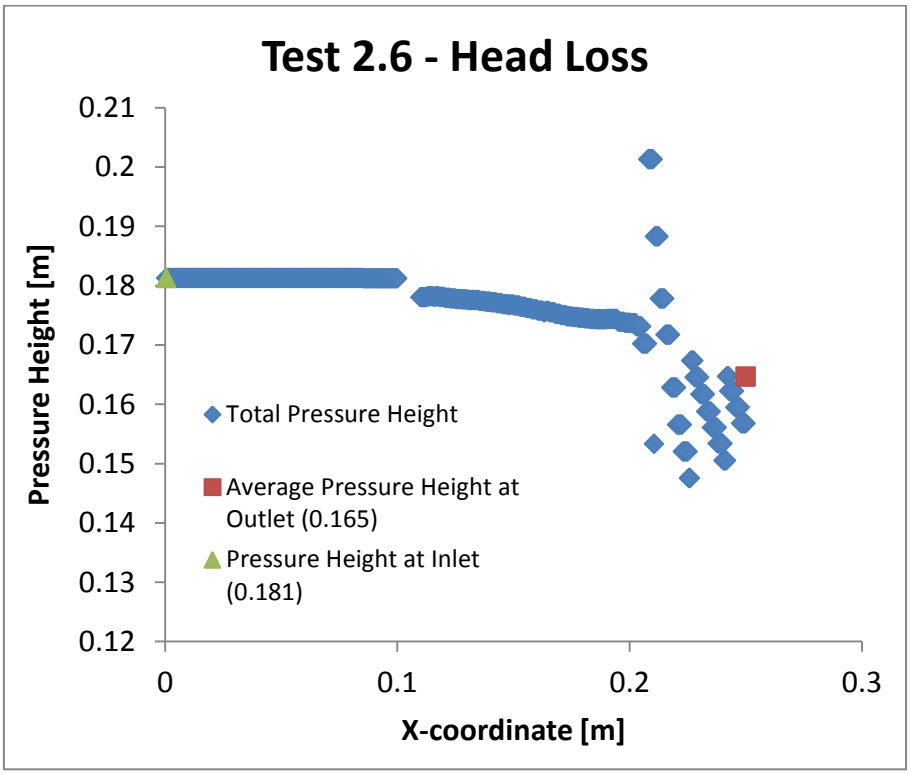


**Figure 6-29: Head loss for test 2.6 – The Demonstration Model**

### 6.3.7. Test 2.7 – The Scale Model (Long)

Test 2.7 is performed on model 4a, the Scale Model with an L/D relationship of 6. As the test simulates normal production the inlet and the outlet boundary conditions are activated. The results for test 2.7 are further portrayed here.

The streamlines in test 2.7 is portrayed in figure 6-30. The main streamlines passes through the trash rack and moves horizontally along the surface until it reaches the right wall where the streamlines bend and passes through the outlet. A slow moving secondary flow is forming by the foot of the weir on the downstream side of the model.

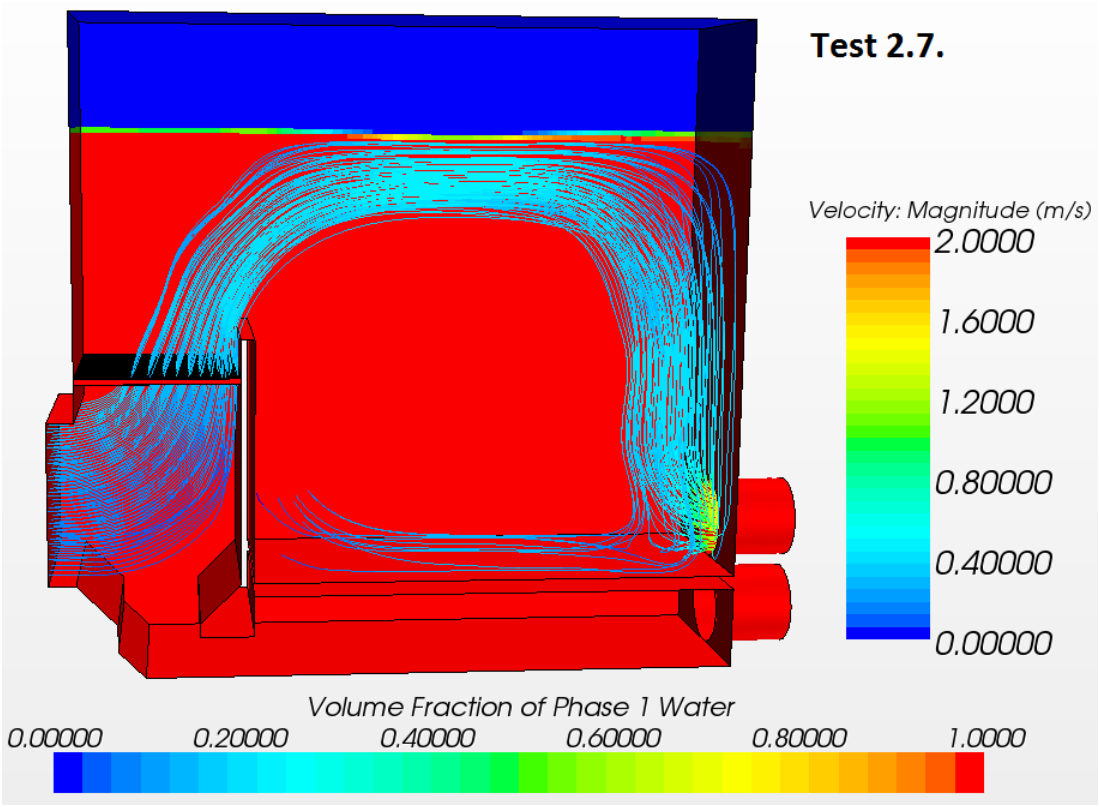


**Figure 6-30: Streamlines and volume fraction of water for test 2.7 – The Scale Model (Long)**

The TKE-value at the outlet for test 2.7 is portrayed in figure 6-31. The TKE values are symmetrically distributed over the outlet. The highest TKE-concentration is located in a confined area in the upper part of the pipe. Average TKE is measured as 0.041 J/kg.

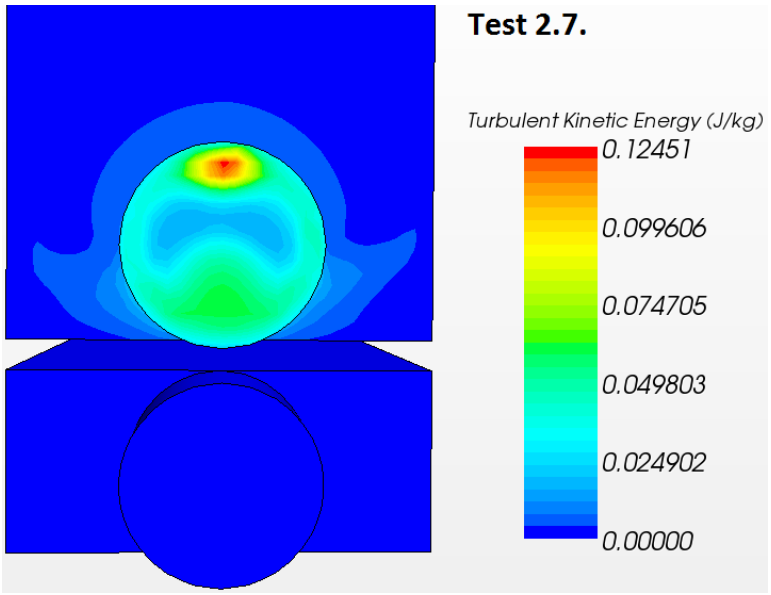


**Figure 6-31: Turbulent kinetic energy (TKE) for test 2.7 – The Scale Model (Long)**

The total head loss for test 2.7 is calculated as 0.015 m by using the graph displayed in figure 6-32.

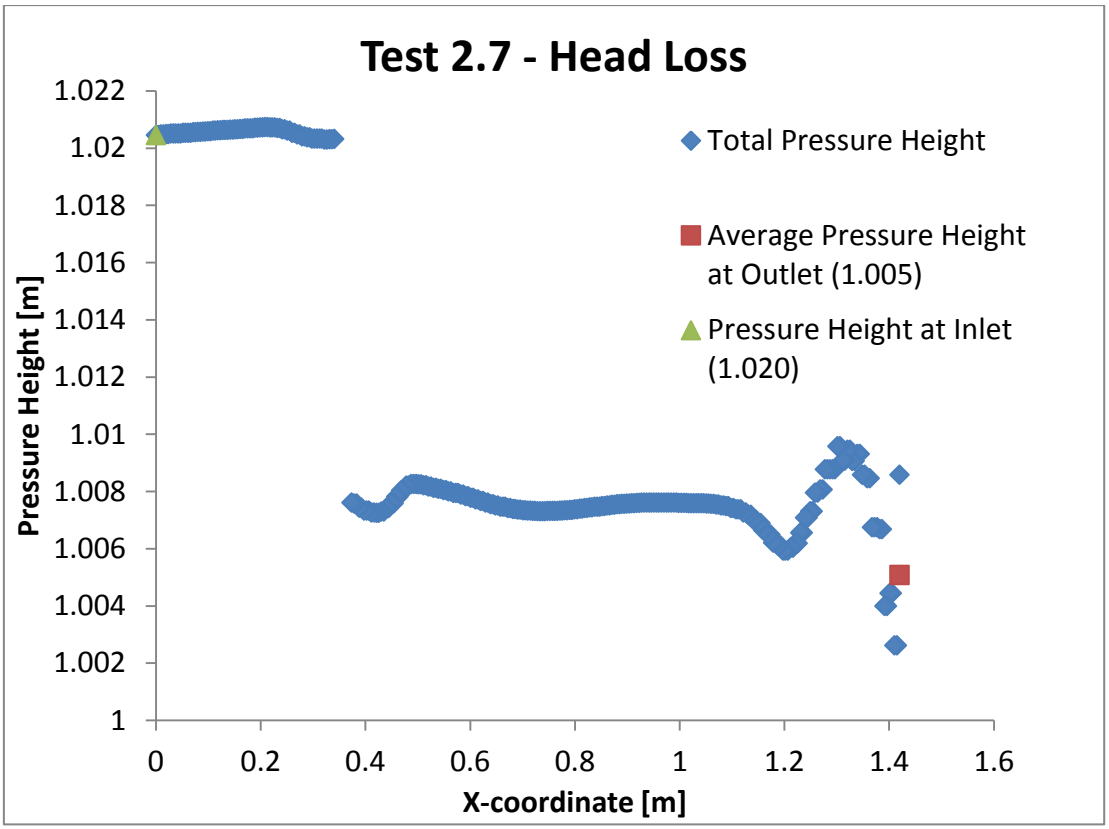


**Figure 6-32: Head loss for test 2.7 – The Scale Model (Long)**

### 6.3.8. Test 2.8 – The Scale Model (Short)

Test 2.8 is performed on model 4c, the Scale Model with a low L/D Relationship of 2. As the test simulates normal production the inlet and the outlet boundary conditions are activated. The results for test 2.8 are further portrayed here.

The streamlines in test 2.8 is portrayed in figure 6-33. The main streamlines passes through the trash rack and bend over the weir and down through the outlet to the right in the model. A recirculation zone is forming at the foot of the weir at the downstream side.

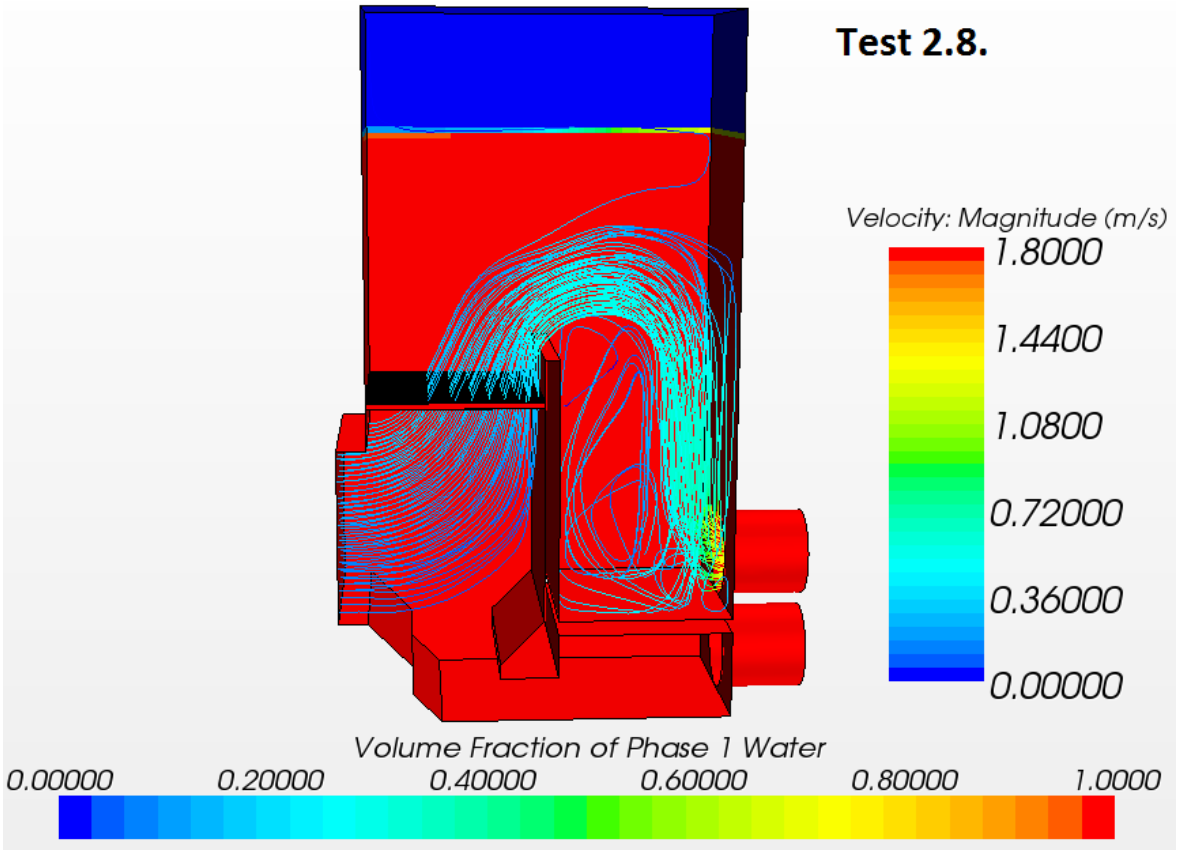


**Figure 6-33: Streamlines and volume fraction of water for test 2.8 – The Scale Model (Short)**

The TKE-values at the outlet for test 2.8 are portrayed in figure 6-34. The TKE values are roughly symmetrically distributed over the outlet. The highest TKE-concentration is located in large parts of the upper half of the pipe. Average TKE is measured as 0.115 J/kg.

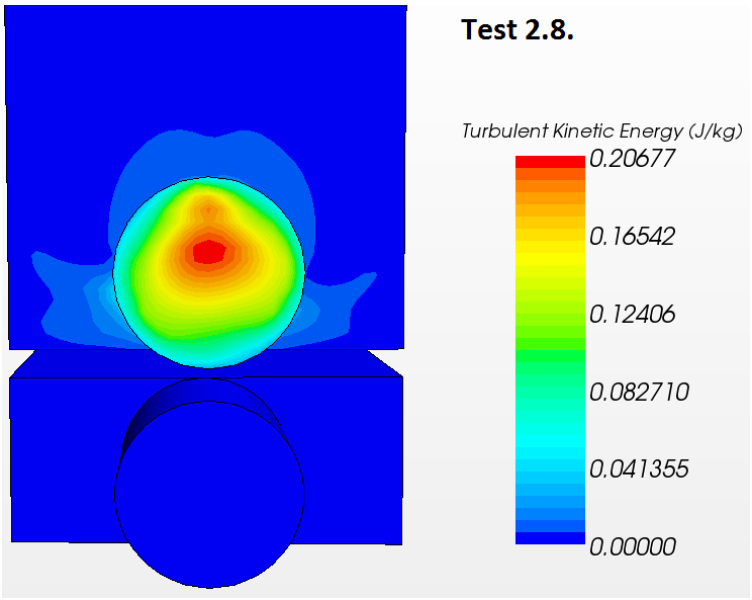


**Figure 6-34: Turbulent kinetic energy (TKE) for test 2.8 – The Scale Model (Short)**

The total head loss for test 2.8 is calculated as 0.031 m by using the graph displayed in figure 6-35.

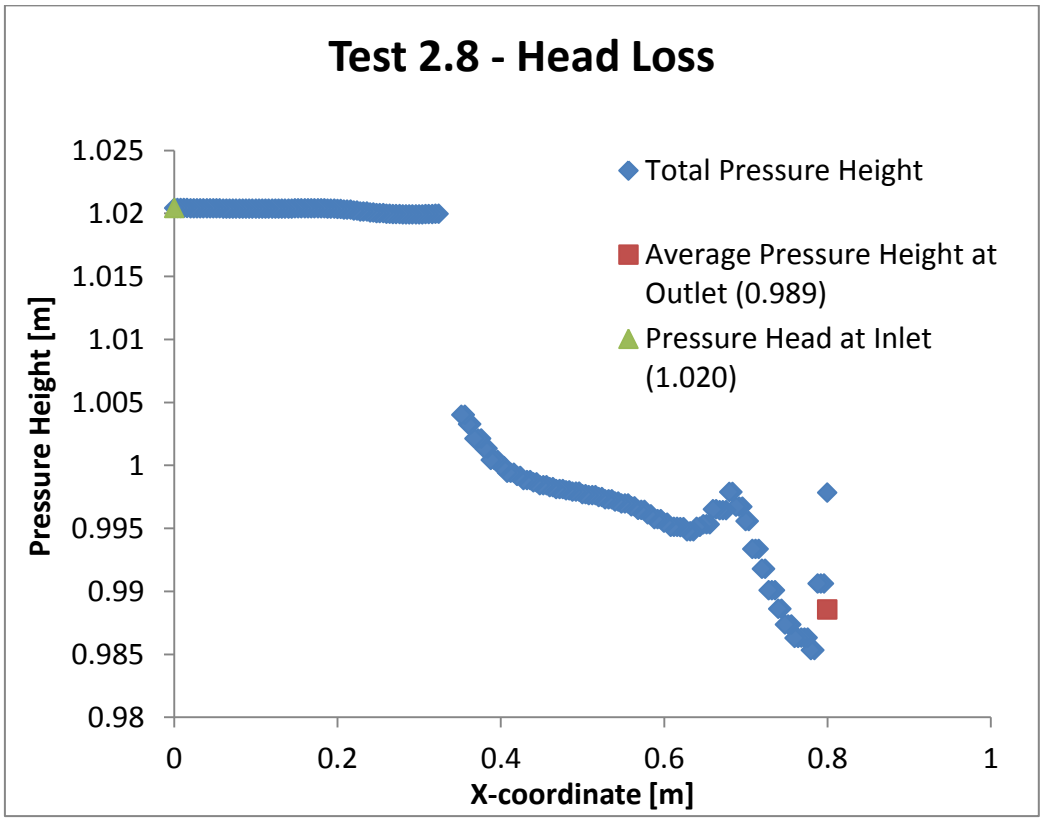


**Figure 6-35: Head loss for test 2.8 – The Scale Model (Short)**

### 6.3.9. Test 2.9 – The Scale Model (High Weir)

Test 2.9 is performed on model 4b, the Scale Model with a high weir. The test simulates normal production where the inlet and the outlet boundary conditions are activated. The results for test 2.9 are further portrayed here.

The streamlines in test 2.9 is portrayed in figure 6-36. The main streamlines passes through the trash rack and bend over the weir and follow the surface before bending down towards the outlet as they reach the right wall. A slow moving secondary flow is forming at the foot of the weir in the downstream side.

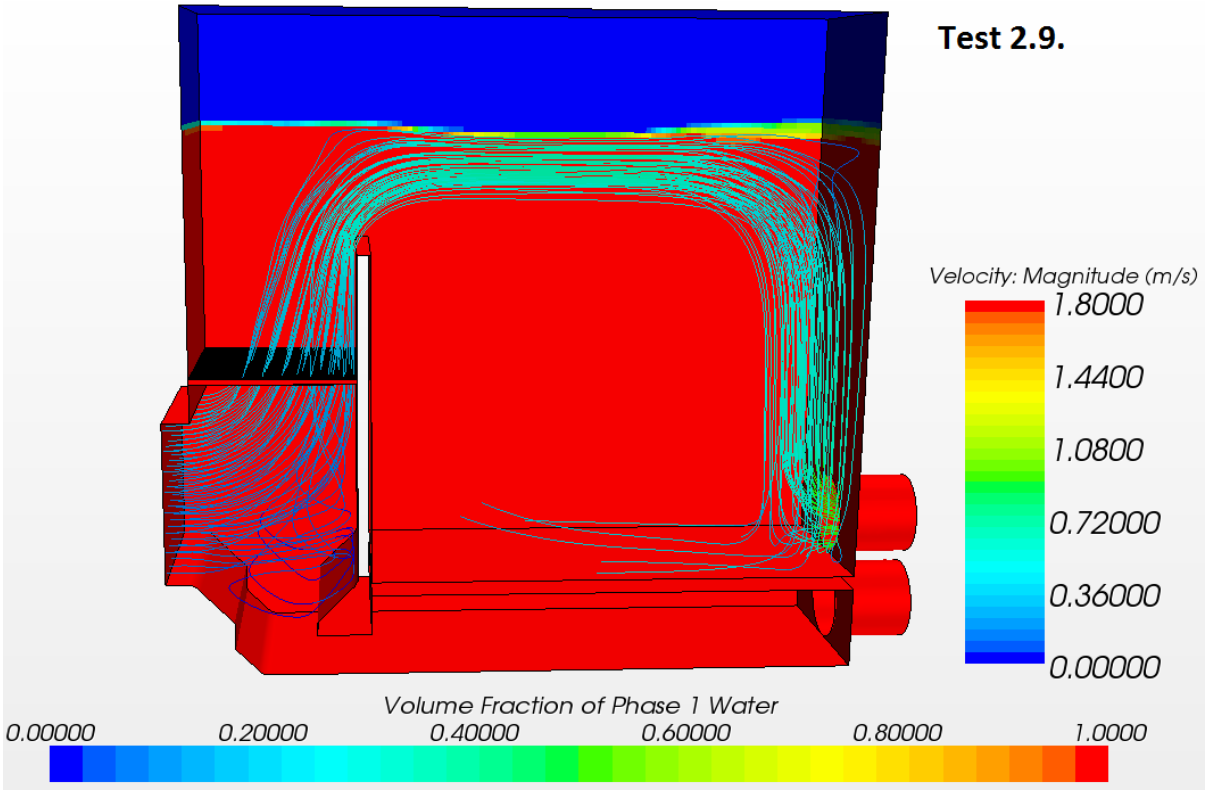


**Figure 6-36: Streamlines and volume fraction of water for test 2.9 – The Scale Model (High Weir)**

The TKE-value at the outlet for test 2.9 is portrayed in figure 6-37. The TKE values are symmetrically distributed over the outlet. The highest TKE-concentration is located in the upper parts of the pipe. Average TKE is measured as 0.074 J/kg.

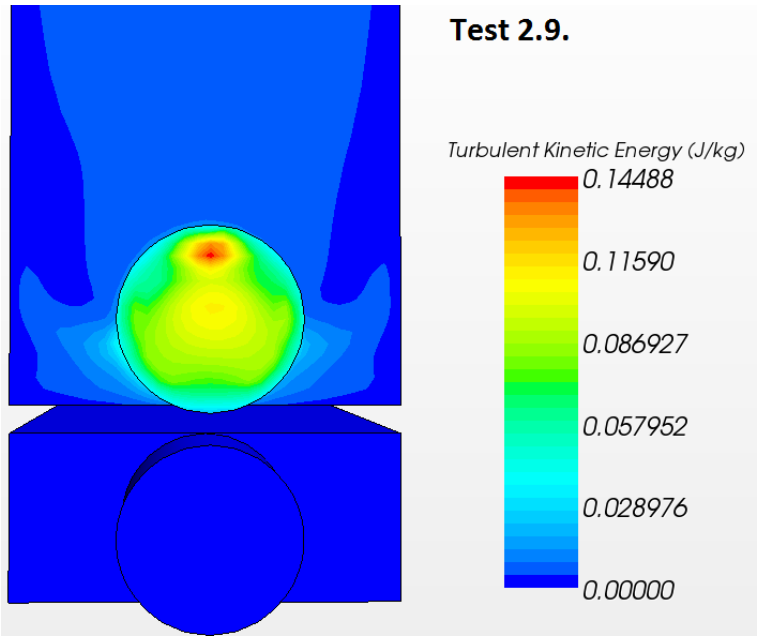


**Figure 6-37: Turbulent kinetic energy (TKE) for test 2.9 – The Scale Model (High Weir)**

The total head loss for test 2.9 is calculated as 0.017 m by using the graph displayed in figure 6-38.

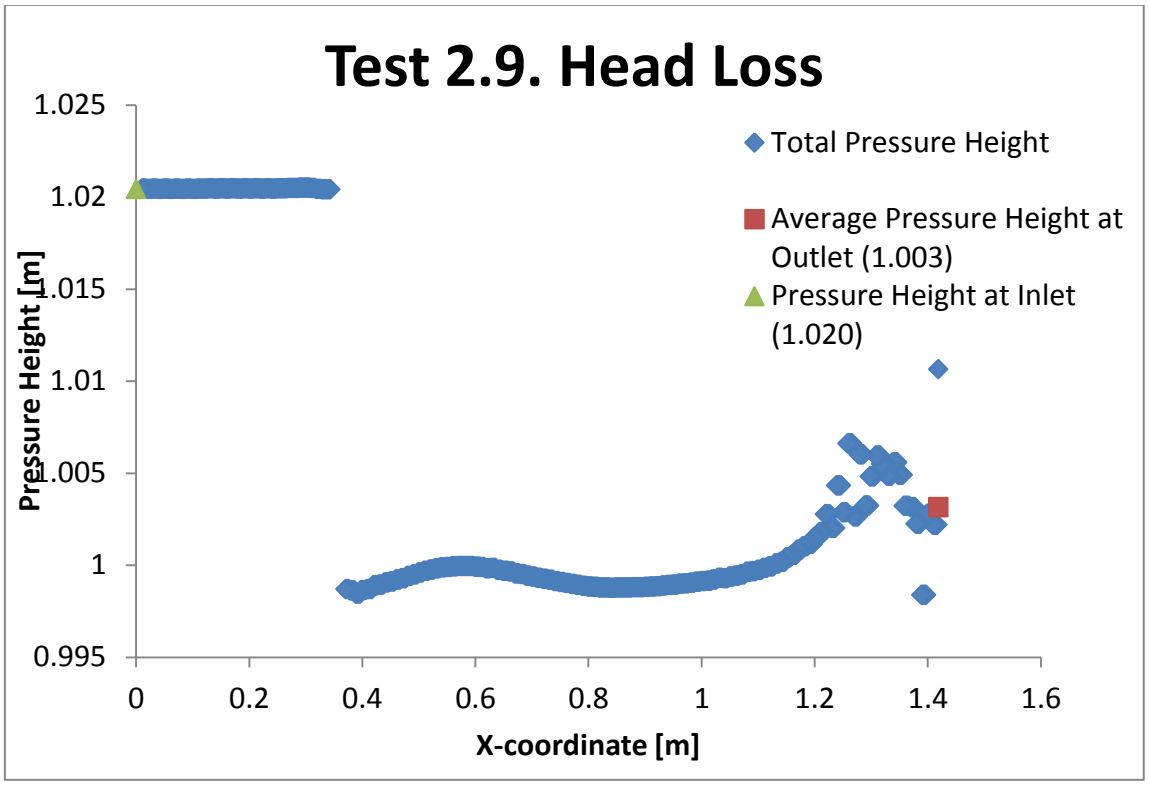


**Figure 6-38: Head loss for test 2.9 – The Scale Model (High Weir)**

# 7. Discussion

This chapter will focus on comparing the test results as well as evaluating the quality of the results. Special attention has been given to the results of the tests performed on the Scale model (model 4), due to its clear results and potential for comparison with tests performed on an identical model built in the lab. The scale model built in the lab is presented in section 7.3 and it is designed as a result of the initial testing and the simulation results. The main test parameters evaluated is the weir height ($H_R$/D), model length (L/D) and water available for flushing ($V_{OTR}$/$V_{UTR}$).

The discussion is concluded by encountering the potential, profitability and the challenges of the horizontal track rack design.

## 7.1. Back Flushing Efficiency

High flushing efficiency is achieved by ensuring a fast and equal pressure difference over the trash rack for a period of time. If the trash rack is exposed to uneven pressures at the initial flushing, it may result in a partially cleaned trash rack, because of water's nature of flowing where it meets lowest resistance through the clean areas of the rack. High energy free surface flow is also effective for detaching debris from the trash rack.

The back flushing efficiency is assessed in the One Chamber Model, the Two Chamber Model and in the Scale Model (test 1.1-1.4). The flushing velocity used for the tests are based on necessary flushing velocities described in chapter 2.6.2 when using a gross velocity of 0.5 m/s through the trash rack during normal operation. Defining a gross velocity of 0.5 m/s through trash racks during normal operation is a good starting point for design because of it often being referred to as the upper limit of recommended velocities.

The One Chamber Model and the Two Chamber Model (test 1.1 and 1.2) are both in full scale and are compared and discussed in this chapter. The back flushing tests performed on the Scale Model (test 1.3 and 1.4) are also compared and discussed, illustrating the effect of different weir heights.

**Test 1.1 and 1.2 – Comparing the One Chamber Model and The Two Chamber Model**
Test 1.1 and 1.2 have design flushing capacities of respectively 4 and 2 $m^3$/s. The design flushing capacity is different because the Two Chamber Model has two small trash racks instead of one large trash rack. When flushing, the Two Chamber Model only needs half the discharge to achieve the same velocity as the One Chamber Model. The One Chamber Model and the Two Chamber Model have equal design flushing velocities of 1 m/s over the trash rack. The flushing discharge for both tests is directly controlled by a constant value. In more realistic circumstances the flushing discharge would vary over time, starting with an acceleration phase where the discharge rises to its limits controlled by the flushing-pipe

capacity, followed by a reduction phase as the pressure height decreases when the water level sinks.

The One Chamber test (test 1.1) simulates flushing and the process lasts for about 8 seconds. The flushing process is initiated with a still surface 2.25 m over the horizontal trash rack and ends as the water level sinks below the horizontal trash rack. Test 1.1 is exposed to an uneven velocity distribution during flushing, which might cause uneven cleaning. At the flushing initiation the trash rack experiences high velocities at its edges and an average velocity of ~0.8 m/s in its central parts. 0.8 m/s is lower than the design flushing velocity, but it might just as well be sufficient for effective flushing if the velocity was uniform over the entire trash rack. As time passes and the water level sinks, more water travels from the right part of the model through the trash rack creating a concentrated flow along the weir (See Fig. 6-3 and Animation 1). The high velocities around the edges of the trash rack can be explained by the geometry of the model. Three of four sides of the trash rack are exposed to sharp edges, the overhang to the left, the overhang ensuring access for maintenance at the back and the weir to the right. The sharp edges create small vortexes which create upwards pointing velocities at confined areas over the trash rack (See Fig. 6-2, 6-3 and 6-4).

The Two Chamber test (test 1.2) differs from the One Chamber test by using a two chamber design with a stationary water level. The two chamber model makes it possible to continue power production (reduced production) leaving one inlet gate open while back flushing one trash rack at the time. The water level is simulated to be stationary by assuming that the open inlet gate can carry forward the needed water for both flushing and power production. In reality, the inertia of water will result in a local reduction of the water level due to the rapid and high flushing discharge. The water-level appears to be disturbed due to the complex water flow pattern and the intensity of the water flow (See Fig. 6-5). The velocity distribution over the trash rack does not change significantly over time when the simulation has reached convergence and mass balance (See Fig. 6-5). The mass flow plot indicates that the simulation has reached sufficient balance after 30 000 iterations (See Appendix 5). A sufficient balance is achieved when the line-plot defining the sum of all mass flows, in and out of the model, converges towards 0 with low oscillations.

**Table 7-1: Back flushing efficiency and model parameters for the One Chamber and Two Chamber test**

| Test | Model | Initial Water level [m] | Back Flushing Efficiency | Model Parameters | | |
|---|---|---|---|---|---|---|
| | | | | L/D | $H_R/D$ | $V_{OTR}/V_{UTR}$ |
| 1.1 | One Chamber | 5 | Uneven | 2.25 | 3.19 | 1.55 |
| 1.2 | Two Chamber | 6 | Less uneven | 2.7 | 2.15 | 2.27 |

Table 7-1 illustrates the test results compared with the model parameters. The flushing efficiency is hard to differentiate between the One Chamber and the Two Chamber test.

**Test 1.3 and 1.4 – Comparing Weir Heights in the Scale Model**

Test 1.3 and 1.4 are performed on the Scale Model with a design flushing discharge of 41 litre/s and a design flushing velocity over the trash rack of 0.39 m/s. The flushing discharge is controlled using pressure outlet as the outlet boundary condition. A pressure outlet is used for accomplishing a more realistic mass flow. The mass flow plot of test 1.3 and 1.4 indicates that the design flushing discharge is reached after only 0.25 seconds (See Appendix 5). The only difference between test 1.3 and 1.4 is the height of the weir. The distance between the trash rack and the weir top is 150 mm higher in test 1.4 than in 1.3, which equals the diameter of the outlet pipe.

The meaning of testing low and high weirs was to identify how different weir heights impact the velocity distribution over the trash rack during back flushing. The results are very clear showing that the weir height does matter when it comes to velocity distribution over the trash rack. A high weir achieves more even velocities within the first second of back flushing than a similar test with a low weir.

The animation of the low weir test (test 1.3) gives us a clear image of the change in velocity distribution and the duration of the process (See animation 2). The process of back flushing in test 1.3 took about 4 seconds from start, with an initial water level 400 mm over the trash rack, to end as the water level sinks below the trash rack. The direction of the velocities is also presented in the results to clarify the flow directions and recirculation zones (See Fig. 6-6, 6-7, 6-8). As presented in the results a recirculation zone is developing by the weir in test 1.3 as the water level sinks. After 1.50 seconds a quarter of the trash rack experiences velocities in the wrong (upward) direction. As time passes more of the trash rack is exposed to the developing recirculation zone, resulting in greater areas exposed to velocities facing the wrong direction working against the effects of back flushing.

An animation of the high weir test (test 1.4) is also presented, displaying the change of velocities over the trash rack (See Animation 3). The duration of the back flushing process in the high weir test is shorter than in the low weir test due to less water available because of the higher weir. The back flushing process in the high weir test took about 3 seconds to finish, starting with an initial water-level 250 mm over the trash rack and ending when the water level is lowered below the trash rack. Design flushing discharge is reached after just 0.25 seconds and the velocity over the trash rack is perfectly even within the first second with a value of ~0.42 m/s (See Fig. 6-9). It is interesting that the simulation catches the creation of a free surface flow moving from left to right over the trash rack as the water level sinks, resulting in high velocity areas effective for detaching debris (See Fig. 6-10, 6-11). The low weir test does not experience the same extent of free surface flow due to its low weir.

**Table 7-2: Back flushing efficiency and model parameters for the Scale Model with low and high weir**

| Test | Model | Initial Water level [m] | Back Flushing Efficiency | Model Parameters | | |
|---|---|---|---|---|---|---|
| | | | | L/D | $H_R/D$ | $V_{OTR}/V_{UTR}$ |
| 1.3 | Scale Model (Low Weir) | 1 | Continuously uneven velocity | 6 | 3 | 3.94 |
| 1.4 | Scale Model (High Weir) | 1 | Even velocity during initiation | 6 | 4 | 2.40 |

Table 7-2 illustrate the back flushing efficiency compared to the model parameters for the tests with low and high weir in the Scale Model. Better back flushing efficiency is achieved with higher $H_R/D$ relationship as long as the water level assures enough water available for flushing.

## 7.2. Hydraulic Performance during Normal Operation

The concept of using back flushing with horizontal trash racks has to work efficiently both during flushing and under normal operation in order to function as an adequate intake construction. The hydraulic performance during normal power production is assessed here by presenting and comparing the test results. The test results during normal operation is presented in table 7-3, displaying head loss, initial water level, TKE and the model parameters.

**Table 7-3: Test results during normal operation**

| Test | Model | Head Loss [m] | Initial Water-level [m] | Head Loss [%] | TKE-Average [J/kg] | Model Parameters | | |
|---|---|---|---|---|---|---|---|---|
| | | | | | | L/D | $H_R/D$ | $V_{OTR}/V_{UTR}$ |
| 2.1 | 1. One Chamber | 0.143 | 5 | 2.9 | 0.698 | 2.25 | 3.19 | 1.55 |
| 2.2 | 2a.Two Chamber | 0.008 | 6 | 0.1 | 0.139 | 2.7 | 2.15 | 2.27 |
| 2.3 | 2a.Two Chamber | 0.032 | 4.5 | 0.7 | 0.150 | 2.7 | 2.15 | 0.88 |
| 2.4 | 2b. Two Chamber | 0.034 | 6 | 0.6 | 0.182 | 2.7 | 2.15 | 2.27 |
| 2.5 | 2c. Two Chamber | 0.018 | 6 | 0.3 | 0.310 | 2.7 | 2.15 | 2.27 |
| 2.6 | 3.Demonstra-tion Model | 0.016 | 0.18 | 8.9 | 0.158 | 3.3 | 3 | 1.32 |
| 2.7 | 4a. Scale Model | 0.015 | 1 | 1.5 | 0.041 | 6 | 3 | 3.94 |
| 2.8 | 4c. Scale Model | 0.031 | 1 | 3.1 | 0.115 | 2 | 3 | 1.31 |
| 2.9 | 4b. Scale Model | 0.017 | 1 | 1.7 | 0.074 | 6 | 4 | 2.40 |

**Test 2.1 – The One Chamber Model**
Test 2.1 is performed on the One Chamber model with a design discharge of 2 $m^3/s$. Because of the model's lack of hydraulic design and its low L/D relationship the test suffers high head losses and high TKE values compared to the other tests (See Table 7-3).

**Test 2.2 – The Two Chamber Model**
Test 2.2 is performed on the Two Chamber Model with a design discharge of 2 $m^3/s$. The result from the Two Chamber model may be compared with the results from the One Chamber model due to its similar design discharge and equal trash rack area. Test 2.2 has a higher L/D relationship than test 2.1 and the head loss and TKE-values are much lower in comparison with test 2.1 (See Table 7-3). Why the head loss in test 2.2 is so extremely small is discussed in section 7.3.

**Test 2.3 – The Two Chamber Model (Low Water Level)**
Test 2.3 is performed on the same model as test 2.2, the Two Chamber Model, but with a lower water level resulting in a low $V_{OTR}/V_{UTR}$ relationship of 0.88. The water surface is located 2 m above the top of the outlet pipe, which is just within the limit of necessary submerging (using equation 2-4 and 2-5).The measured head loss and TKE-values for test 2.3 show that a lower water level increases both head loss and TKE-values (See table 7-3). A lower water level reduces the available vertical flow area over the trash rack resulting in higher velocities and velocity changes and therefore also higher energy losses. The surface interface is also less defined in the low water level test (test 2.3) than in the test 2.2 which most likely is a result of higher local velocities (See Fig. 6-15 and 6-18). Another explanation of the less defined surface interface might be lack of mass balance due to a lower number of performed iterations for test 2.3. This explanation is easy rejected when comparing the mass balance plot for both tests show that both tests are equally converged (See Appendix 5).

**Test 2.4 – The Two Chamber Model (with Trash Rack)**
The model used for test 2.4 is the same as in test 2.2 but it includes a modeled trash racks. The idea behind simulating with and without the trash rack was to identify the isolated head loss through the horizontal trash rack. The difference between the total head loss for test 2.2 and 2.4 gives us a local head loss of 0.024 m over the trash rack. There is off course uncertainties in this approach in terms of the quality of the numerical result. The measured head loss through the trash rack is therefore compared with the head loss calculated using Kirschmer-Mosonyis formula. The Kirschmer-Mosonyis formula is presented in chapter 2.3 and equation 2-1.

The head loss over the trash rack is calculated as 0.0045 m by using the Kirschmer-Mosonyis formula. The calculated head loss using Kirschmer-Mosonyis formula is 5 times smaller than the head loss calculated using the numerical results, which indicates that the numerical head loss measurements are imprecisely measured. The geometry, the gross velocity over

the trash rack and the average flow angle over the trash rack (*α)* were used as inputs in the Kirschmer-Mosonyis approach.

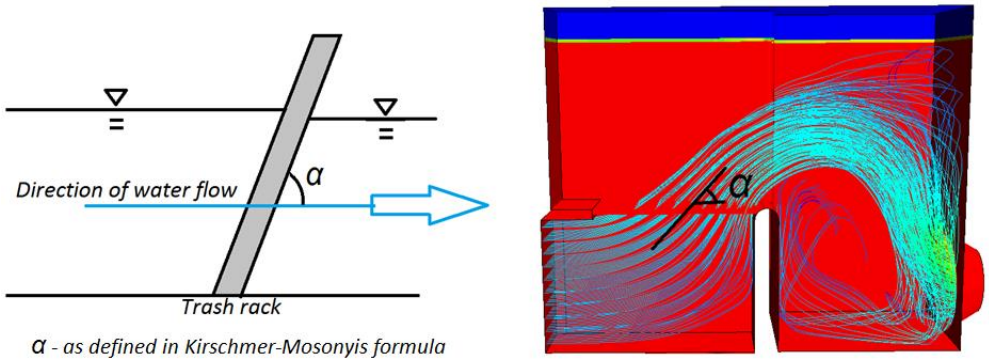


**Figure 7-1: Determination of the angle *α* in test 2.4 – The Two Chamber Model**

Figure 7-1 illustrates the analog qualities for the angle between the trash rack and the horizontal plane (to the left) and the angle between the average flow direction and the trash rack (to the right). Appendix 8 presents how the head loss varies depending on the angle *α.* The angle (*α)* is valued as 40 degrees for test 2.4.

**Test 2.5 – The Two Chamber Model (with Modified Weir)**

Test 2.5 is the fourth and last test performed on the Two Chamber Model. The goal of test 2.5 was to identify how much energy loss is caused by the recirculation zone emerging by the foot of the weir in the other Two Chamber tests (test 2.2, 2.3 and 2.4). The recirculation zone was eliminated by modifying the weir (See Fig. 6-24). However, the total head loss is higher than the head loss in the original model (test 2.2). By analyzing the streamlines for test 2.5, some disturbance in the water flow is located underneath the trash rack by the flushing outlet. The increased head loss for test 2.5 may be explained by or a combination of the disturbance developing by the flushing outlet, flow variations over time, the modified weir itself or faulty numerical results. The TKE-values are also high and asymmetrical, most likely because of the disturbance created at the flushing outlet which propagates through the model.

**Test 2.6 – The Demonstration Model**

Test 2.6 is performed on model 3, which is identical to the small demonstration model which has been built and is displayable in the lab. Test 2.6 was performed in order to identify the similarities between the streamlines in the real model and in the numerical model. The comparison between the real and the numerical model is discussed in the following section, section 7.3. By analyzing the streamlines in test 2.6 it is concluded that there is a recirculation zone downstream the weir similar to the previous tests (See Fig. 6-27). TKE-values and total pressure are measured 10 cm inside the outlet pipe in order to achieve more steady measurements. The previous tests, the tests performed on the One Chamber Model and the Two Chamber Model, are modeled with only a short pipe socket which might explain the unsteady head loss measurements.

**Test 2.7 and 2.8 – Identifying the importance of the L/D relationship**

Test 2.7 simulates streamlines, head loss and TKE-values during normal operation for the stretched edition of the Scale Model. The model has a length between the weir and outlet (L) of 900 mm resulting in a high L/D relationship. The streamlines in test 2.7 does not bend down towards the outlet before it meets the right wall of the model, similar to the shorter models (See Fig. 6-30). The simulation is ran for 16 physical seconds and 64 000 iterations, yet the recirculation zone has not completely emerged. The total head loss for test 2.7 appears to be more accurate than the extremely low head loss measured for the Two Chamber Model (See table 7-3). The reason for a more accurate head loss measurement in the Scale Model might be because of the longer outlet pipe ensuring better conditions for measuring the average pressure height.

Test 2.8 simulates the short edition of the Scale Model during normal operation, with a length between the weir and the outlet (L) of 300 mm resulting in a low L/D relationship. The streamlines in test 2.8 show that the flow does not move along the surface as for test 2.7 due to the short length of the model (See Fig. 6-33). The simulation is ran for 16 seconds and 64 000 iterations and sufficient mass balance is achieved (See Appendix 5).

Test 2.7 is directly comparable with test 2.8 and the comparison identifies the difference in hydraulic performance between a long and a short model. The change in flow direction is higher in the short model (test 2.8) than in long model (test 2.7) due to the length difference, which also creates higher turbulence and energy loss. The comparison between test 2.7 and 2.8 is presented in table 7-4 which also includes the important model parameter L/D.

**Table 7-4: Results of test 2.7 and 2.8 including the L/D relationship**

| Test | Head Loss (m) | Head Loss Full scale (m) | Head Loss (%) | TKE-Average | L/D | $H_R/D$ | $V_{OTR}/V_{UTR}$ |
|---|---|---|---|---|---|---|---|
| **2.7** | 0.015 | 0.10 | 1.5 | 0.041 | 6 | 3 | 3.94 |
| **2.8** | 0.031 | 0.21 | 3.1 | 0.115 | 2 | 3 | 1.31 |

The length of the model does afflict the head loss as predicted. The head loss is twice as high in test 2.8 compared with test 2.7. The head loss is also calculated as percentage of the initial water depth and in full scale as the tests are performed on a 1:6.67 scaled model. The profitability behind choosing a long versus a short construction is further adduced in chapter 7.4.

**Test 2.7 and 2.9 – Identifying the importance of the $H_R$/D relationship**

Test 2.9 simulates the streamlines, head loss and TKE-values for the stretched edition of the Scale Model and with a higher weir than in test 2.7. The weir in test 2.9 is 150 mm (D) higher than in test 2.7. The flow in the test with high weir (test 2.9) is more concentrated along the surface than in the test with low weir (test 2.7) (See Fig. 6-30, 6-36). The concentrated flow in test 2.7 is also disturbing the surface interface; especially in the right end of the model.

**Table 7-5: Results of test 2.7 and 2.9 including the $H_R$/D relationship**

| Test | Head Loss (m) | Head Loss Full scale (m) | Head Loss (%) | TKE-Average | L/D | $H_R$/D |
|---|---|---|---|---|---|---|
| **2.7** | 0.015 | 0.10 | 1.5 | 0.041 | 6 | 4 |
| **2.9** | 0.017 | 0.11 | 1.7 | 0.074 | 6 | 3 |

There are small but noticeable differences between head loss and TKE when comparing different $H_R$/D relationships in test 2.7 and 2.9 (See Table 7-5). As previously stated, a high weir results in better flushing efficiency. Because the increase in head loss is as low as stated in table 7-5 it is still recommended to introduce a high weir in overall.

## 7.3. The Reliability of the Numerical Results and Further Testing

The numerical results in this study are most likely to have some sort of error, as error and uncertainties are common in CFD-modeling. Based on the results of the tests performed in this study, the most important factors for achieving good numerical results are the grid resolution, the degree of mass balance and convergence and a realistic numerical setup. The best way of validating numerical results is to perform similar tests on physical models.

**Comparing CFD (test 2.6) with the physical Demonstration model**

As presented in the results, streamline and water level tests were performed on the physical Demonstration Model in order to validate the results in test 2.6.

The streamlines in the physical test proved to be fairly similar to the streamlines in the numerical simulation. The only difference between the streamlines is the occurrence of a small secondary flow as the water flow reaches the upstream wall of the weir (See Fig. 6-1). Why the secondary flow at the upstream wall of the weir is absent in the numerical result might be of casual causes or by numerical flaws. The placement of the origin of the streamlines in test 2.6 might be one of the casual reasons why the secondary flow is absent. A finer grid and more iterations may result in more precise streamlines and better measurements in general.

The head loss in the physical model was hard to define as the measured water level by the outlet was (in average) 0.3 mm higher than upstream the intake (See Fig. 6-1). Therefore, the water level was measured directly at several points in the physical model and compared with the water level in the numerical model (See Appendix 7). By the outlet in the numerical model, the water level is measured as 1.6 mm lower than initial water level, which is far from the physical result. The difference between the numerical and the physical result is not easily explained. There are also low coexistences between the measured head loss and the water level by the outlet in the numerical model or in the physical model. Based on the numerical and physical test results of the Demonstration Model, it is often hard to establish the exact head loss in the system by assessing the water level alone.

**Further Testing in Lab**

The numerical tests performed on the Scale Model assessed the back flushing efficiency as well as the hydraulic performance during normal operation by looking at different model parameters. The different model parameters tested are the length of the lower chamber, the height of the weir and the volume of water available for back flushing. In order to validate the result of the numerical simulations and for running more tests with different model parameters, it has been chosen to build a physical model similar to the Scale Model used for test 1.3, 1.4, 2.7, 2.8 and 2.9. The physical model is built in the hydraulic lab at the Department of Hydraulic and Environmental Engineering and the testing is to be performed in immediate future. The geometry and design of the scale model as well as a test program for the scale model are further described here.

The geometry of the physical model is based on the CFD-simulations performed in this study where important model parameters have been identified. The design of the physical model is presented in appendix 9 and a photo of the almost complete model is presented in appendix 10. The model is scaled 1 to 6.67 using Froude similarities and is based on the available outlet pipes in the lab and common velocities in penstocks and over the trash rack for small hydro power plants (See Appendix 10). The model is designed with notice on the need of performing tests with different model parameters, which means varying geometry. The intake construction itself varies in length between 0.60 m and 1.20 m. The model includes a reservoir to ensure steady inflow to the intake construction. The total height of the model is 1.20 m.

The test program for the physical model is presented in table 7-6.

**Table 7-6: Test program for the physical model built in the lab**

| **Main tests:** | **Sub tests:** | **$Q_{Production}$** | **$Q_{Flushing}$** |
|---|---|---|---|
| **A**. Measuring head loss during normal operation | **1.** L1* position with varying height of the weir | 20,5 l/s | - |
| | **2.** L2* position with varying height of the weir | 20,5 l/s | - |
| | **3.** L3* position with varying height of the weir | 20,5 l/s | - |
| | **4.** Vertical trash rack comparison | 20,5 l/s | - |
| **B**. Measuring back flushing efficiency | **1.** Flushing efficiency with varying height of the weir and trash rack | - | 20 - 40 l/s |

*L1, L2 and L3 describe the length of the model as displayed in the drawing of the physical model in appendix 9.

The tests are divided in two main groups, measuring head loss during normal operation (A) and measuring back flushing efficiency (B). The first 3 sub tests in test A measure head loss with varying lengths of the model and height of the weir. Test A4 measure head loss by installing the trash rack vertically in the position of the weir for comparison purposes. Test B1 measure the back flushing efficiency by varying the height of the weir as well as the position of the trash rack. Each sub test should be performed with at least 3 different weir heights to establish the changes in head loss and flushing efficiency. The production and flushing discharges are based on Froude similarity scaling (See Appendix 11). The head loss is measured by a laser logging the water level or by pressure sensors in the outlet pipe if necessary. The back flushing efficiency is best measured by applying debris to the trash rack and visually monitoring the flushing progress.

## 7.4. Potential, Profitability and Challenges for the Horizontal Trash Rack Concept

There are obvious advantages in the use of the horizontal trash rack concept. The concept eliminates the need of manual labour for trash rack cleaning and flushing can be remotely controlled whenever needed. However, there are some challenges to cope with.

**Potential for the horizontal trash rack concept**

The horizontal trash rack concept has its main potential of use in small run of the river power plants where the load of debris is high. Back flushing is a good substitute to manual cleaning of the trash rack not only considering its possibilities of being remotely controlled, but also by increasing the safety of service. The horizontal trash rack concept may be used in future headworks design. In existing headworks where debris is causing problems and high costs, it is believed that modules of the horizontal trash rack concept may be directly installed in front of the existing intake or next to it.

**Profitability**

The head loss difference between test 2.7 and 2.8, a long and a short model, was only measured as 0.016 m (See Table 7-4). The corresponding full scale head loss would be 0.11 m (as the model is scaled 1:6.67). The total lengths of the short and long model are 0.60 m and 1.20 m equivalent to 4 m and 8 m in full scale. The question raised is if it is feasible building a long model when the head loss change is only 0.11 m. A model with moderate length, somewhere between test 1.3 and 1.4, might be a more suitable design.

It is obvious that the water used for flushing is water lost for production and therefor has a given value. The value of the flushing water depends on the amount and its potential energy. The water amount used for flushing will vary depending on the design. If we use the stretched model in test 1.4 as an example, the maximum water available for flushing would be equivalent to 50 $m^3$ with a flushing duration of about 15 seconds in full scale (See Appendix 11). If the power plant is designed with discharge capacity of 2 $m^3/s$ and a pressure head of 100 meters the corresponding value of the flushing water would not exceed more than 4.5 NOK (using turbine and generator efficiency of 86% and 95% and 0.40 NOK/KWh). In addition to the water value there is lost production time, start up and shut down time of the aggregate. The costs per flushing might be compared to the costs of performing one manual clean of the trash rack. If the intake is remotely placed and manual labour is scarce the costs of one cleaning process might well exceed several hundred NOK. Intakes having frequent problems with clogging of the trash rack may experience huge cost reduction by using the concept of back flushing.

**Challenges**

When designing a full scale intake using the horizontal trash rack concept there is several aspects to consider. The design of the trash rack itself, the design of the inlet gate, the design of the flushing gate/valve and maintenance and access are some aspects to consider.

The horizontal trash rack must be carefully designed to ensure it will withstand the forces of the water especially during flushing. The worst case scenario is during flushing where the trash rack is fully clogged resulting in full water pressure above the trash rack and low pressure under. Using the Scale Model and the physical model built in the lab as an example, the equivalent water pressure against the trash rack in a full scale intake would be approximately 40KPa (4 tons per $m^2$).

The inlet gate in a one chamber design of the horizontal trash rack concept is closed during flushing. The design force on the inlet gate is full water pressure at the external side and atmospheric pressure at the inner side.

The flushing gate or flushing valve has to open as fast as possible to ensure efficient flushing by exploiting the high initial pressure difference over the trash rack. The flushing gate is limited by the opening speed and strength. A smaller flushing pipe, compensated by increasing the drop, might open opportunities for usage of a globe-valve. A globe-valve might be more suitable than a gate in forms of opening speed and strength.

The intake must be designed in a way that ensures access to every construction part requiring maintenance. Access to the area between the trash rack and the flushing outlet would be critical, in order to perform maintenance on the trash rack, removing debris clogging the flushing gate or just general maintenance on the inlet gate from the inside. Access might be given by installing a hatch on a ledge level to the trash rack or simply through the weir. Entering the intake should be done from the roof through a hatch, as most of the exterior walls are surrounded by water.

# 8. Conclusions

This study has concentrated on using CFD-modelling as a tool to evaluate the performance of an intake design using the concept of back flushing with a horizontally fixed trash rack.

Several numerical tests have been performed on different models and important model parameters have been revealed. The model parameters affecting the flushing efficiency and the hydraulic performance during normal production is the height between the weir and the trash rack, the vertical position of the trash rack and the length between the weir and the outlet.

A high weir results in an even velocity distribution over the trash rack during the initiation of the flushing. As the water level is reduced a free surface flow over the trash is created using a high weir. Even velocities and creation of free surface flows are both effective for detaching clogged debris on the trash rack. A high weir will also increase the head loss and TKE-values during normal operation.

The vertical position of the trash rack decides how fast debris is transported to the flushing outlet and downstream back to the natural run of the river. A lower placed trash rack results in faster and more effective flushing due to higher water pressure and more water available for flushing.

The length between the weir and the outlet affects the head loss and the TKE-values measured at the outlet, where a longer design reduced both head loss and TKE. By comparing two models where one of them are 3 times as long, the resulting head loss is 50% less in the long model.

The numerical results are preferred to be validated by comparing with physical models. A demonstration model has been built in this study and compared with a numerical model. The result of the comparison shows that the numerical model managed to imitate the streamlines of the physical model.

Further research should include testing the back flushing efficiency and the hydraulic performance of the scale model built and designed in this study. The test program for the scale model is presented in this study. The goal of the test program is to identify the optimum limits between height of the weir and length of the model by looking at model performance during both flushing and normal production.

# 9. References

Aune, E.R. (2011) *Inntak Viddal – Hydraulisk utforming av inntak med tilbakespyling.* Master-Thesis. NTNU, Department of Hydraulic and Environmental Engineering.

CD-Adapco. (2012) *User Guide – STAR CCM+Version 7.04.006*

Courant, R., Friedrichs, K., Lewy, H. (1967) *On the Partial Difference Equations of Mathematical Physics.* IBM Journal of Research and Development.

Durbin, P.A., Petterson Reif, B.A. (2011) *Statistical Theory and Modelling for Turbulent Flows, Second Edition.* John Wiley & Sons, Ltd.

Ferziger, J.H. & Peric, M. (2002). *Computational Methods for Fluid Dynamics.* Springer-Verlag.

Fladen, B., Holmqvist, E., Bachke, D., SWECO Norge. (2010) *Veileder i planlegging, bygging og drift av små kraftverk.* NVE.

Gotvassli, I. (2012) *Kartlegging av heft mellom drivgods og inntaksrista.* Project-Thesis. NTNU, Department of Hydraulic and Environmental Engineering.

Guttormsen, O. (1989). *Vassdragsteknikk II.* NTNU, Department of Hydraulic and Environmental Engineering.

Holmeset, F. (2012) *Numerisk modellering av intakshydraulikk på Furset kraftverk*. Project-Thesis. NTNU, Department of Hydraulic and Environmental Engineering.

Jenssen, L., Tesaker, J., Lund, S., Huber, D., Støle, H. (2006) *Inntakshåndboken.* NVE.

NVE, 2013. *Rekordmange konsesjoner i 201*2 [Online], Available: http://www.nve.no/no/Nyhetsarkiv-/Pressemeldinger/Rekordmange-konsesjoner-i-2012-/ [Accessed 05.06.2013]

Johnson, P.L. (1988). *Hydro-Power Intake Design Considerations*. ASCE

Jørstad, O.A. (2010) *Bergedammen – Verifisering av selvrensende inntak.* Master-Thesis. NTNU, Department of Hydraulic and Environmental Engineering.

Knauss, J. (1987) *Swirling Flow Problems at Intakes.* Hydraulic Structures Design Manual. Rotterdam, Balkema.

Lysne, D., Glover, B., Støle, H., Tesaker, E. (2003). *Hydraulic Design*. NTNU, Department of Hydraulic and Environmental Engineering.

Mesa Associates Inc, Oak Ridge National Laboratory (2011) *Best Practice Catalog – Trash Racks and Intakes.* U.S. Department of Energy.

Nøvik, H., Jørstad, O.A. (08.03. 2011) *Tilbakespyling – En alternativ renskemetode for varegrinder?* [Online], Available: http://www.energinorge.no/getfile.php/FILER/KALENDER/Foredrag%202011/PTK2011/Tirsdag_Sesjon_A/05_2011-03-08_PTK_Novik_og_Jorstad.pdf [Accessed 10.04.2013]

Nøvik, H., Lia, L., Jørstad, O.A. (2011) *Back Flushing of Trash Racks at Intakes to Small Hydro Power Plants.* NTNU, Department of Hydraulic and Environmental Engineering.

Olsen, N. R. (2011) *Numerical Modelling and Hydraulics.* NTNU, Department of Hydraulic and Environmental Engineering.

# Appendix 1 – The Demonstration Model

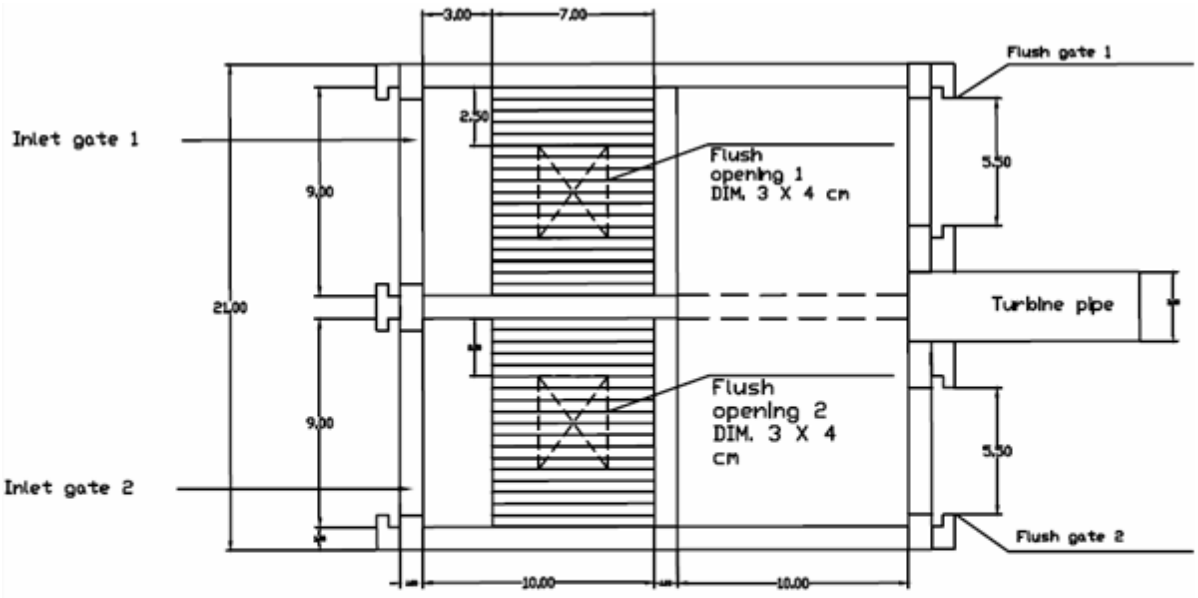


Horizontal Plane

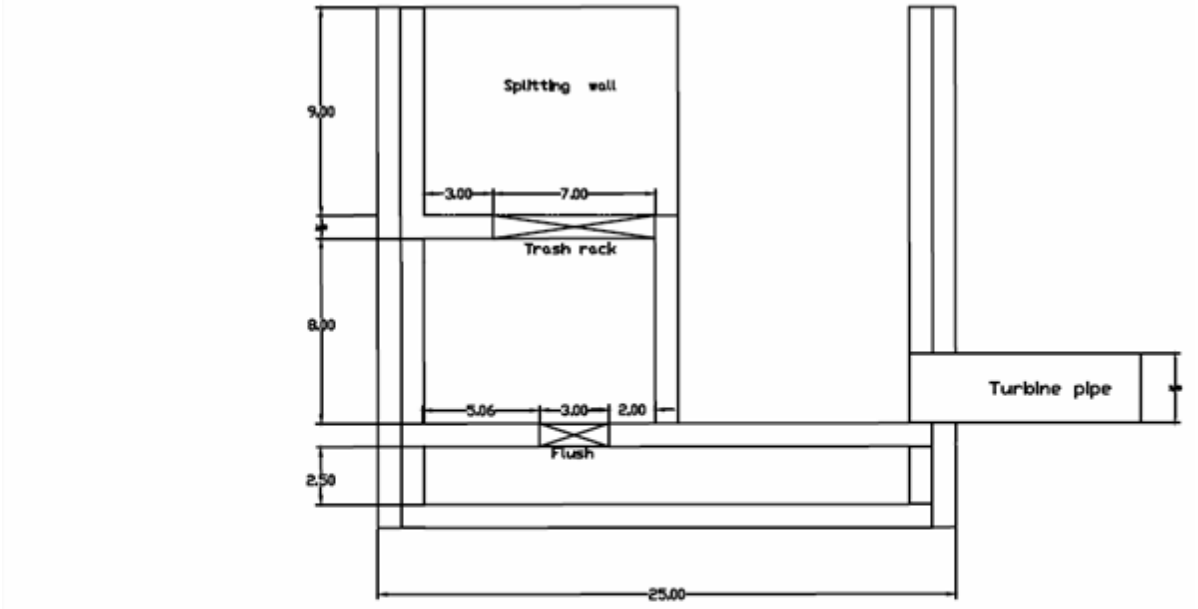


Vertical Plane

# Appendix 2 – Boundary Conditions for the Numerical Simulations

| Test 1.1. | Type | Flow-rate/ Pressure | Volume Fraction |
|---|---|---|---|
| **1. Inlet** | Wall (Inactive) | - | - |
| **2. Outlet (Normal Production)** | Wall (Inactive) | - | - |
| **3. Outlet (Flushing)** | Mass Flow Inlet | -4000 kg/s | Only water |
| **4. Outlet (Roof)** | Pressure Outlet | 0 Pa | Only air |

| Test 1.2. | Type | Flow-rate/ Pressure | Volume Fraction |
|---|---|---|---|
| **1. Inlet 1**<br>**Inlet 2** | Wall (Inactive)<br>Pressure Outlet | -<br>Field function 1 | -<br>Only water |
| **2. Outlet (Normal Production)** | Mass Flow Inlet | -300 kg/s | Only water |
| **3. Outlet 1 (Flushing)**<br>**Outlet 2 (Flushing)** | Mass Flow Inlet<br>Wall (Inactive) | -2000 kg/s<br>- | Only water<br>- |
| **4. Outlet (Roof)** | Pressure Outlet | 0 Pa | Only air |

| Test 1.3, 1.4. | Type | Flow-rate/ Pressure | Volume Fraction |
|---|---|---|---|
| **1. Inlet** | Wall (Inactive) | - | - |
| **2. Outlet (Normal Production)** | Wall (Inactive) | - | - |
| **3. Outlet (Flushing)** | Pressure Outlet | 0 Pa | Water and air |
| **4. Outlet (Roof)** | Pressure Outlet | 0 Pa | Only air |

| Test 2.1. | Type | Flow-rate/ Pressure | Volume Fraction |
|---|---|---|---|
| **1. Inlet** | Pressure Outlet | Field function 1 | Only water |
| **2. Outlet (Normal Production)** | Mass Flow Inlet | -2000 kg/s | Only water |
| **3. Outlet (Flushing)** | Wall (Inactive) | - | - |
| **4. Outlet (Roof)** | Pressure Outlet | 0 Pa | Only air |

| Test 2.2. | Type | Flow-rate/ Pressure | Volume Fraction |
|---|---|---|---|
| **1. Inlet 1**<br>**Inlet 2** | Pressure Outlet | Field function 2 | Only Water |
| **2. Outlet (Normal Production)** | Mass Flow Inlet | -2000 kg/s | Only water |
| **3. Outlet 1 (Flushing)**<br>**Outlet 2 (Flushing)** | Wall (Inactive) | - | - |
| **4. Outlet (Roof)** | Pressure Outlet | 0 Pa | Only air |

| Test 2.3, 2.4, 2.5. | Type | Flow-rate/ Pressure | Volume Fraction |
|---|---|---|---|
| **5. Inlet 1<br>Inlet 2** | Pressure Outlet | Field function 1 | Only Water |
| **6. Outlet (Normal Production)** | Mass Flow Inlet | -2000 kg/s | Only water |
| **7. Outlet 1 (Flushing)<br>Outlet 2 (Flushing)** | Wall (Inactive) | - | - |
| **8. Outlet (Roof)** | Pressure Outlet | 0 Pa | Only air |

| Test 2.6. | Type | Flow-rate/ Pressure | Volume Fraction |
|---|---|---|---|
| **1. Inlet 1<br>Inlet 2** | Pressure Outlet | Field function 3 | Only water |
| **2. Outlet (Normal Production)** | Mass Flow Inlet | -1.2 kg/s | Only water |
| **3. Outlet 1 (Flushing)<br>Outlet 2 (Flushing)** | Wall (Inactive) | - | - |
| **4. Outlet (Roof)** | Pressure Outlet | 0 Pa | Only air |

| Test 2.7, 2.8, 2.9. | Type | Flow-rate/ Pressure | Volume Fraction |
|---|---|---|---|
| **1. Inlet 1<br>Inlet 2** | Pressure Outlet | Field function 4 | Only water |
| **2. Outlet (Normal Production)** | Mass Flow Inlet | -20.5 kg/s | Only water |
| **3. Outlet 1 (Flushing)<br>Outlet 2 (Flushing)** | Wall (Inactive) | - | - |
| **4. Outlet (Roof)** | Pressure Outlet | 0 Pa | Only air |

# Appendix 3 – Courant Number Comparison Test

| High Courant Numbers | Low Courant Numbers |
| --- | --- |
| **Time-steps**:<br>0.01 s for 48 000 iterations | **Time-steps**:<br>0.01 s for 48 000 iterations<br>+ 0.001 s for 2 000 iterations |
| **Convective Courant Number**<br> 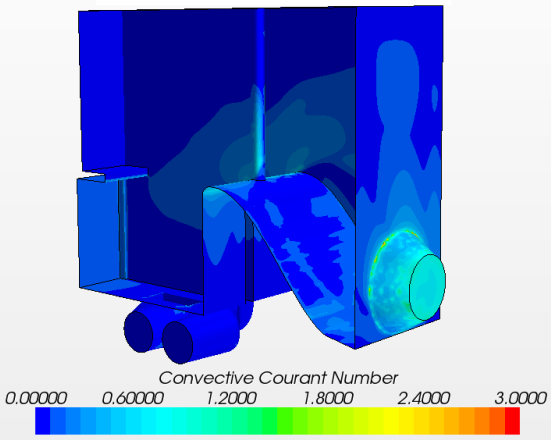 <br> | **Convective Courant Number**<br> 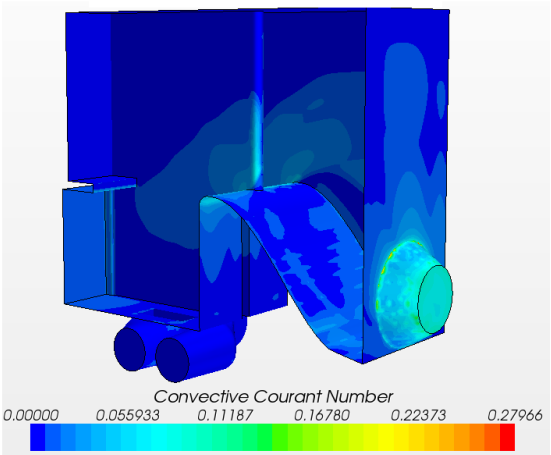 <br> |
| **Turbulent Kinetic Energy**<br> 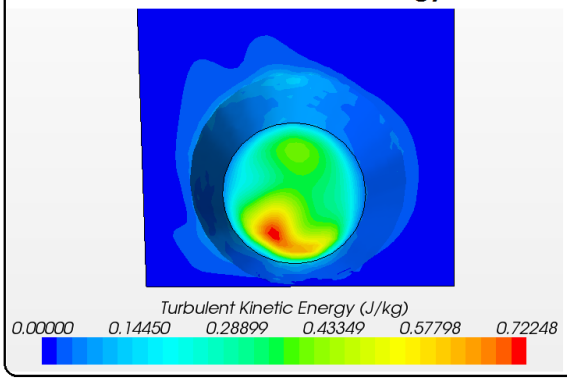 <br> | **Turbulent Kinetic Energy**<br> 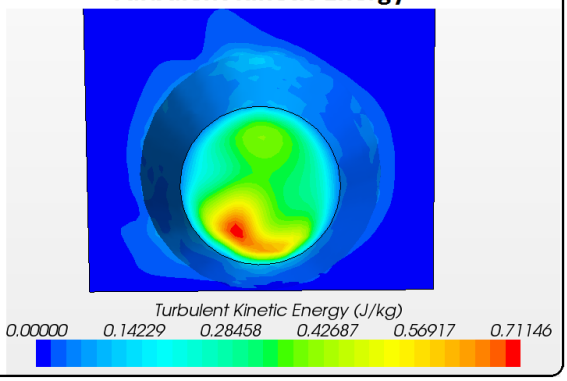 <br> |

# Appendix 4 – Residuals

**Test 1.1. Residuals**

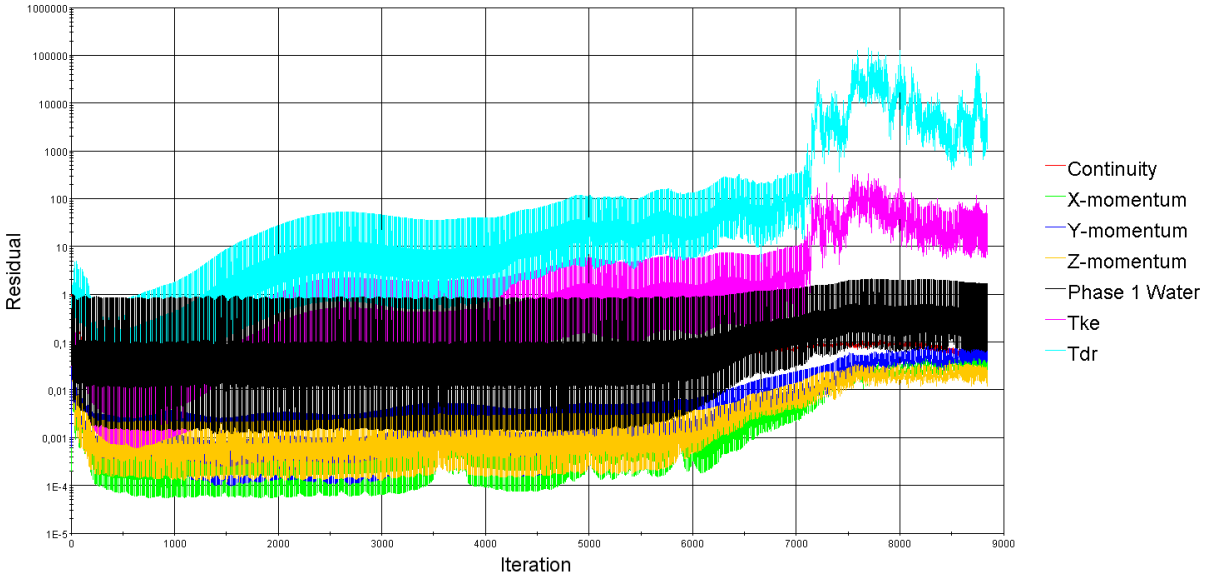


**Test 1.2. Residuals**

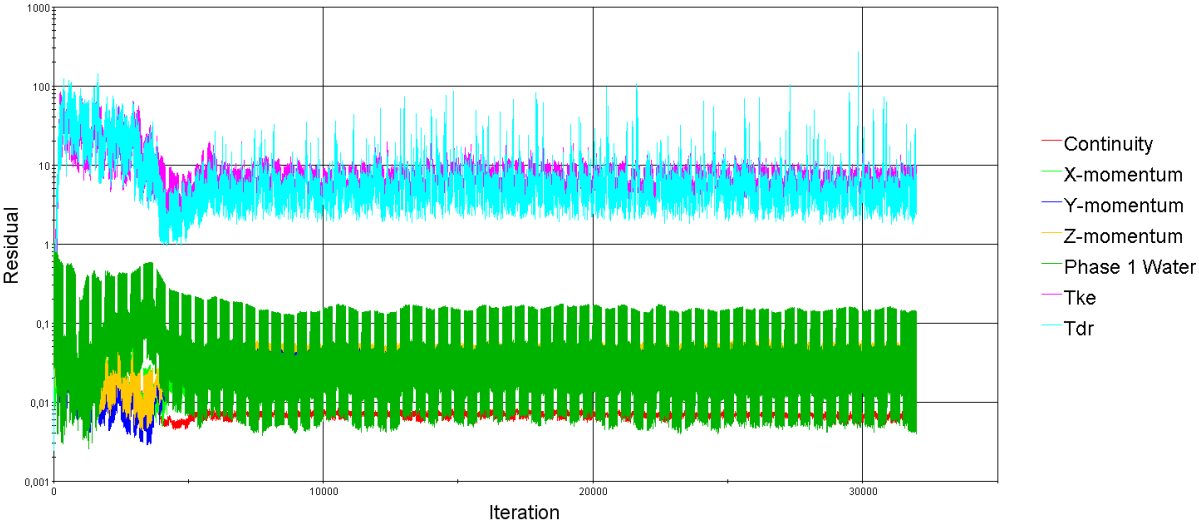

## Test 1.3. Residuals

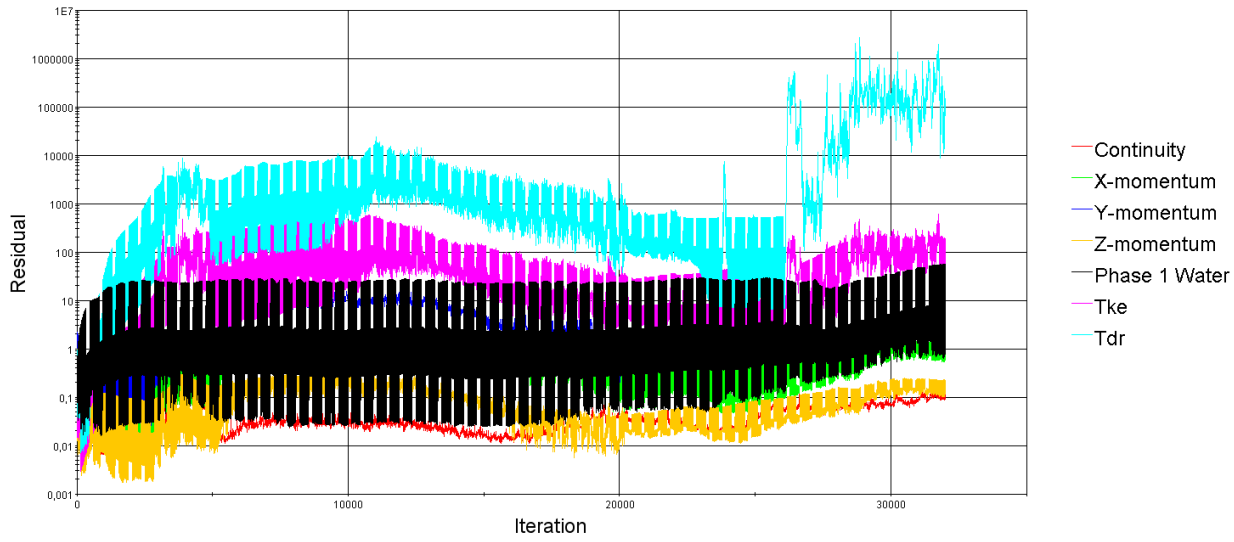


## Test 1.4. Residuals

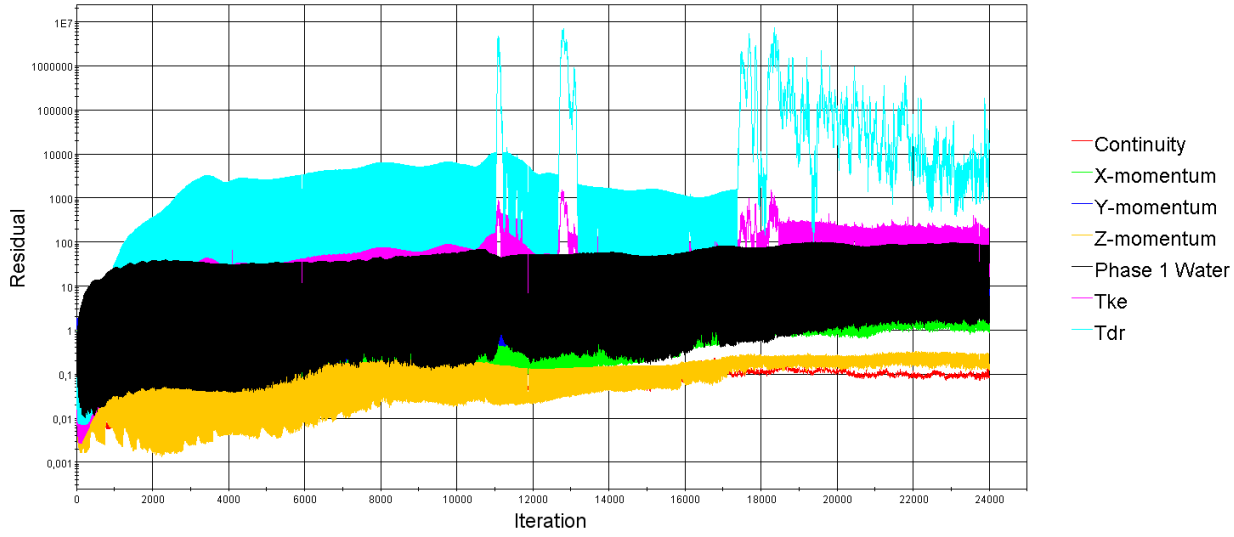


## Test 2.1. Residuals

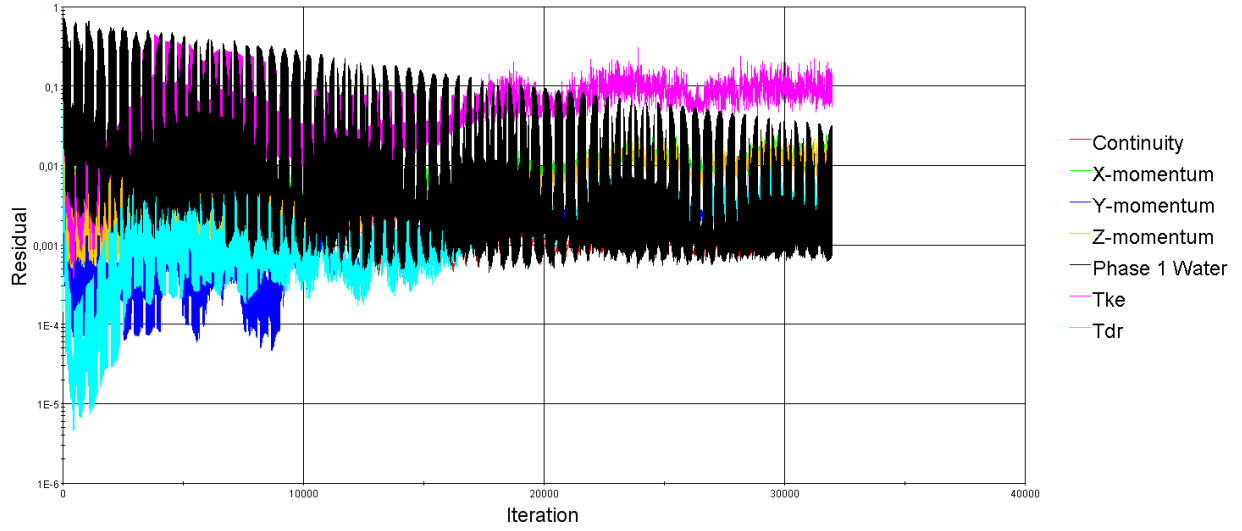

## Test 2.2. Residuals

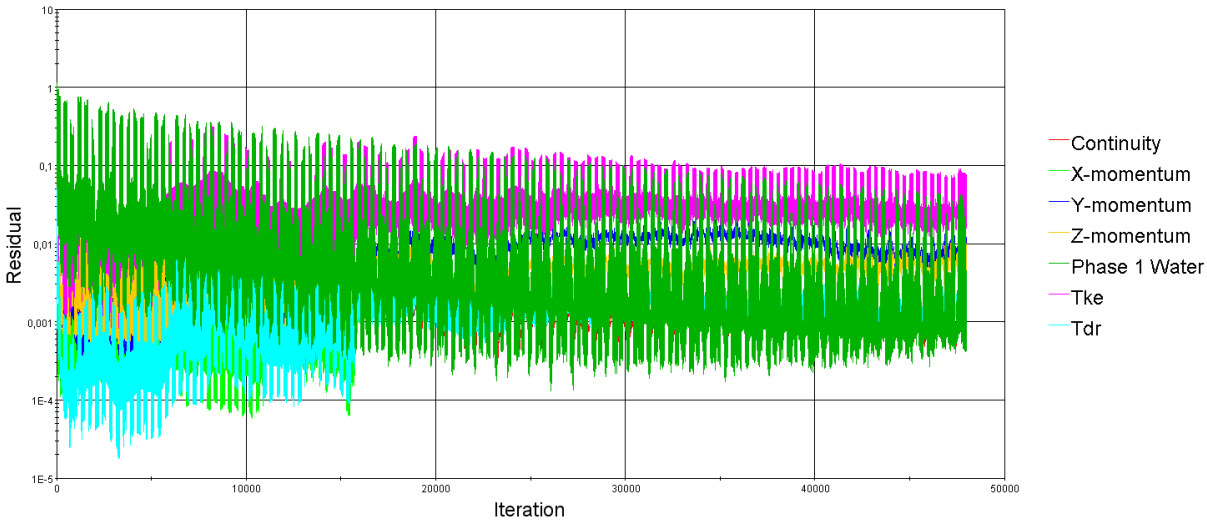


## Test 2.3. Residuals

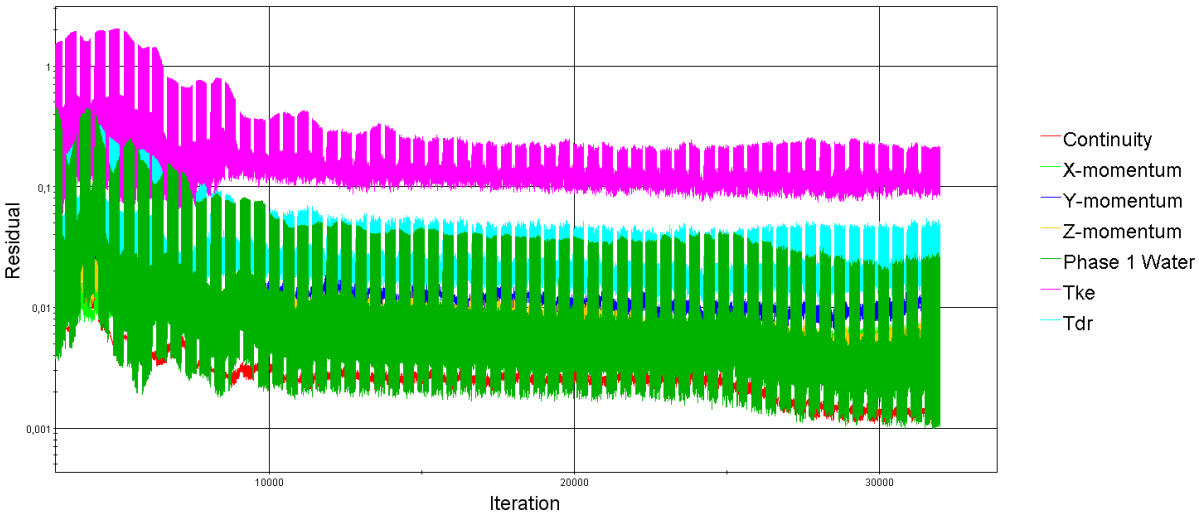


## Test 2.4. Residuals

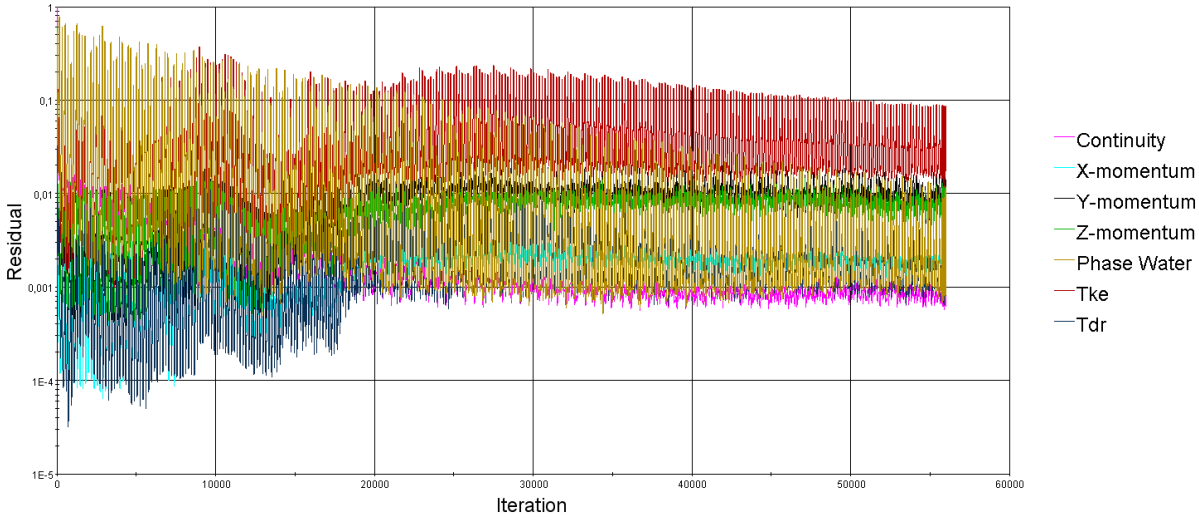

## Test 2.5. Residuals

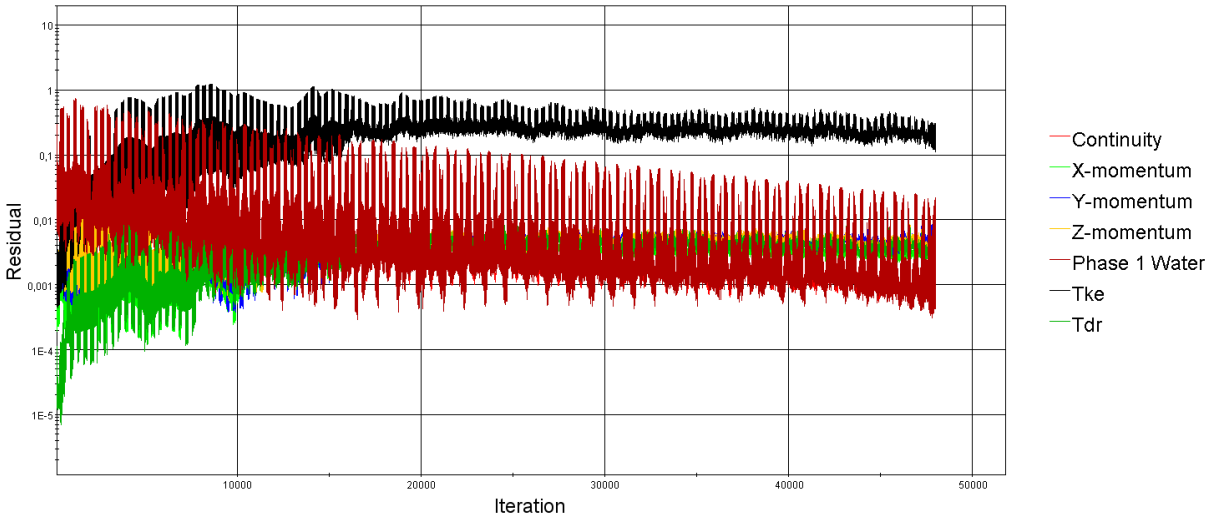


## Test 2.6. Residuals

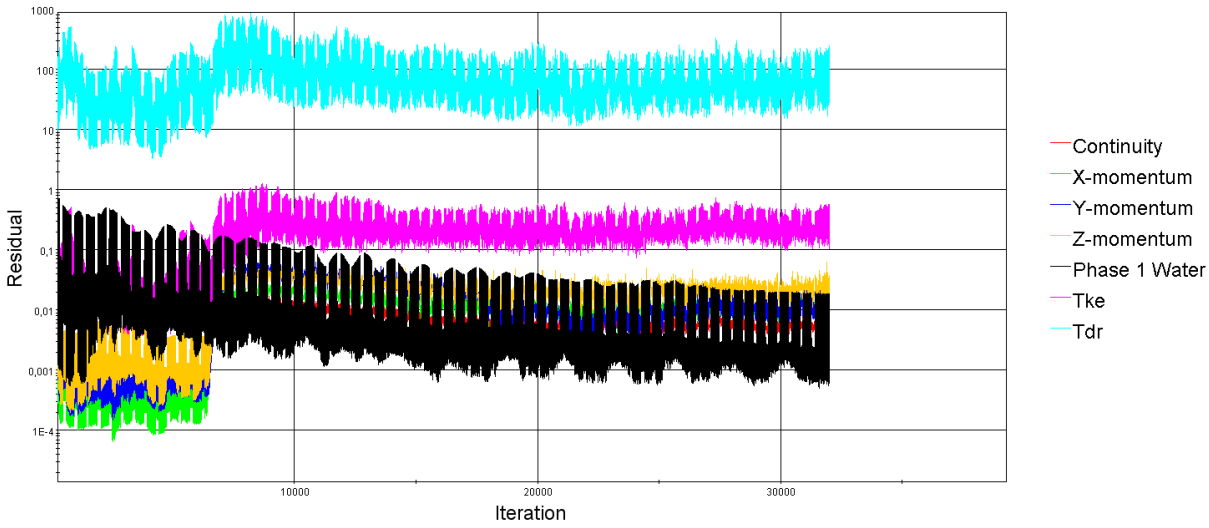


## Test 2.7. Residuals

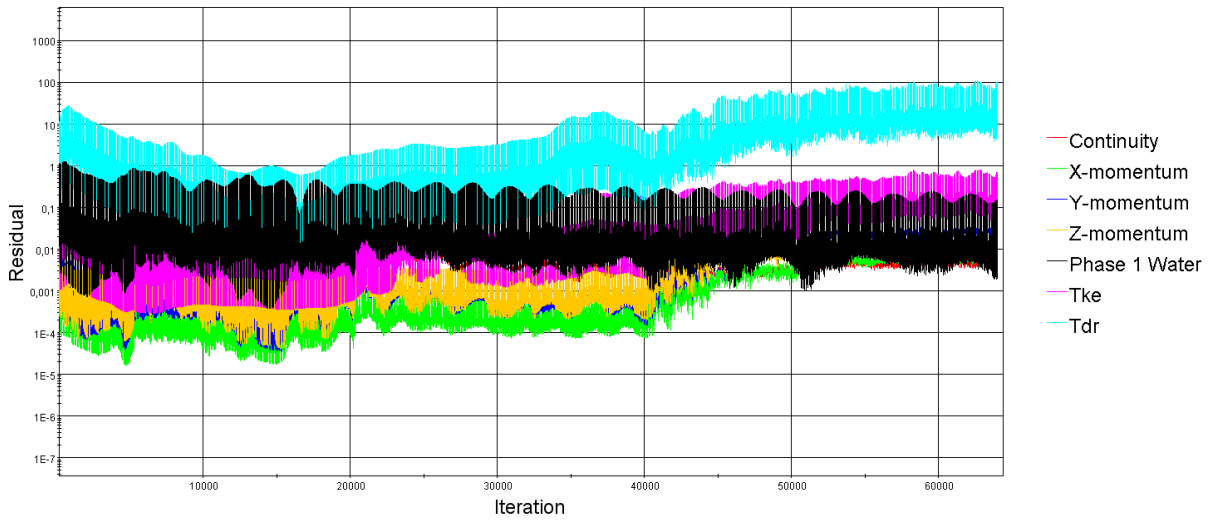

**Test 2.8. Residuals**

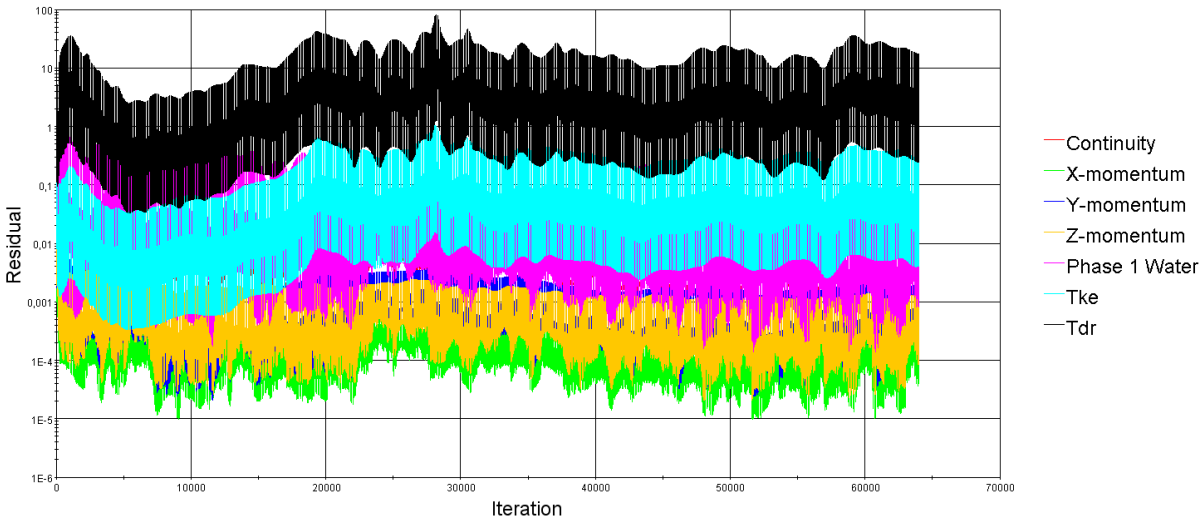


**Test 2.9. Residuals**

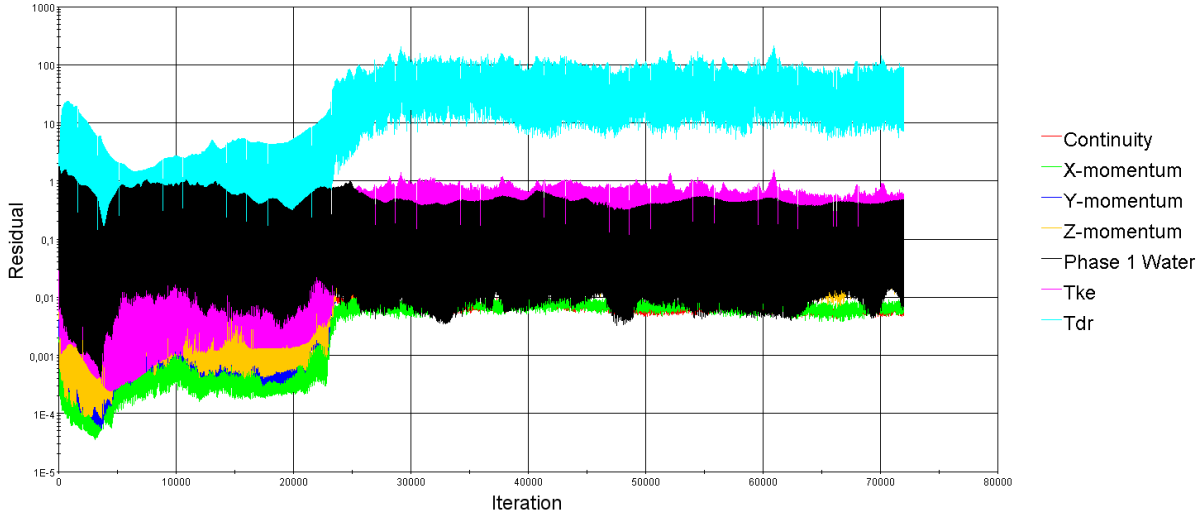

# Appendix 5 – Mass Flow Plots

**Test 1.2. Mass Flow Monitor Plot**

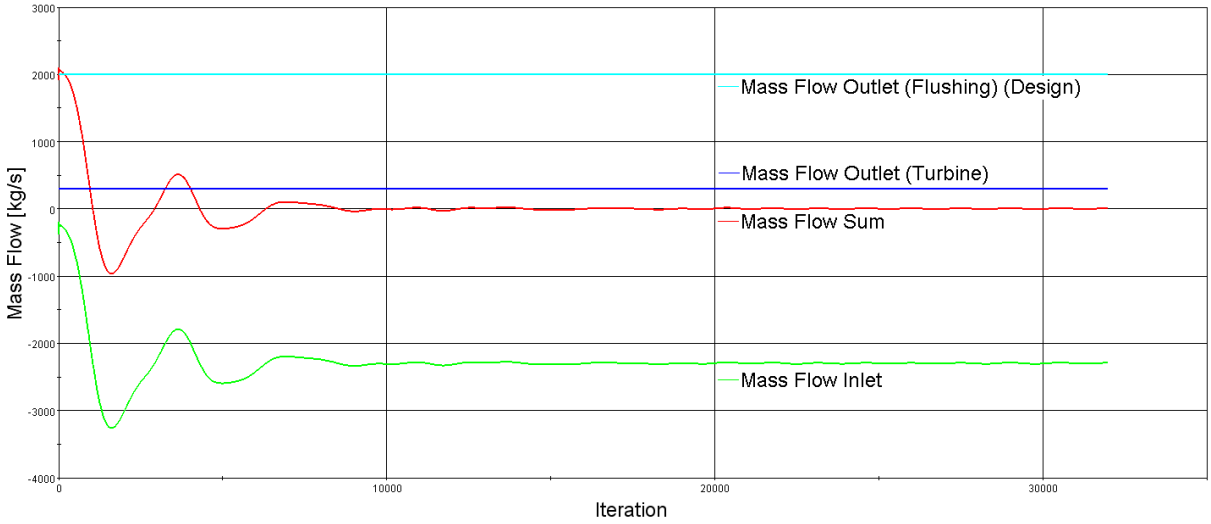


**Test 1.3. Mass Flow Monitor Plot**

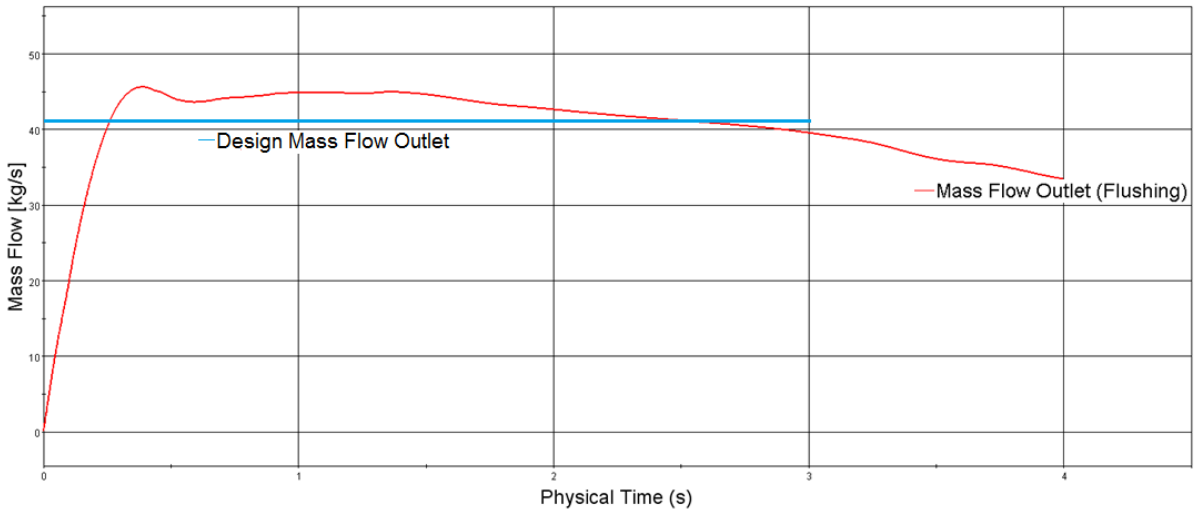

**Test 1.4. Mass Flow Monitor Plot**

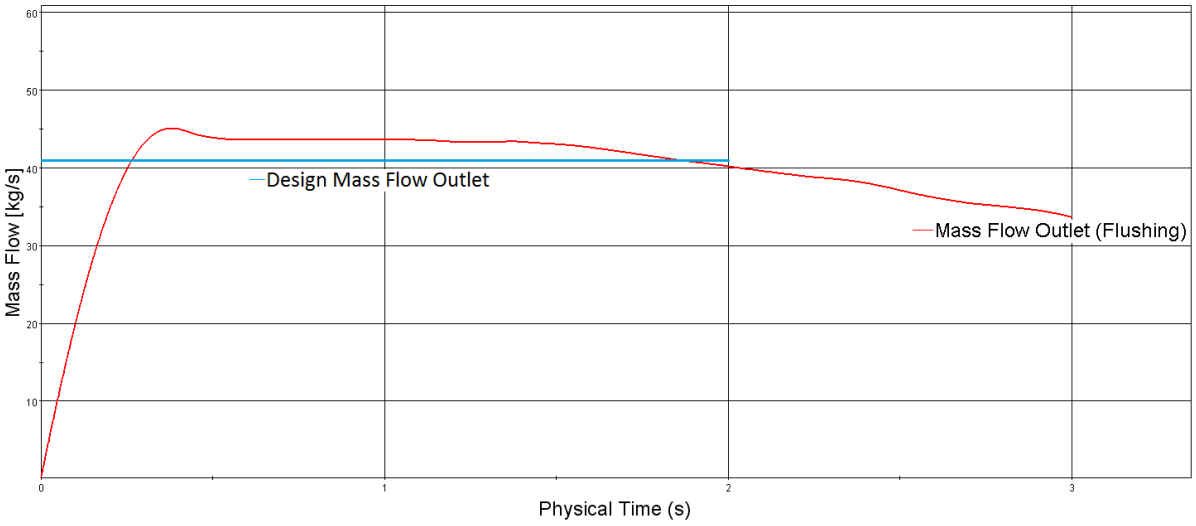


**Test 2.1. Mass Flow Monitor Plot**

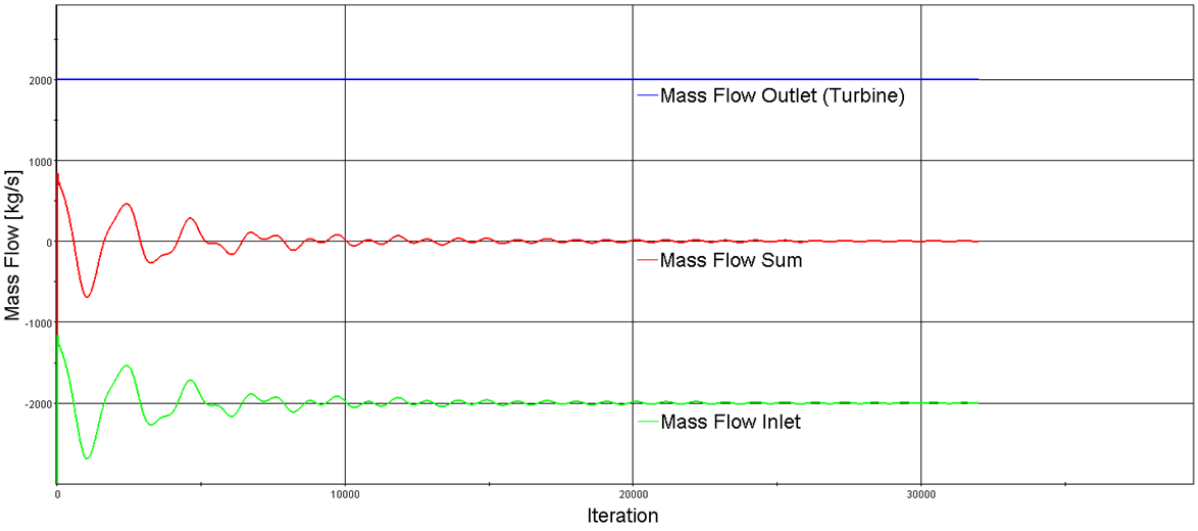


**Test 2.2. Mass Flow Monitor Plot**

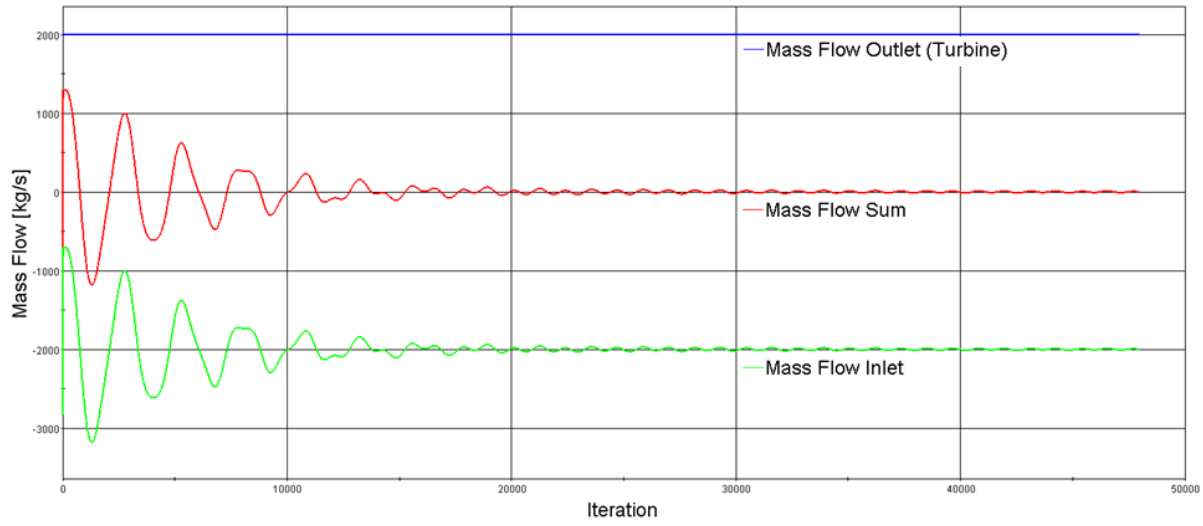

**Test 2.3. Mass Flow Monitor Plot**

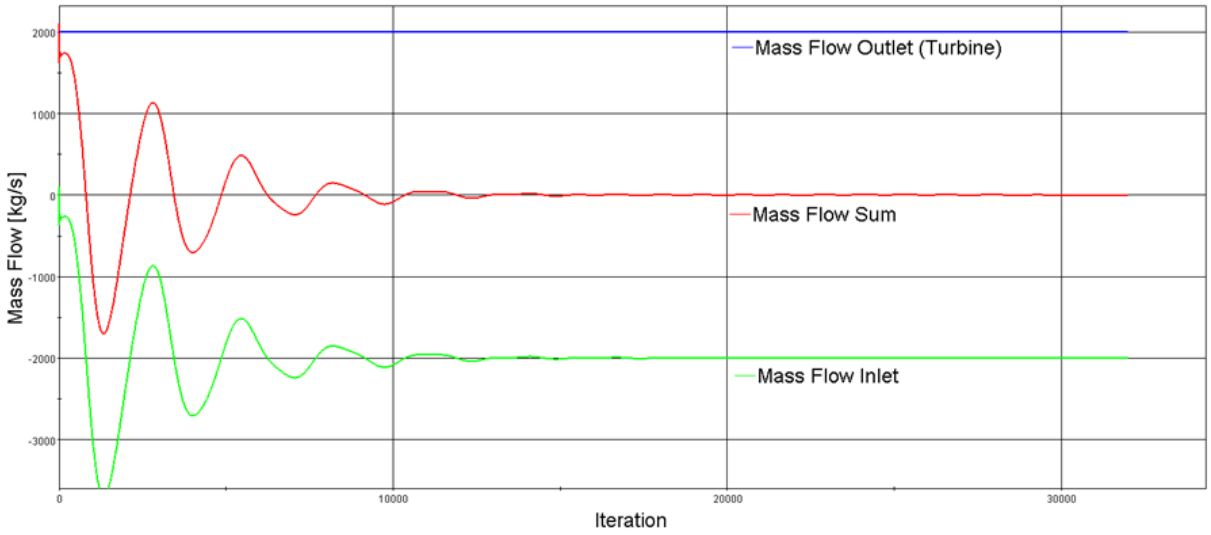


**Test 2.4. Mass Flow Monitor Plot**

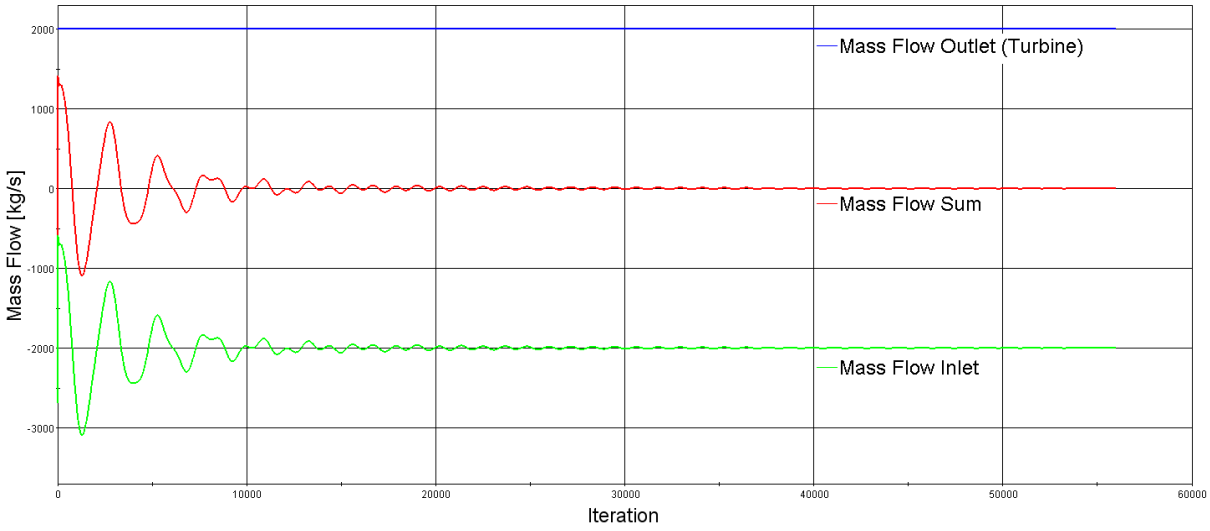


**Test 2.5. Mass Flow Monitor Plot**

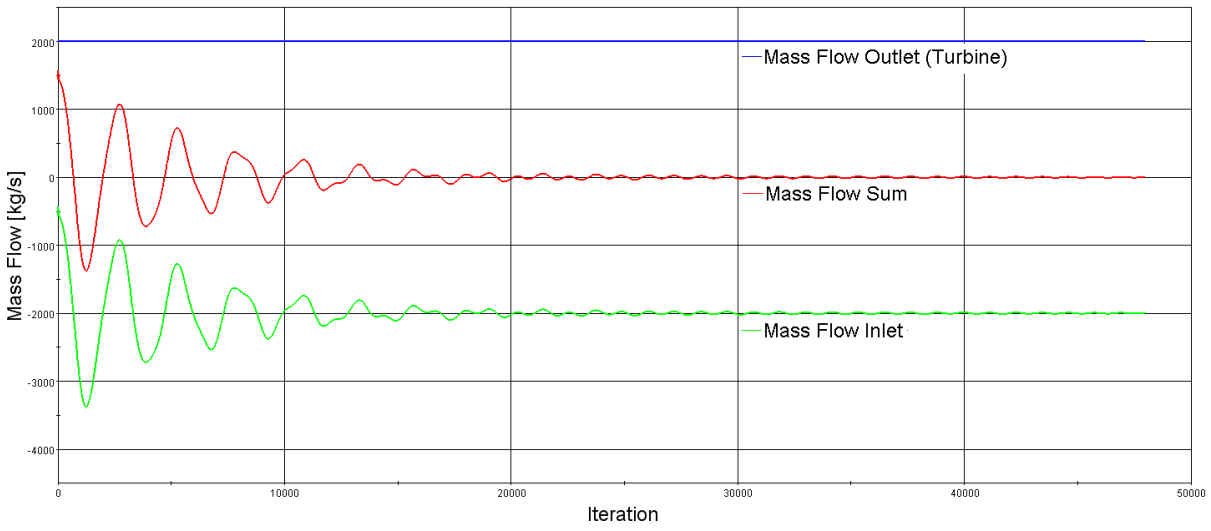

**Test 2.6. Mass Flow Monitor Plot**

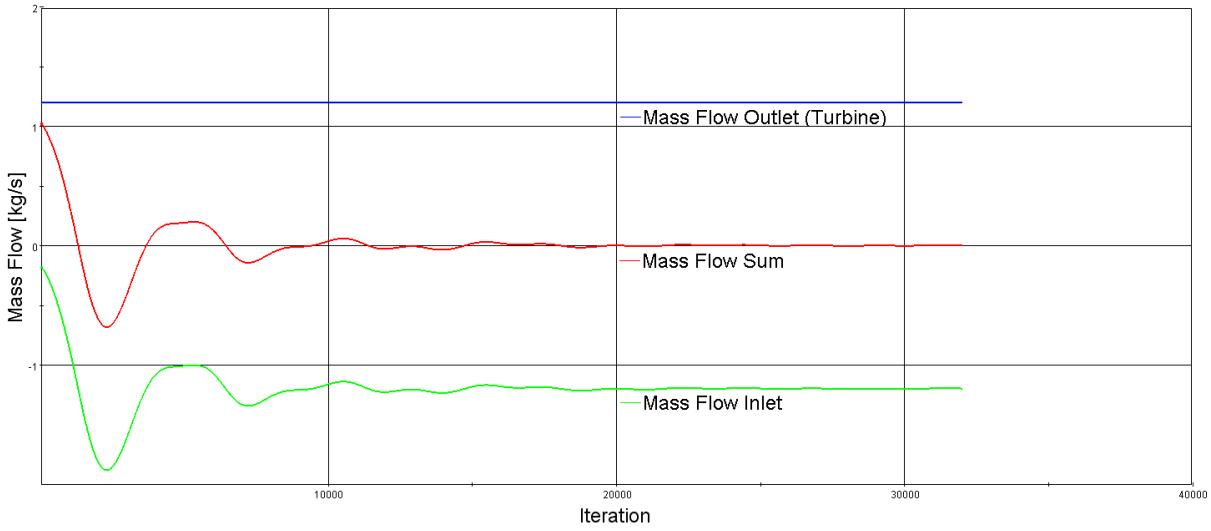


**Test 2.7. Mass Flow Monitor Plot**

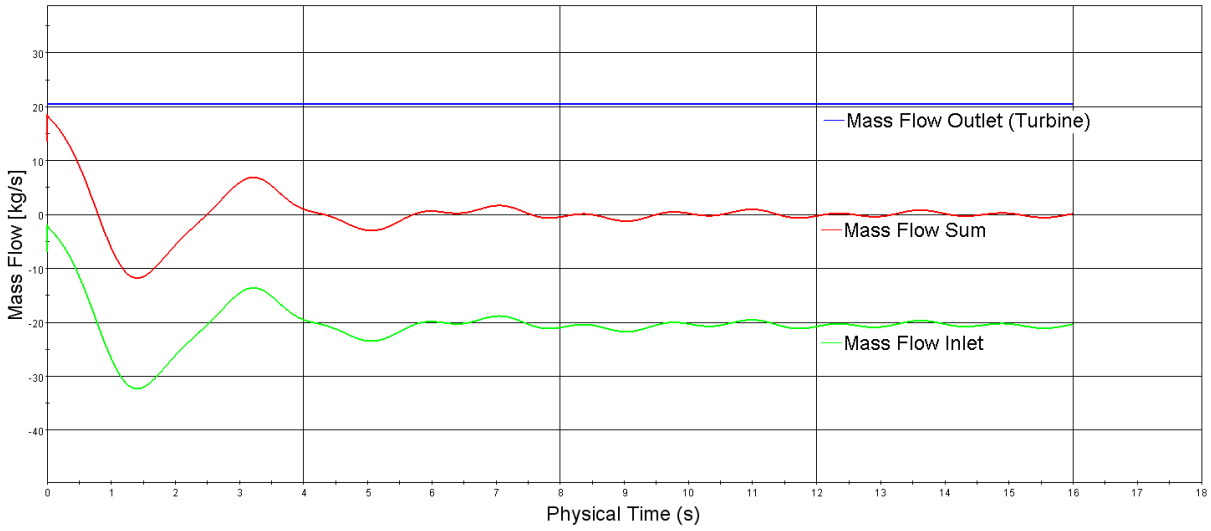


**Test 2.8. Mass Flow Monitor Plot**

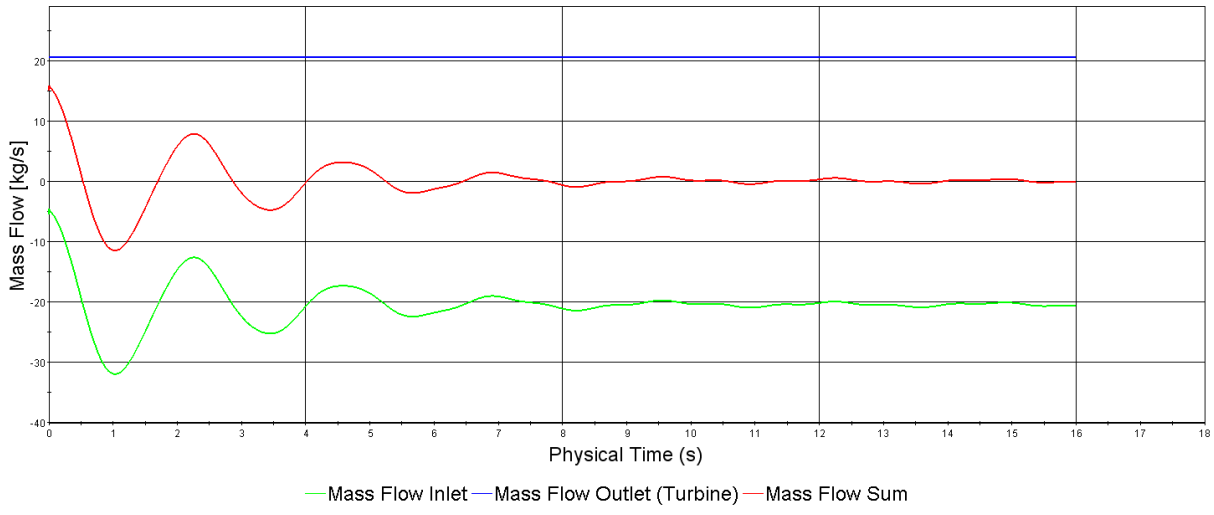

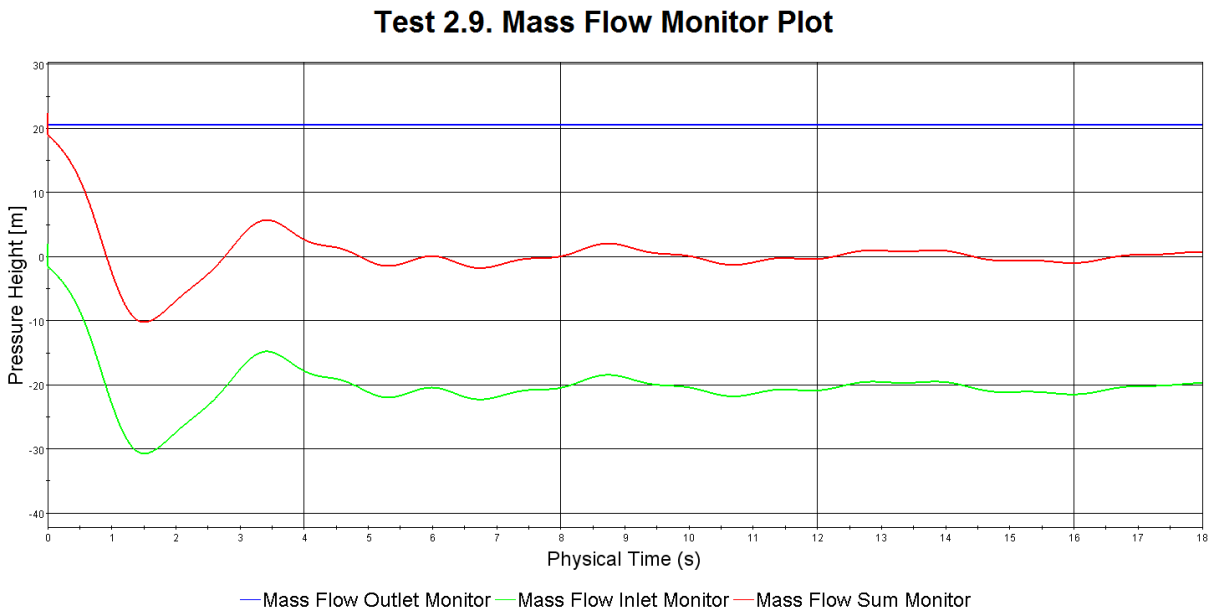
Test 2.9. Mass Flow Monitor Plot
Pressure Height [m]
30
20
10
0
-10
-20
-30
-40
0
1
2
3
4
5
6
7
8
9
10
11
12
13
14
15
16
17
18
Physical Time (s)
Mass Flow Outlet Monitor
Mass Flow Inlet Monitor
Mass Flow Sum Monitor

# Appendix 6 – Velocity Distribution during Normal Production

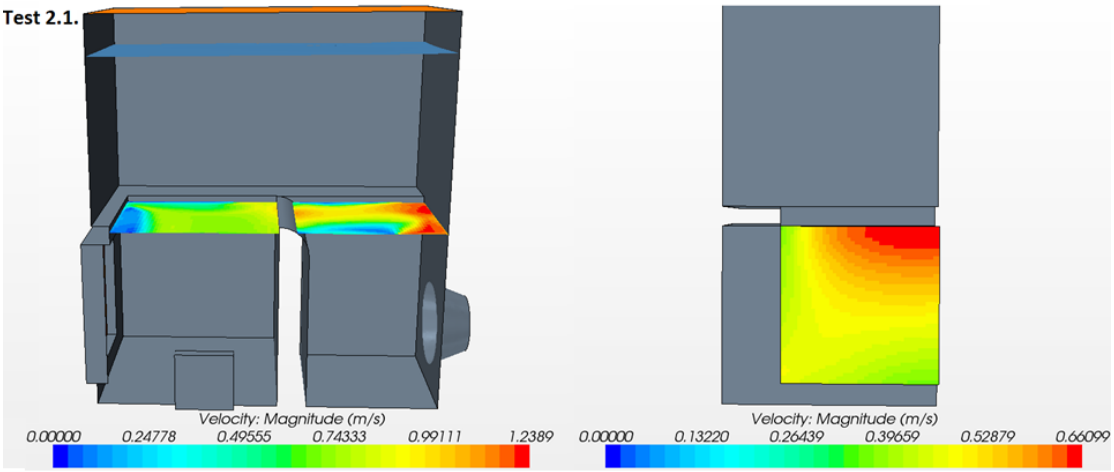


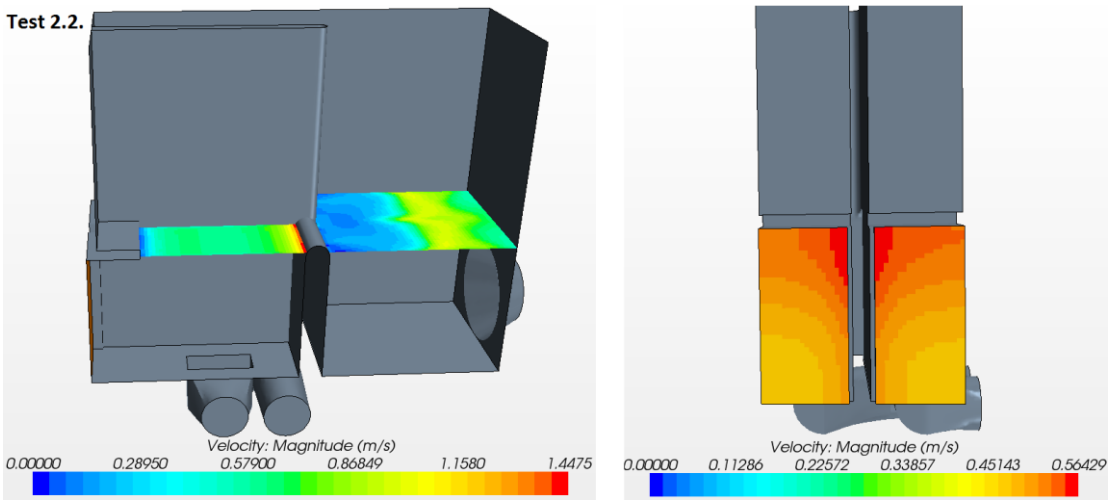


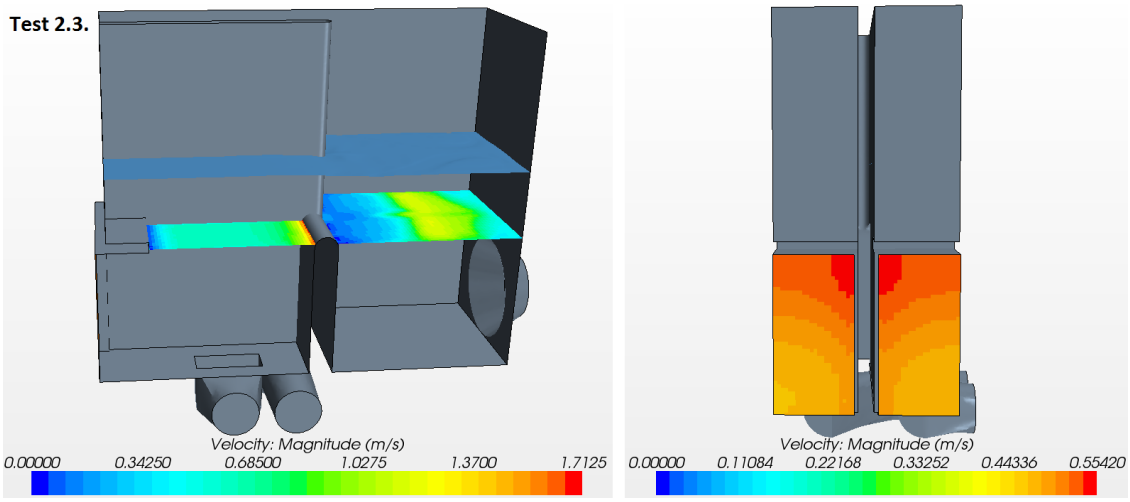

**Test 2.4.**

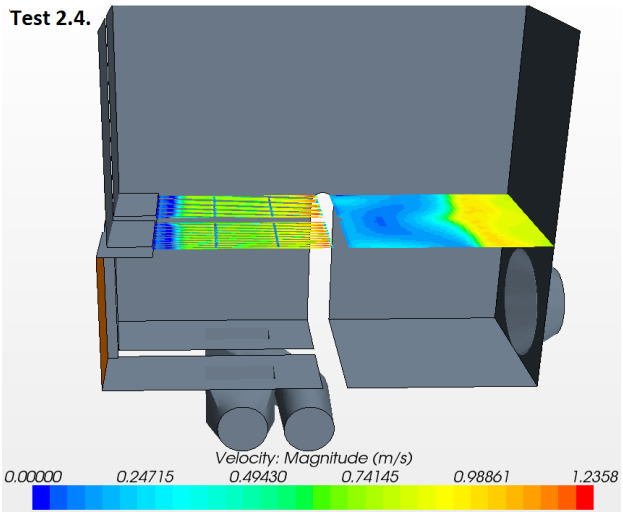


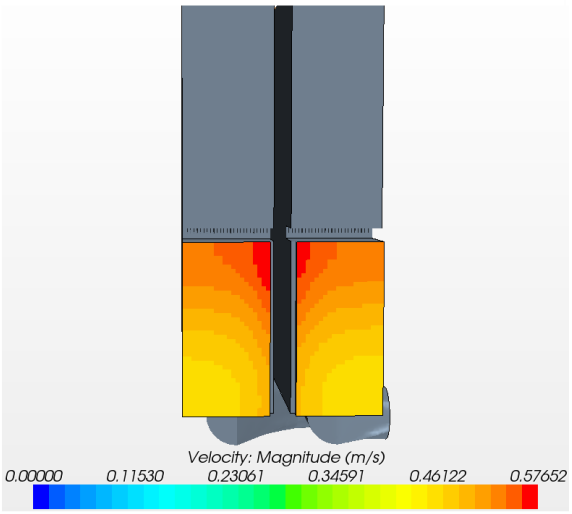


**Test 2.5.**

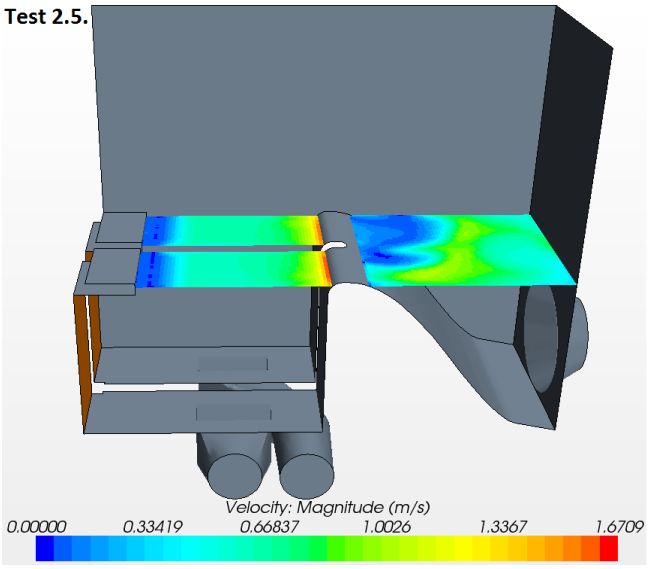


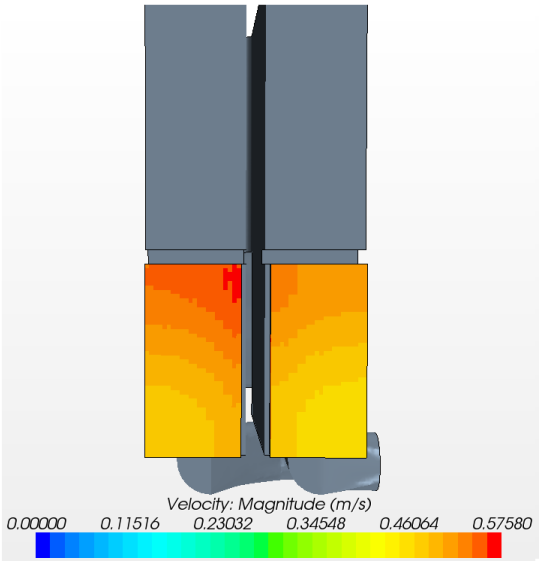


**Test 2.6.**

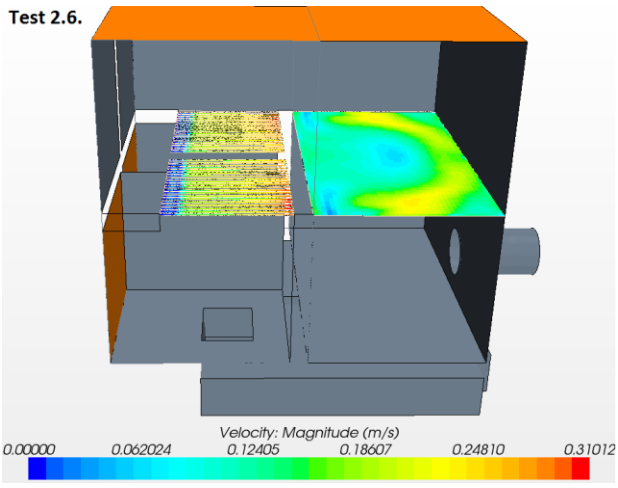


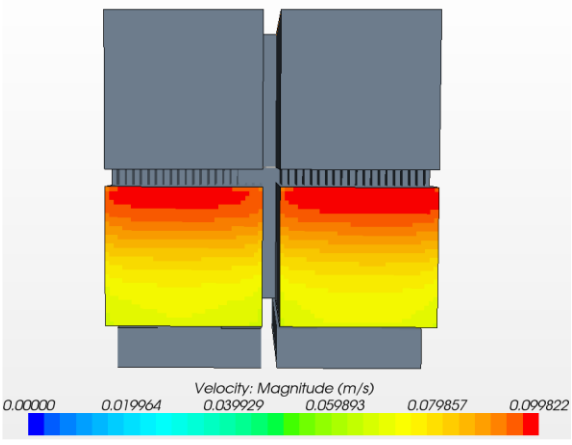

**Test 2.7.**

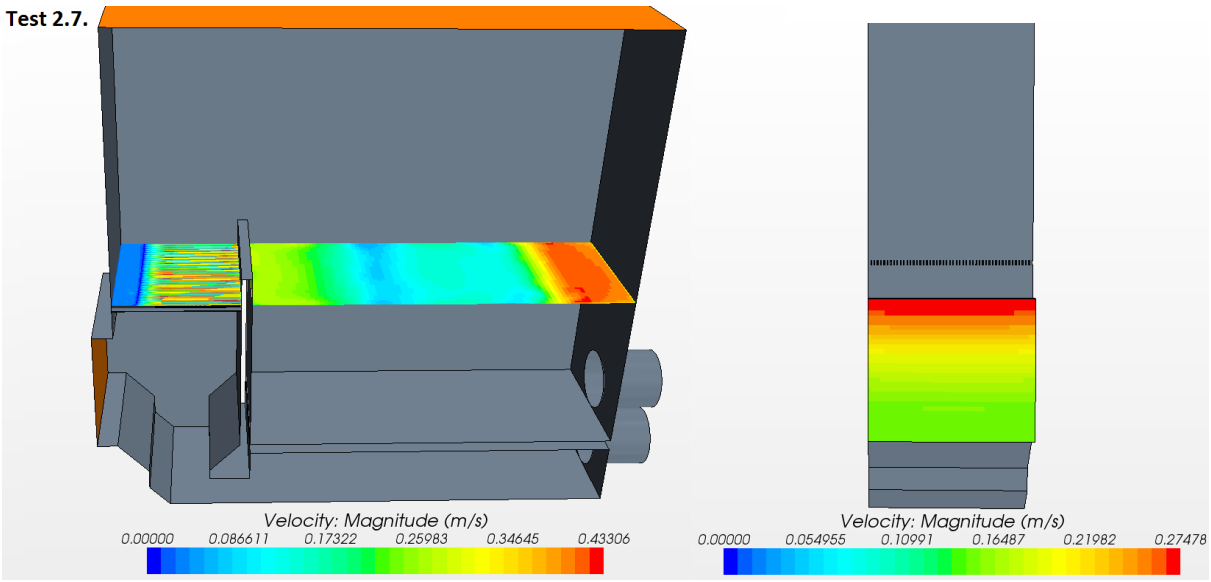


**Test 2.8.**

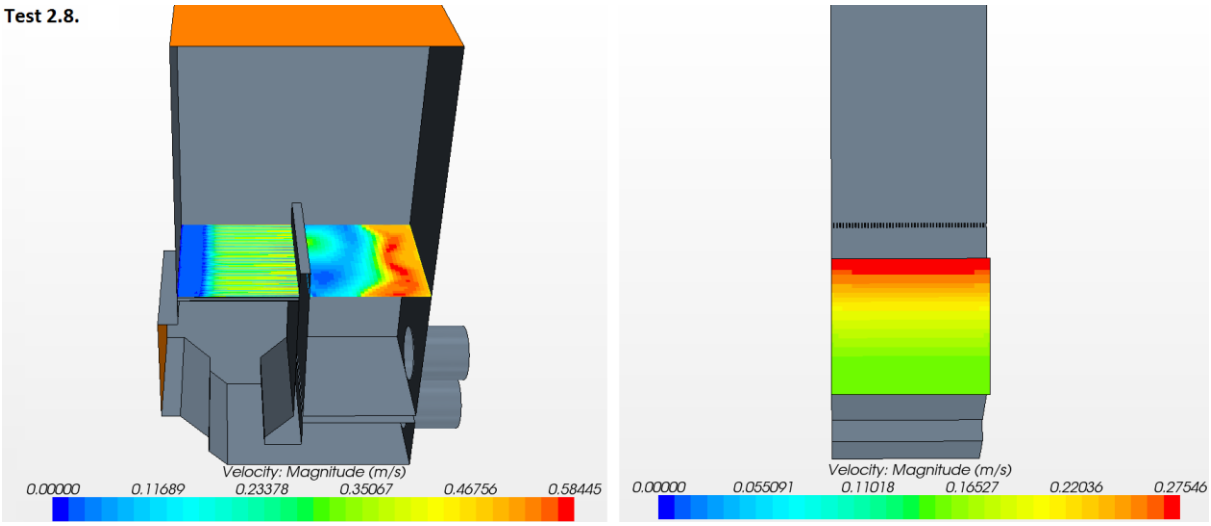


**Test 2.9.**

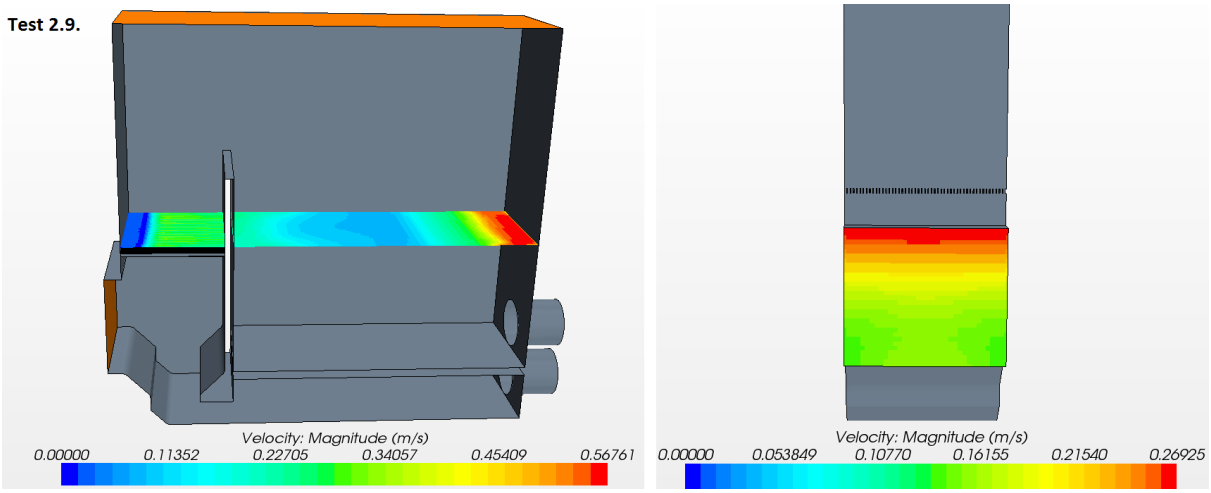

# Appendix 7 – Water Level Change in Test 2.6 – The demonstration Model

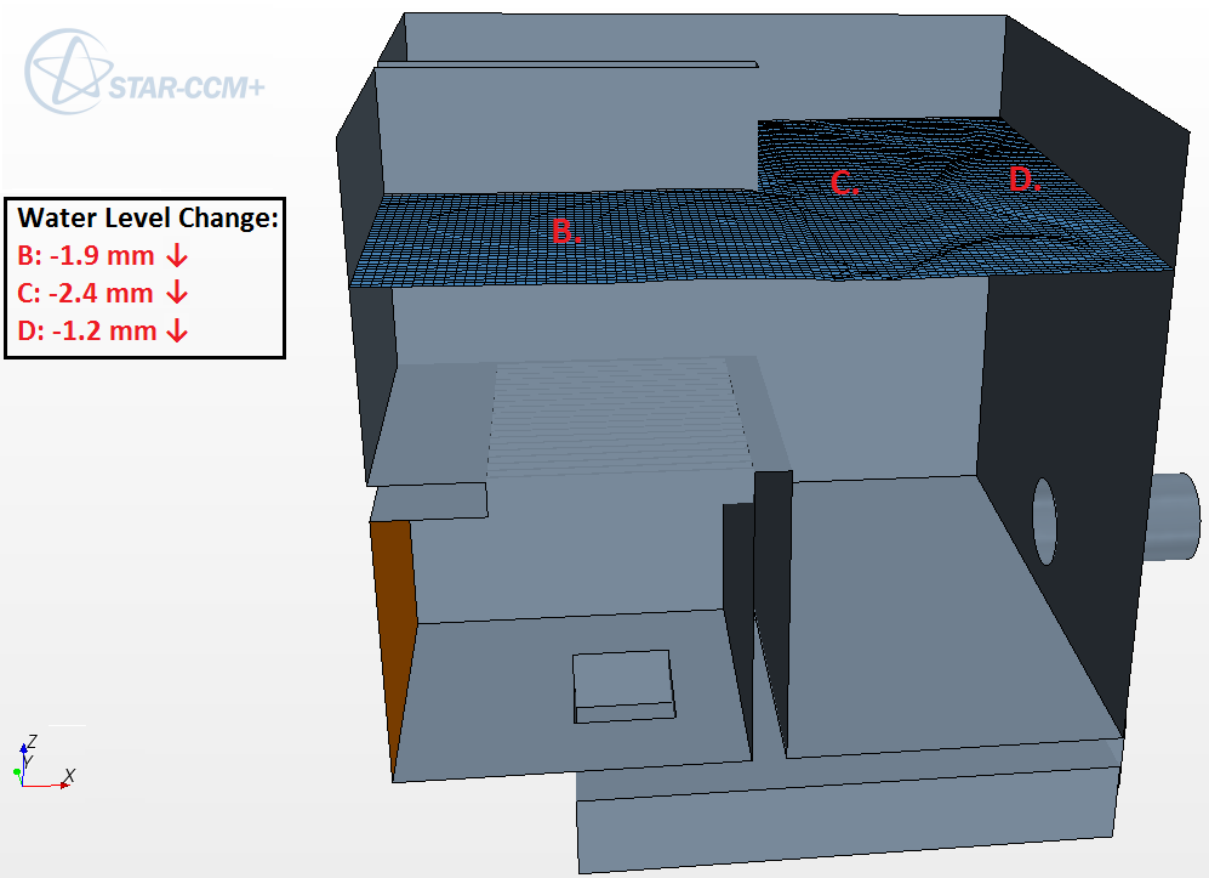

# Appendix 8 – Head Loss Variations in Kirschmer-Mosonyis Formula

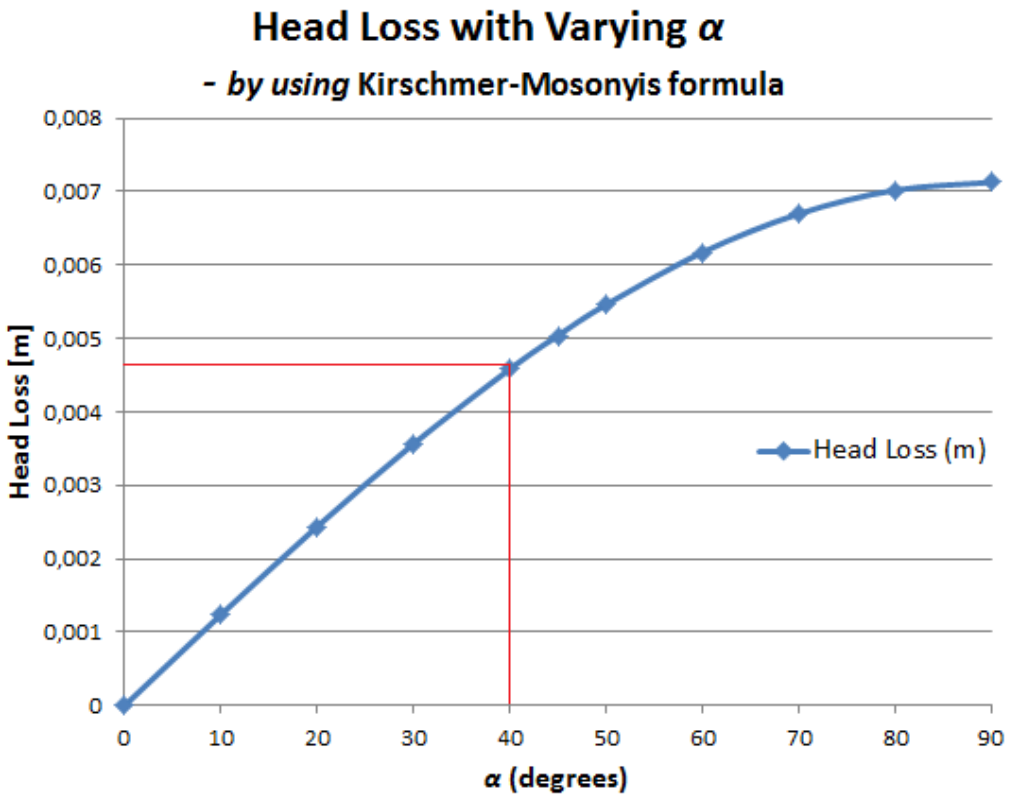

# Appendix 9 – Drawing of the Physical Scale Model

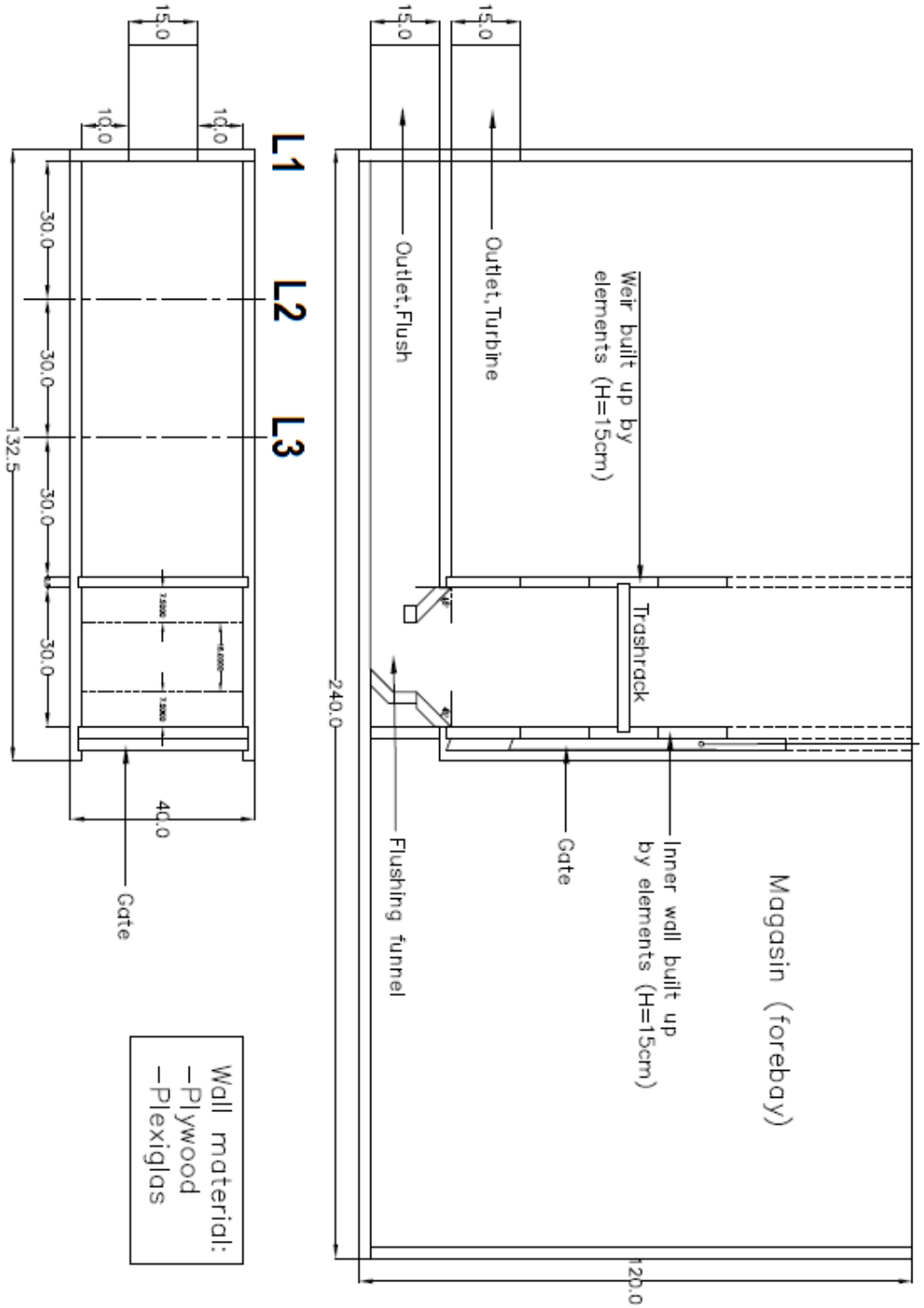

# Appendix 10 – Photo of the Scale Model

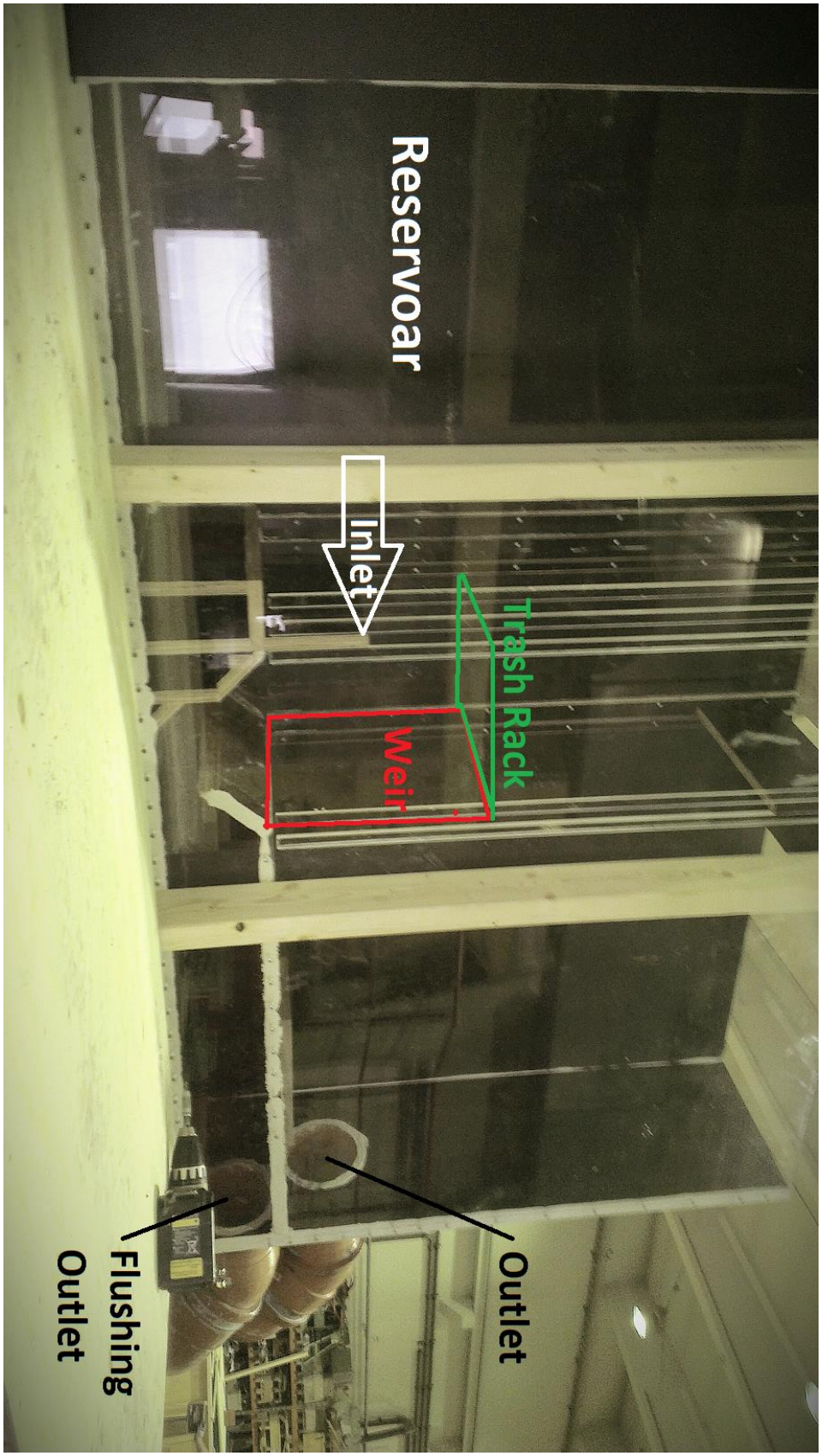

# Appendix 11 – Model Scaling using Froude Similarity

## Froude Similarity

| | Scale Model: | Prototype: | | |
|---|---|---|---|---|
| $D_{outlet\ pipe}$ | 0,15 | 1 | Lr: | 6,667 |
| $A_{trash\ rack}$ | 0,105 | 4,666667 | | |
| TR width | 0,35 | 2,3 | Vr: | 2,582 |
| TR length | 0,3 | 2,0 | Qr: | 114,76 |
| v | 0,1936 | 0,5 | | |
| Q | 0,02033 | 2,333 | | |
| Fr | 0,112881 | 0,112881 | | |
| | | | | |
| $A_{outlet\ pipe}$ | 0,017671459 | 0,785398 | | |
| $V_{outlet\ pipe}$ | 1,161895004 | 3 | | |
| Q | 0,02053238 | 2,3562 | | |
| | | | | |
| **Trash Rack:** | | | | |
| Bearings (m) | 0,0045 | 0,03 | m | |
| Bar width (m) | 0,0015 | 0,01 | m | |
| $v_{normal\ operation}$ | 0,1936 | 0,5 | m/s | |
| $v_{flushing}$ | 0,3873 | 1 | m/s | |
| | | | | |
| $Q_{normal\ operation}$ | 0,0205 | 2,3562 | m3/s | |
| $Q_{flushing}$ | 0,0411 | 4,712389 | m3/s | |